CHARACTERIZATION OF THE SUBUNIT INTERFACE RESIDUES AND THEIR EFFECTS ON ENZYME PROPERTIES OF GLUTATHIONE S-TRANSFERASES

JUTHAMART PIROMJITPONG

**A THESIS SUBMITTED IN PARTIAL FULFILLMENT OF
THE REQUIREMENTS FOR THE DEGREE OF
MASTER OF SCIENCE
(MOLECULAR GENETICS AND GENETIC ENGINEERING)
FACULTY OF GRADUATE STUDIES
MAHIDOL UNIVERSITY
2004**

ISBN 974-04-5171-3

Thesis
Entitled

CHARACTERIZATION OF THE SUBUNIT INTERFACE RESIDUES AND THEIR EFFECTS ON ENZYME PROPERTIES OF GLUTATHIONE S-TRANSFERASES

Juthamart Piromjitpong
Miss Juthamart Piromjitpong
Candidate

Albert J. Ketterman
Assoc. Prof. Albert J. Ketterman, Ph.D.
Major-Advisor

C. Krittanai
Asst. Prof. Chartchai Krittanai, Ph.D.
Co-Advisor

Lect. Duncan R. Smith, Ph.D.
Co-Advisor

Rassmidara Hoonsawat
Assoc. Prof. Rassmidara Hoonsawat, Ph.D
Dean
Faculty of Graduate Studies

V. Akkarapatumwong
Asst. Prof. Varaporn Akkarapatumwong, Ph.D
Chair
Master of Science Programme in Molecular Genetics and Genetic Engineering
Institute of Molecular Biology and Genetics

Thesis
Entitled

CHARACTERIZATION OF THE SUBUNIT INTERFACE RESIDUES AND THEIR EFFECTS ON ENZYME PROPERTIES OF GLUTATHIONE S-TRANSFERASES

was submitted to the Faculty of Graduate Studies, Mahidol University
For the degree of Master of Science (Molecular Genetics and Genetic Engineering)
on
1 September 2004

Juthamart Piromjitpong
Miss Juthamart Piromjitpong
Candidate

Assoc. Prof. Albert J. Ketterman,
Ph.D.
Chair

Asst. Prof. Chartchai Krittanai,
Ph.D.
Member

Pimchai Chaiyen
Asst. Prof. Pimchai Chaiyen
Ph.D.
Member

Lect. Duncan R. Smith,
Ph.D.
Member

Assoc. Prof. Rassmidara Hoonsawat,
Ph.D.
Dean
Faculty of Graduate Studies
Mahidol University

Asst. Prof. Chartchai Krittanai,
Ph.D.
Acting Director
Institute of Molecular Biology and Genetics
Mahidol University

ACKNOWLEDGMENTS

I wish to express my appreciation of the generosity of many persons, particularly my supervisor, Dr. Albert J. Ketterman, who provided invaluable advice and all the encouragement during this course and for the thesis preparation. I am also grateful to my co-advisors, Dr. Chartchai Krittanai and Dr. Duncan R. Smith for their helpful comments, advice and discussion for this research.

I wish to thank Asst. Prof. Pimchai Chaiyen, from Biochemistry Department, Faculty of Science, for kindness in providing the fluorescence spectrophotometer and suggestions for improvement.

My appreciation is also extended to Mr.Apichai Bourchookarn and Mr. Weerachon Taepanun for their spectroscopic techniques assistance. I would also like to thank many members of GST laboratory especially Ms. Jantana Wongsantichon, Ms. Ardcharaporn Vararattanavech and Mr. Pakorn Winayanuwattikun for their advice, great assistance in solving technical problems and their friendship.

I am grateful to all the teachers and staffs of the Institute of Molecular Biology and Genetics for their valuable assistances and thanks also to my friends for their kind support.

I also thank the Development and Promotion of Science and Technology Talent Project (DPST) that provided me financial support and the good opportunity for doing this project.

Finally I would like to thank my parents, my sister and my brother for their encouragement, love and patience.

Juthamart Piromjitpong

CHARACTERIZATION OF THE SUBUNIT INTERFACE RESIDUES AND THEIR EFFECTS ON ENZYME PROPERTIES OF GLUTATHIONE S-TRANSFERASES

JUTHAMART PIROMJITPONG 4536667 MBMG/M

M.Sc. (MOLECULAR GENETICS AND GENETIC ENGINEERING)

THESIS ADVISORS: ALBERT J. KETTERMAN, Ph.D., CHARTCHAI KRITTANAI, Ph.D., DUNCAN R. SMITH, Ph.D.

ABSTRACT

The purpose of this research was to investigate the molecular basis for catalytic differences between closely related GSTs from the same class which have nucleotide and amino acid sequence similarities. Two closely related GSTs, namely adGSTD3-3 and adGSTD4-4, purified from *Anopheles dirus*, are of interest because they arise from alternate splicing and their crystal structures are available. These two isozymes have 68% amino acid identity and have very similar tertiary structures. Among 77 different amino acid residues in these two isozymes, there are nine residues at the subunit interface where the same residue position from both subunits fold to interact with each other. The interface interactions demonstrate three major areas; the conserved square electrostatic interactions at the top, the hydrophobic interactions at the center and the ionic interactions at the edge of the subunit interface. The results of the present work demonstrate that the conserved electrostatic interactions at the top of the subunit interface, which are formed by two glutamate75 and two arginine96 of adGSTD4-4, as well as the charge-charge network interactions at the edge of adGSTD4-4 subunit interface between glutamate116 and arginine134 are critical interactions that help to maintain the catalytic activity and conformation of the enzymes as shown by altering the kinetic parameters, refolding properties, thermal stability and florescence spectra. Moreover, we also observed that three variant hydrophobic amino acids at the center of the subunit interface influenced the specific properties of the adGSTD3-3 and adGSTD4-4. This was shown by amino acid replacement that changed the protein properties although the replacement did not differ much in amino acid properties; that is, tyrosine and phenylalanine, methionine and valine, and glycine and alanine.

Although adGSTD3-3 and adGSTD4-4 are highly homologous proteins, they display non-identical conformational dynamics. AdGSTD3-3 is soluble in the unfolding solution and the unfolding occurs via four-state pathway ($N_2 \leftrightarrow I_2 \leftrightarrow 2I \leftrightarrow 2U$) while adGSTD4-4 is aggregated in various concentrations of the unfolding solutions. Therefore, the unfolding pathway of adGSTD4-4 is still unknown. The native tertiary structures of adGSTD3-3 and adGSTD4-4 are similar as shown by similar tryptophan environments. However, their N_2 subunit interfaces are not identical as reflected by their different fluorescent dye binding spectra and the electrostatic field and the solvent-exposed cleft at the subunit interface. The subunit interface of adGSTD4-4 showes less polarity and provides a greater amount of fluorescent dye binding sites when compared with adGSTD3-3. This feature may be a factor that influences the different folding dynamics of the two splicing products.

KEY WORDS: GLUTATHIONE S-TRANSFERASES, SUBUNIT INTERFACE, DIMERIC PROTEIN, UNFOLDING PATHWAY

163 pp. ISBN 974-04-5171-3

การศึกษาอิทธิพลของกรดอะมิโนในบริเวณรอยต่อระหว่างโมเลกุลที่ส่งผลกระทบต่อคุณสมบัติของเอนไซม์กลูตาไธโอน เอสทรานสเฟอเรส (CHARACTERIZATION OF THE SUBUNIT INTERFACE RESIDUES AND THEIR EFFECTS ON ENZYME PROPERTIES OF GLUTATHIONE S-TRANSFERASES)

จุฑามาศ ภิรมจิตรผ่อง 4536667 MBMG/M
วท.ม. (อณูพันธุศาสตร์และพันธุวิศวกรรมศาสตร์)
คณะกรรมการควบคุมวิทยานิพนธ์: ALBERT J. KETTERMAN, Ph.D., ชาติชาย กฤตนัย, Ph.D., DUNCAN R. SMITH, Ph.D.

บทคัดย่อ

งานวิจัยนี้เป็นการศึกษาเอนไซม์กลูตาไธโอน เอสทรานสเฟอเรสในกลุ่มเดลตาสองชนิด คือ adGSTD3-3 และ adGSTD4-4 เอนไซม์ทั้งสองนี้ผลิตจากยีนเดียวกันแต่ให้รูปแบบของโปรตีนที่แตกต่างกัน เมื่อเปรียบเทียบลำดับกรดอะมิโนพบว่ามีความเหมือนกัน 68% และ มีความคล้ายคลึงกันในเชิงโครงสร้างสามมิติ แต่เมื่อเปรียบเทียบคุณสมบัติของเอนไซม์ทั้งด้านการเร่งปฏิกิริยาและเสถียรภาพต่อความร้อนพบว่ามีความแตกต่างกัน จากการวิเคราะห์โครงสร้างสามมิติในบริเวณกึ่งกลางระหว่างรอยต่อของโมเลกุลที่ประกอบด้วยสองหน่วยย่อย พบว่าบริเวณดังกล่าวมีกรดอะมิโน 18 ตำแหน่งม้วนพับมาทำปฏิกิริยากัน การศึกษานี้ได้ทำการสร้างโปรตีนกลายพันธุ์โดยการเปลี่ยนแปลงกรดอะมิโนเฉพาะที่จำนวน 12 ชนิดเพื่อศึกษาอิทธิพลของกรดอะมิโนที่ตำแหน่งดังกล่าวต่อคุณสมบัติของเอนไซม์ พบว่าปฏิกิริยาไฟฟ้าทางสถิตย์ระหว่างอาร์จินีน96 และ กลูตาเมต75 และโครงข่ายปฏิกิริยาไอออนิกระหว่างกลูตาเมต116 และอาร์จีนีน134 ที่บริเวณรอยต่อระหว่างโมเลกุลของ adGSTD4-4 มีความสำคัญต่อการเร่งปฏิกิริยาและการคงสภาพโครงสร้างของโปรตีน นอกจากนี้ยังพบว่าความแตกต่างกันของกรดอะมิโนสามตำแหน่งที่มีคุณสมบัติไม่ชอบน้ำ(hydrophobic) ตรงบริเวณกึ่งกลางของรอยต่อได้แก่ ไทโรซีน98 เมทไธโอนีน101 และไกลซีน102 ของ adGSTD3-3 และ ฟีนิลอะลานีน104 เวลีน107 และ อะลานีน108 ของ adGSTD4-4 มีบทบาทต่อคุณสมบัติที่จำเพาะเจาะจงของโปรตีนทั้งสองชนิด ดังจะเห็นได้จากการที่คุณสมบัติของโปรตีนกลายพันธุ์ทั้ง 8 ชนิดเปลี่ยนไปทั้งด้านการเร่งปฏิกริยาและโครงสร้างของโปรตีนเมื่อเปรียบเทียบกับโปรตีนต้นแบบ

จากการศึกษาขั้นตอนการคลายตัว (unfolding pathway) ของเอนไซม์ทั้งสองรูปแบบ พบว่าการเปลี่ยนแปลงโครงสร้างทางจลศาสตร์ของเอนไซม์ทั้งสองชนิดมีความแตกต่างกัน โดย adGSTD3-3 สามารถละลายได้ในสารละลาย GuHCl และคลายตัวโดยผ่านกระบวนการสี่ขั้นตอน ($N_2 \leftrightarrow I_2 \leftrightarrow 2I \leftrightarrow 2U$) ในขณะที่ adGSTD4-4 ตกตะกอนในสารละลายดังกล่าว ทำให้ไม่สามารถวิเคราะห์กระบวนการคลายตัวได้

163 หน้า ISBN 974-04-5171-3

.

CONTENTS

CONTENTS (continued)

CONTENTS (continued)

CONTENTS (continued)

CONTENTS (continued)

CONTENTS (continued)

LIST OF TABLES

LIST OF TABLES (continued)

LIST OF TABLES (continued)

LIST OF FIGURES

LIST OF FIGURES (continued)

LIST OF FIGURES (continued)

LIST OF FIGURES (continued)

LIST OF FIGURES (continued)

LIST OF ABBREVIATIONS

ANS	8-anilino-1-naphthalenesulfonate
CD	Circular dichroism
CDNB	1-chloro-2,4-dinitrobenzene
CTAB	Cetyltrimethyltrichloroethane
DCNB	1, 2–dichloro-4-nitrobenzene
GSH	Glutathione
GSTs	Glutathione S-transferases
IPTG	Isopropyl-β-D-thiogalactopyranoside
LB	Luria-Bertani medium
TCA	Trichloroacetic acid
TEMED	N,N,N',N'tetramethylene-ethylenediamine

CHAPTER 1
INTRODUCTION

1.1 Glutathione S-Transferases (GSTs)

Glutathione S-transferases (EC 2.5.1.18), first described in 1961(1), are a supergene family of multifunctional enzymes which are widely distributed in nature and found in most aerobic eukaryotes and prokaryotes. There are both membrane-bound and soluble GSTs. Microsomal glutathione transferase (MGST1) is a homotrimeric protein that is present at high concentrations both in the endoplasmic reticulum and the mitochondria outer membrane(2). The soluble or cytosolic GSTs are stable dimeric enzymes that occur in all organisms. Of these two GSTs, the cytosolic form has been most extensively investigated.

The dimeric cytosolic GSTs catalyze a broad range of substrates and play an important role in detoxification of xenobiotic compounds (e.g. drugs, herbicides and insecticides) (3). GSTs catalyze the S-conjugation between the thiol group of glutathione (GSH, γ-glutamyl-L-cysteinyl-glycine) and the electrophilic center of a range of endogenous hydrophobic molecules. A simplified enzyme catalysis scheme for GSTs first involves GSH substrate binding to the active site, then GSH ionization to form a nucleophilic thiolate anion (GS^-), followed by substrate conjugation, product formation and finally product release (4-7). The GS-xenobiotic conjugate is too hydrophilic to diffuse freely from the cell, and must be pumped out actively by a transmembrane ATPase such as the GS-R pump. This results in the unidirectional excretion of the xenobiotic from the cell, since the hydrophilic GSH moiety prevents re-diffusion across the plasma membrane.

$$\underset{\text{Glutathione}}{GS\text{-}H} + \underset{\substack{\text{Xenobiotic compounds}\\(R = \text{electrophilic group})}}{R\text{-}X} \xrightarrow{GST} \underset{\substack{\text{Products}\\(\text{less reactive and more soluble})}}{GS\text{-}R} + X\text{-}H$$

GSTs display marked differences in their abilities to conjugate glutathione with various electrophiles. Some substrates are valuable tools for the characterization and identification of the different forms of GSTs. The important substrate for GST is 1-chloro-2,4-dinitrobenzene (CDNB) (**Figure 1.1: A**). Class pi GSTs are highly active with ethacrynic acid ([2,3-dichloro-4-(2-methylenebutyryl)-phenoxy]acetic acid) (**Figure 1.1: B**). Class mu GSTs display comparatively high activity with 1,2-dichloro-4-nitrobenezene (DCNB) and 4-nitrobenzyl chloride (4-NBC) (**Figure 1.1: C, D**). Human theta class GSTs have been shown to have activity toward 4-nitrophenethyl bromide (4-NPB) (**Figure 1.1: E**).

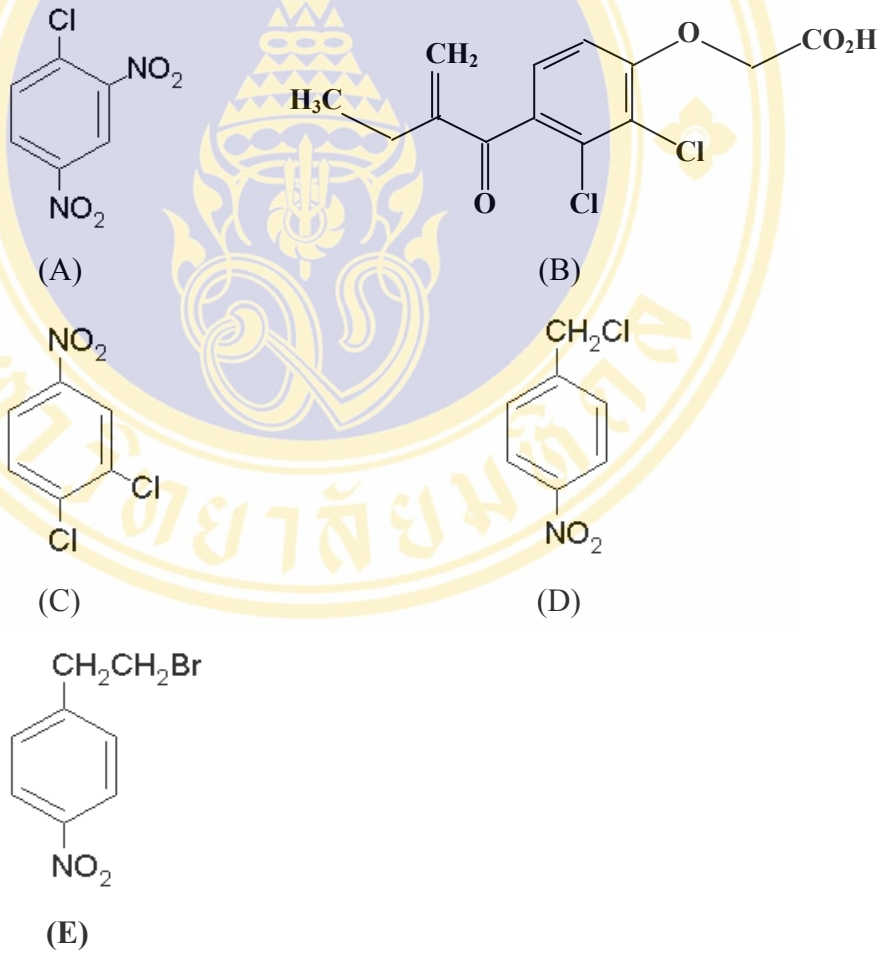

Figure 1.1 The chemical structures of GSTs substrates

(A) 1-chloro-2,4-dinitrobenzene (CDNB); (B) ethacrynic acid (EA) (C) 1,2-dichloro-4-nitrobenezene (DCNB); (D) p-nitrobenzyl chloride (PNBC); (E) p-nitrophenethyl bromide (PNPB)

1.2 The Functions of GSTs

The conjugation between GSH and electrophiles always yield a conjugate that is less reactive and more soluble than the parental compound therefore the actions of GSTs generally result in detoxification. The enzymes can protect cells against chemical-induced toxicity and stress as a mechanisms of resistance e.g. resistance of insects to insecticides (8), resistance of parasites to drug treatment (9), resistance of plants to herbicides (10), resistance of tumor cells to anticancer drugs (11) and bacterial resistance to antibiotics including herbicides (12). The molecular basis of GST-based resistance was thought to be involved with up-regulation of one or more GSTs in resistant insects that seems to be due to a trans-acting regulator (13).

GSTs also show other biological functions which can be divided into two categories; enzymatic functions and non-enzymatic functions.

1.2.1 Enzymatic functions

Several GSTs have been show to have secondary catalytic activities including a peroxidase activity with lipid peroxidation products such as 4-hydroxynon-2-enal (HNE) in hGSTA4, formerly GST A4-4, (14) and tobacco GST (15) and steroid isomerization by catalyzing the isomerization of Δ^5-androstene-3, 17, dione (AD) and Δ^5-pregnene-3, 20-dione, precursors of testosterone and progesterone respectively (16;17) in GST alpha class. Glutathione also functions by acting as a cofactor for the enzyme. It was found that hGSTA3, formerly GST A3-3, was the most efficient enzyme that can catalyze the isomerization reaction (18). HGSTP1 can interact with physiological nitric oxide (NO) carriers such as S-nitrosoglutathione (GSNO) and dinitrosyl-diglutathionyl iron complex (DNDGIC). In the absence of GSH, GSNO causes rapid and stable S-nitrosylation of both Cys47 and Cys101 residues. The nitrosylation of Cys47 decreases the affinity toward GSH approximately 10-fold therefore it acts as a NO protein carrier without detriment to its detoxicating activity. When GSH is in excess, DNDGIC can bind with the G-site of the enzyme. The GSH molecule is stabilized by the interactions of the G-site with its natural substance; the NO moieties are stabilized by van der Waal's and polar interactions. When the excess GSH is removed, one of the two GSH molecules or the bound DNDGIC is lost from the complex, and Tyr-7 and enzyme-bound GSH could be

involved in the coordination of the iron atom. Binding of DNDGIC triggers a conformational change in the vacant subunit, which lowers its affinity for the complex (19).

1.2.2 Non-enzymatic functions

Apart from their enzymatic roles, GSTs have the ability to bind many ligands such as hemin, bilirubin, bile salts, steroids, thyroid hormones, fatty acids and drugs. In pi class GST, the ligandin-binding site was studied using X-ray crystallography and it was found that ligandin occupies part of one of the substrate-binding sites (20). In hGSTA1, formerly, hGST A1-1, the ligandin binding site remains unclear since the modification of Cys 112 which blocks the intersubunit cleft did not affect the binding of non-substrate ligands. Therefore the ligandin binding was proposed to occur in the hydrophobic substrate site (21). In contrast, the ligand binding site was also reported at the dimer interface in hGSTA1. This was shown by binding of the non-substrate ligand 8-aniline-1-naphthalene sulphonate (ANS) in Phe51Ser mutant, this residue is located in a loop connecting α2 and β3 (22). Recently identified functions of GSTs include roles in signal transduction. GST pi class can function as a Jun N-terminal kinase (JNK) inhibitor (23). In stress conditions, UV irradiation or H_2O_2 treatment, GST pi oligomerizes and dissociates from the GSTp-JNK complex. The interaction between hGSTP1 and JNK was studied and found that the GST interacts with the C-terminus of JNK (residues 200-424) (24). Moreover, GST mu was reported to inhibit apoptosis signal-regulating kinase 1 (ASK1) (25) the upstream activator of JNK. The interaction was formed between the C-terminal portion of mGSTM1 and the N-terminal region of ASK1. Ion channel modulation was studied with Omega class GST (hGSTO1) that revealed significant sequence similarity with members of the chloride intracellular channel (CLIC) family of proteins (26). CLIC1 is a member of the highly conserved class of chloride ion channels. The protein is monomeric and structurally homologous to the GST superfamily (27). HGSTO1 reduced cardiac RyR2 activity approximately 50% but skeletal muscle RyR1 activity was potentiated. The results suggested that RyR2 has two binding sites for hGSTO1. When the enzyme binds to one site, it activates the channel whereas the enzyme binds to the second site it inhibits the channel.

1.3 GST Structure and Dimerization

Many forms of cytosolic GST have been reported and there have been many attempts to classify the different forms of GSTs. At present there are 7 classes of mammalian GSTs; alpha, mu, pi, theta, kappa, omega and zeta, grouped on the basis of extensively characterized physiochemical properties, immunological properties and amino acid sequence identity (28-30). A number of GSTs in non-mammalian sources have also been reported e.g. sigma in cephalopods and arthropods, zeta and epsilon in plant, beta in bacteria, fungal GSTs, phi and tau classes in plant, delta class in insect and helminth GSTs (31). GSTs within the same class normally demonstrated more than 40% amino acid identity whereas GSTs between classes share less than 30% identity (32).

Three dimensional structures of several cytosolic GSTs have been elucidated and these reveal a conserved overall folding topology (**Figure 1.2**). Each subunit comprises two structurally distinct domains, N-terminal and C-terminal domains respectively. The N-terminal domain or domain I constituting roughly one-third of the protein is an α/β-structure containing most of the residues involved in the glutathione-binding site (G-site). The C-terminal domain or domain II constituting roughly two-thirds of the protein is all α-helical with a unique protein fold. This domain provides a binding site of the hydrophobic substrates (4) called H-site. The xenobiotic moiety of the product is located in the crevice between the two domains and makes a number of contacts with residues in domain II, particularly along the face of the α4-helix and the C-terminal tail. Thus, domain II appears to provide structural elements for the recognition of the substrates and helps to define the substrate selectivities of the various isozymes (33). In spite of similar overall topologies, the structures differ considerably with respect to a number of details. The most notable topological differences include the mu-loop and the α9-helix of the class mu and alpha, respectively (34;35). The features of subunit-subunit recognition also differ between enzyme families (4).

The dimerization of the GSTs not only allow for the construction of a fully functional active site, part of which is situated near the subunit interface, but also contributes to the stabilization of the subunit tertiary structure. Homodimers, identical subunits, and heterodimers, non-identical subunits, within classes can be formed by a

good geometric complementary which is essential for specific molecular recognition. Therefore, no heterodimers between different classes have been described.

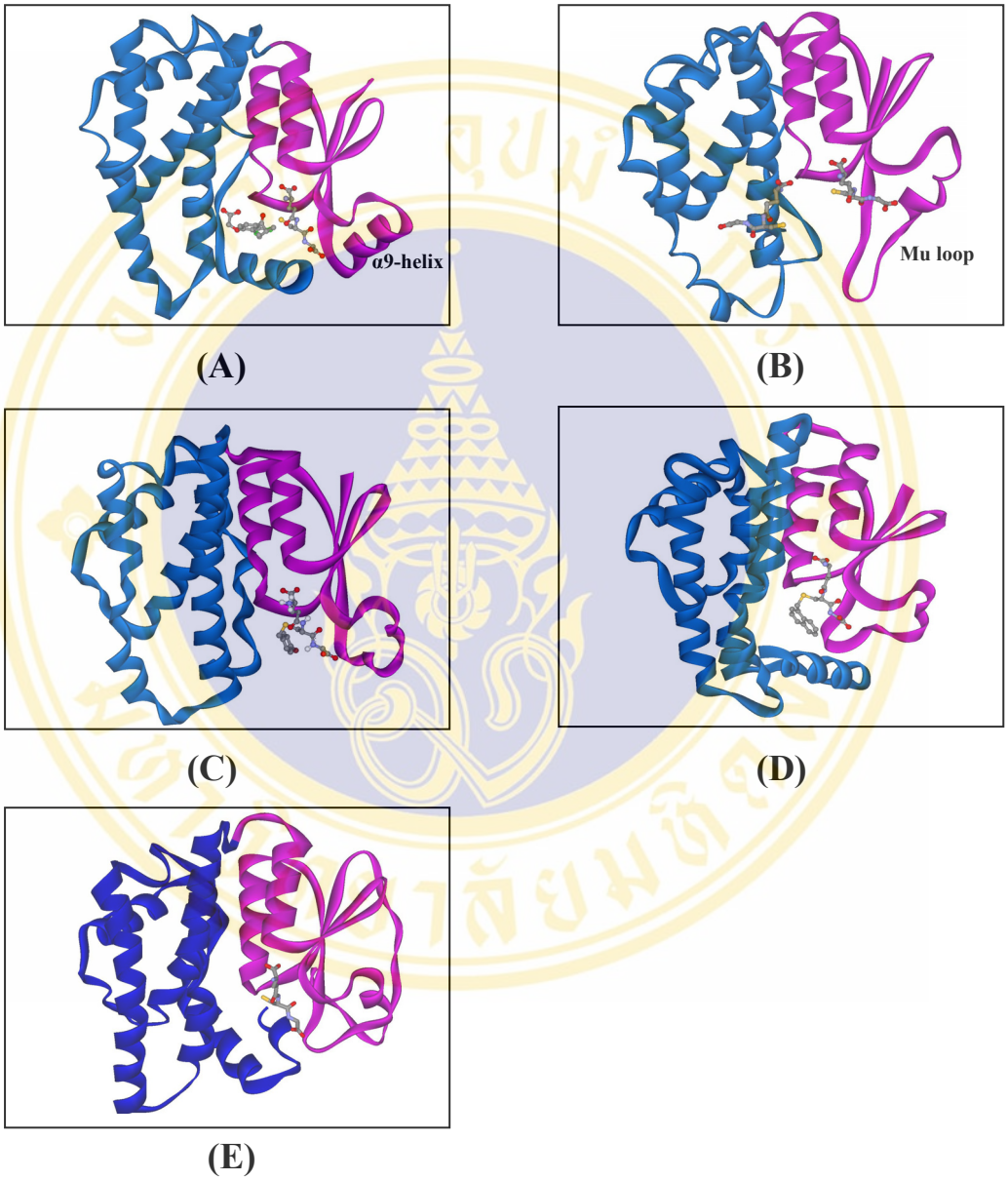

Figure 1.2 GSTs crystal structures

GST domains are distinguished by different colors (domain I is pink, domain II is blue). The ligands are shown in ball and stick form, identifying the location of the active site. (A) alpha-class human GST A1 (35), (B) mu-class human GST M2 (36), (C) pi-class human GST P1 (34), (D) theta-class human GST T2 (37) and (E) omega-class human GST O1 (38).

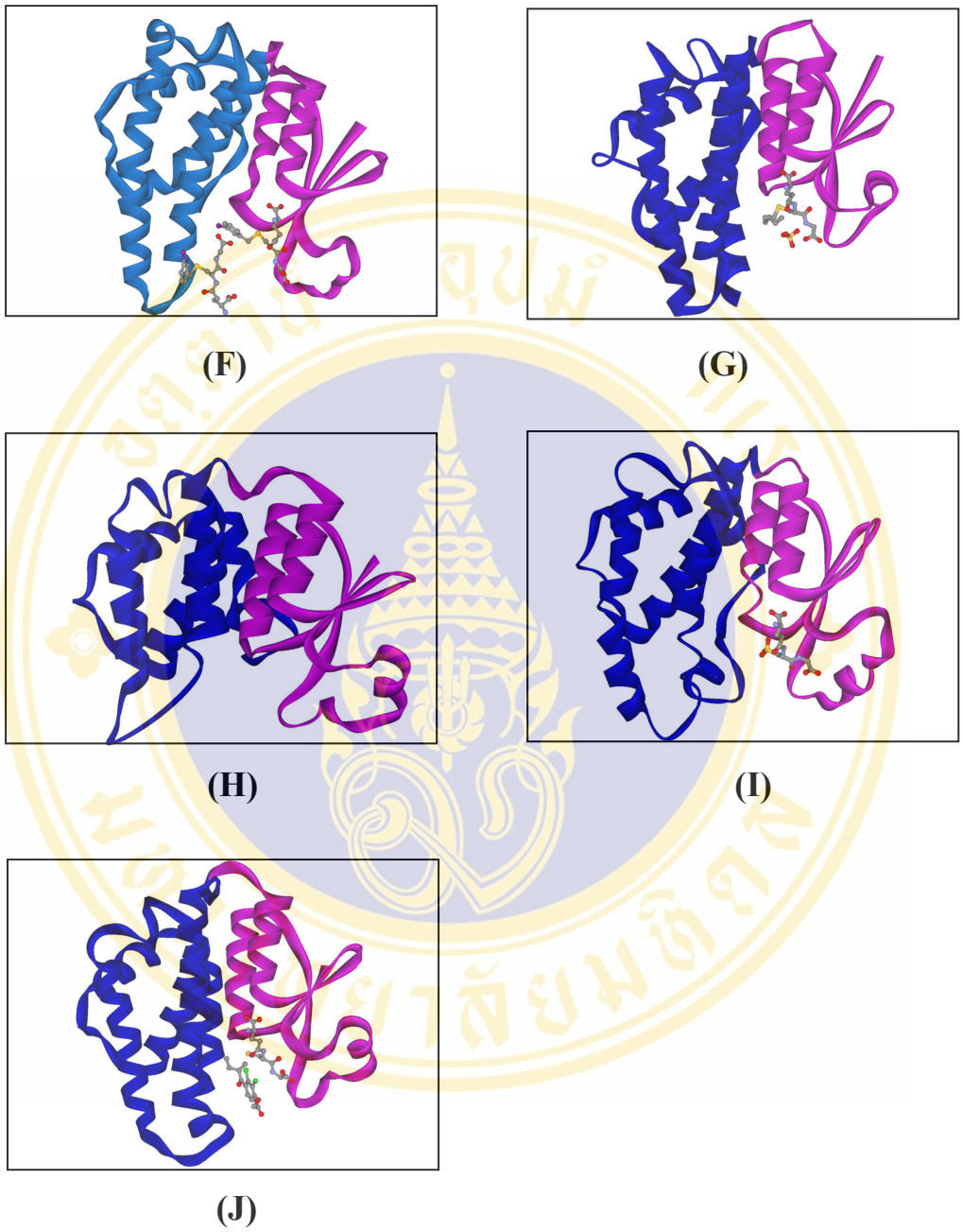

Figure 1.2 GSTs crystal structures (continue)

GST domains are distinguished by different colors (domain I is pink, domain II is blue). The ligands are shown in ball-and-stick form, identifying the location of the active site. (F) Sigma-class squid GST (39), (G) Tau-class wheat GST (40), (H) Zeta class Arabidopsis GST, (I) Mu-class *Schistosoma japonicum GST* (41) and (J) Delta-class insect GST (33).

1.4 GST Subunit Interface

Although tertiary structures of all classes of GSTs are similar, dimerization is highly specific and occurs only between subunits within the same class. It is assumed that the difference in the structure of the subunit interface among the various GSTs is the basis for this discrimination. The principal intersubunit interactions occur between domain I of one subunit and domain II of the other subunit. Recently, the structural features at the dimer interface of the GSTs suggest at least two major areas of interactions, a hydrophobic ball-and-socket and electrostatic interactions at the subunit interface.

1.4.1 The hydrophobic "ball-and-socket" interactions.

Inspection of the structural features at the subunit interface of the different GST classes indicates the existence of two major types of the interfaces in this area; the α/μ/π/Sj26 subunit type and the σ/θ subunit type. The former interface type is curved, hydrophobic, and involves a prominent hydrophobic lock-and-key motif **(Figure 1.3)**. However, the interface of the latter group is flatter, more hydrophilic, and lacks the lock-and-key motif (42) **(Figure 1.4)**.

1.4.1.1 The α/μ/π/Sj26 subunit type

Comparison of the mammalian alpha, mu and pi structures demonstrated the similarities in the types of interaction occurring at the intersubunit interface **(Figure 1.3)**. These are dominated by hydrophobic interaction between residues from domain 1 of one subunit and domain 2 of the other. An aromatic residue (Phe-52 in alpha, Phe-56 in mu and Tyr-49 in pi) acts as a ball protruding from the loop before β3 that fits into a hydrophobic socket provided by residues contributed from helices 4 and 5 of the other subunit (34;35;43). After generation of several mutants at this equivalent position to diminish conformational stability, the results suggest that this residue is important for dimer stability and forming the proper active site pocket (44). Moreover, in zeta class GST, the subunit interface is also dominated by hydrophobic interactions. Residue Met-56, instead of the aromatic residue like mammalian classes, acts as a ball and packs into a hydrophobic socket of the other monomer to stabilize the enzyme structure.

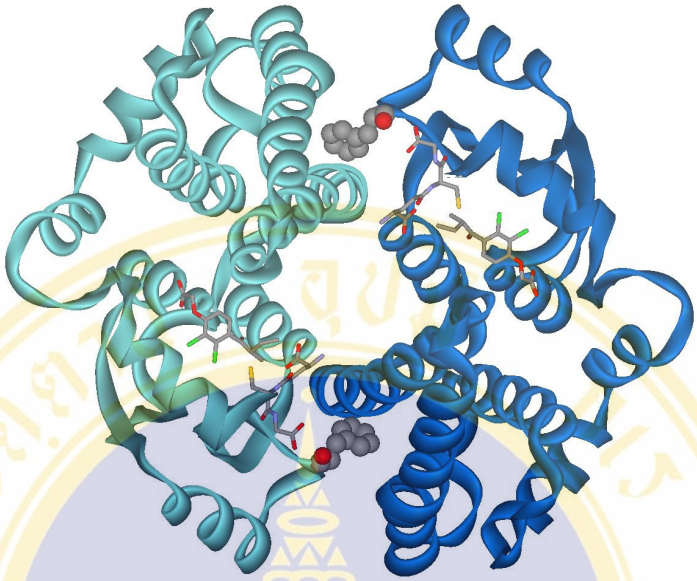

Figure 1.3 Ribbon representation of the α/μ/π/Sj26 subunit type viewed down the 2-fold axis. The ball residues represent the location of the hydrophobic ball-and-socket interaction are shown as CPK models. The ligands bound in the active site area are shown as stick models (35).

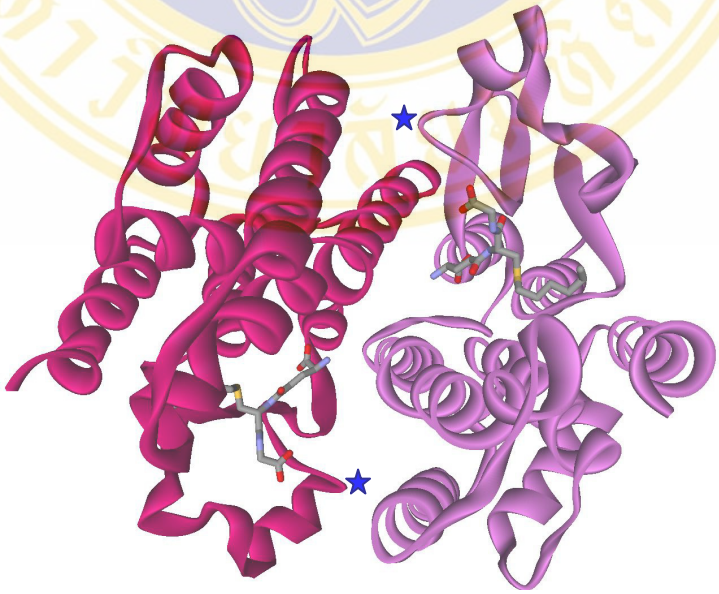

Figure 1.4 Ribbon representation of the σ/θ subunit type viewed down the 2-fold axis. The ball which is absent in this type is shown as by stars and the active site ligands are represented as stick models (39).

1.4.1.2 The σ/θ subunit type

In this subunit type, there is no ball-and-socket motif as found in the previous type. This is due to the fact that the key (Phe) residue and the loop on which it is located are absent. The dimer interface of the squid sigma enzyme is more hydrophilic than others. The enzyme dimer has the canonical GST fold with GSH ordered in only one of the two binding sites. For the H-site, helix 6 demonstrated a novel topography resulting in a largely flat and without a prominent hydrophobic-binding pocket making it high selectivity for lipid peroxidation product (45). In insect delta class, the dimer interface features extensive hydrophobic and hydrogen bonding interaction. Although this GST class does not have the ball-and-socket motif, it shows a hydrophobic interaction at the middle of subunit interface between two aromatic residues, phenylalanine, from both subunits instead. The directions of both phenylalanine rings are parallel like a clasp (**Figure 1.5**).

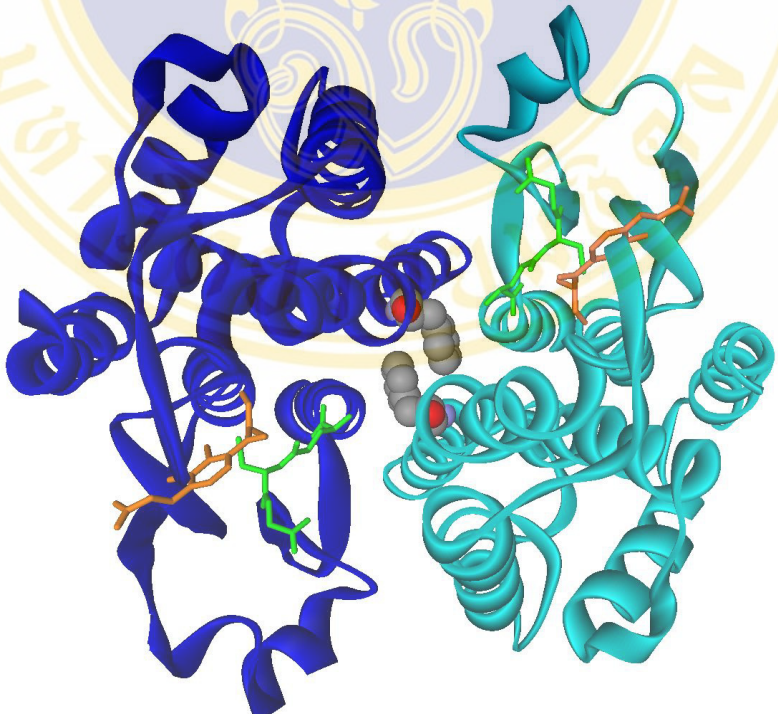

Figure 1.5 Ribbon representation of the clasps at the insect delta class subunit interface. The clasps, phenylalanine, were represented as CPK models. The active site ligands are represented in as stick forms, green are GSH and orange are EA (33).

1.4.2 The electrostatic interactions

In this region, the electrostatic interactions are formed by positive charge residues, arginine, and negative charge residues, glutamate from both subunits. The quanido group (-C-$(NH_2)_2$) of arginine forms a salt link to the carboxylate group (-C00H) of glutamate of both the same subunit as well as the opposite subunit. The locations of the interactions of the different GST classes indicate the existence of two major areas of the interface; the ionic interactions at the edge of the subunit interface and the interactions at the top of subunit interface. The former interface area is conserved among the three human classes, alpha, pi and mu **(Figure 1.6 A)** (46). However, the interface of the latter area is observed in delta, sigma and theta classes (**Figure 1.6 B**).

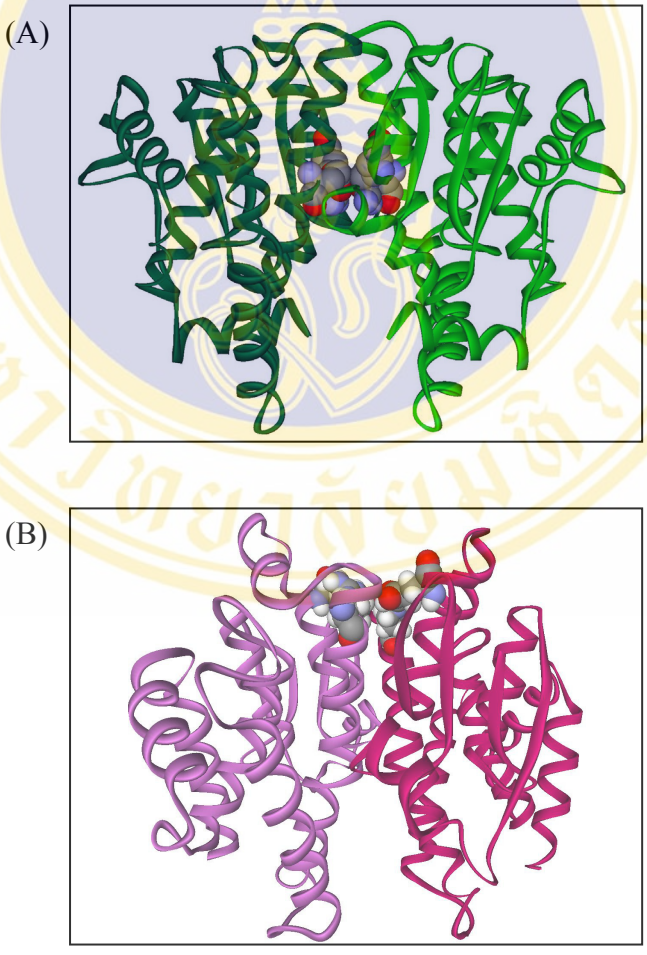

Figure 1.6 The electrostatic interactions at subunit interface.

Arginines and Glutamates represented by CPK models. The difference color of the ribbon illustrates the difference subunit. (A) The ionic interactions at the edge of the subunit interface and (B) The interactions at the top of subunit interface.

1.4.2.1 The electrostatic interaction at the edge of the subunit interface

In alpha class, these interactions are performed by Arg 69 and Glu 97. The directions of both arginine side chains are parallel with 3.77 Å and 3.76 Å between the quanido groups. Moreover, they form a salt-bridge with the glutamate residues from both subunits (**Figure 1.7).** After mutating these residues to evaluate the importance of each at the subunit interface and to determine if monomeric enzymes could be generated. The results show that Arg 69 is the major determinant of the dimer formation because the mutant appeared to be a monomer (46). Moreover, when the heterodimers of wild type and single mutants of these positions, Arg69Gln, Arg69Glu and Glu97Gln, were generated to study whether the subunits are interactive or independent, the results demonstrated that two heterodimer, wild type/Arg69Glu and wild type/Glu97Gln, displayed specific activities much lower than that expected for independent active sites due to new close repulsive interactions and the low activity of one subunit is communicated to the neighboring subunit. In contrast, the other mutant, Arg69Gln, showed specific activity similar to that expected for an independent active site. This is because the closest interaction is not repulsive or occurs over a much longer distance and the subunits act independently.

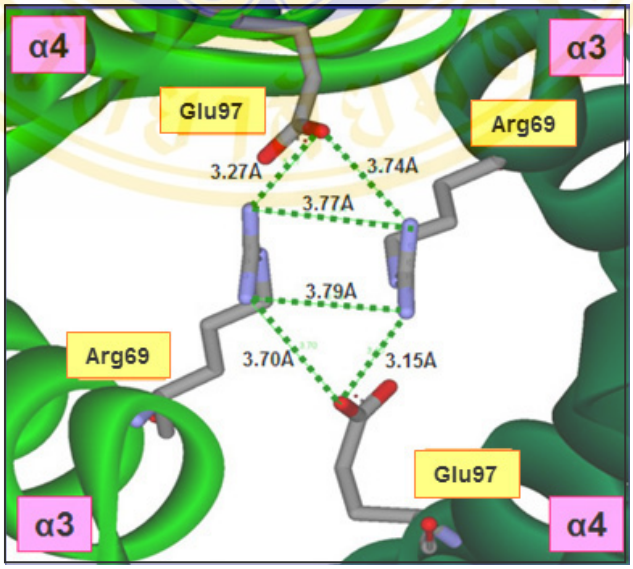

Figure 1.7 The electrostatic interactions at the edge of subunit interface of human alpha class GST (35). Arg 69 and Glu 97 represented by stick models. The different colors of the ribbon show the different subunits.

1.4.2.2 The electrostatic interactions at the top of subunit interface

The charge-charge interactions at this area appear in the insect delta class (33), squid sigma class (39) and mamalian theta class (37). These interactions are more planar than the previous area and the directions of the arginines and the glutamates form a square (**Figure 1.8**). Until now, there are no mutants generated to study the affect of these interactions in any of the three classes.

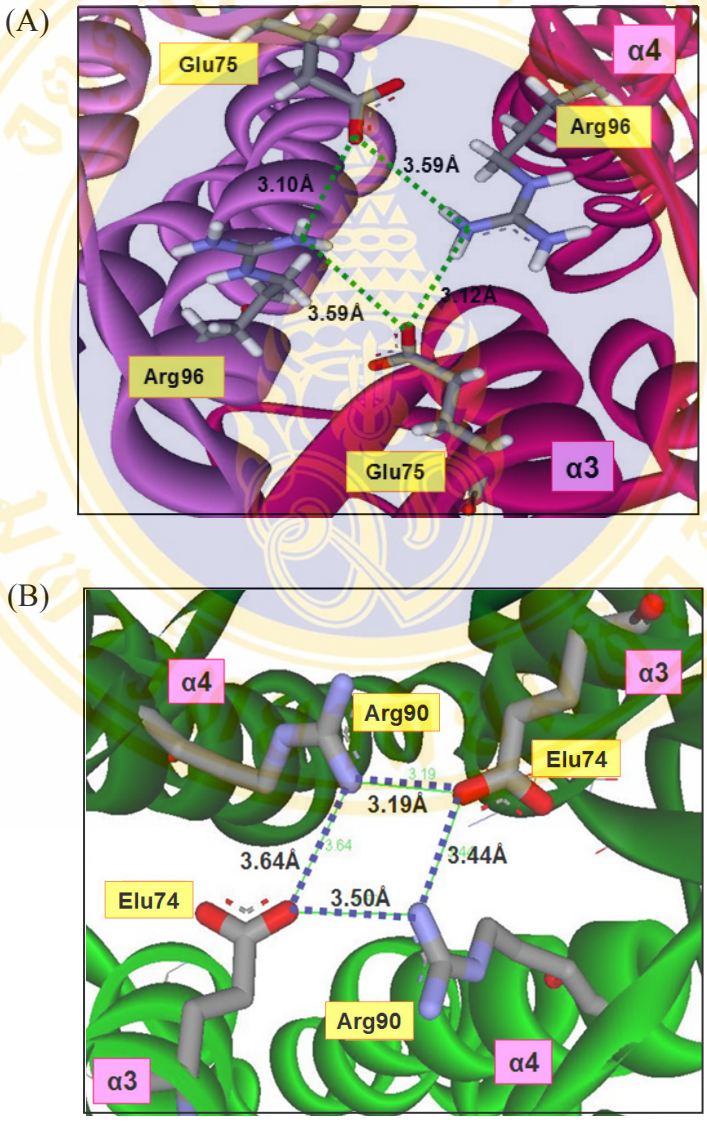

Figure 1.8 The electrostatic interactions at the top of subunit interface.
Arginines and glutamates represented by stick models. The different colors of the ribbon show the different subunits. (A) insect delta class (33), and (B) squid sigma class (39).

1.5 GST Unfolding Pathway

Equilibrium denaturation studies of proteins provide valuable information on the autonomous folding of domains, the relationship of folding and oligomerization process, and determination of the thermodynamic significance of subunit interface interactions. Numerous investigations over the last 40 years have focused on the folding and structural determinants that govern how a polypeptide adopts its native structure. Most of our knowledge on protein folding derives from studies on small monomeric proteins (47;48). However, the majority of native proteins are more complex structures, composed of several subunits that in turn consist of domains. The extrapolation of results obtained in the study of small proteins to larger ones is not always appropriate, and it is therefore important to investigate proteins composed of more than one subunit (49). GSTs provide a useful model for studying stability and folding within a well-characterized super family of dimeric proteins with conserved overall structures and diverse functional properties. GSTs have been the subject of recent studies on protein folding (50-53).

Equilibrium unfolding studies in alpha, pi and mu GSTS demonstrate subunit interaction involves a prominent hydrophobic lock-and-key motif. The results show that alpha and pi classes unfold via a 2 state unfolding pathway with no stable intermediate (54;55;55). Whereas the GST Mu unfolds via a 3 state unfolding pathway with one stable monomeric intermediate (42;56). This is because the mu class has hydrophilic residues, Arg77, which are conserved among this class at the middle of interface (**Figure 1.9**) which help to stabilize the tertiary and quaternary structure of the proteins (57;58).

For the unfolding pathway investigation of the second type of subunit interface, GST sigma which not only lacks a lock-and-key motif at the subunit interface, it also has electrostatic interactions. These features make this class interesting to study in the terms of their functions and stability. The sigma class was shown to unfold via a 4 state pathway with two stable intermediates; dimeric and monomeric intermediates, respectively (49;59). These findings suggest that the dimeric quaternary and subunit interactions are essential for stability of both tertiary and secondary structures of the individual subunit.

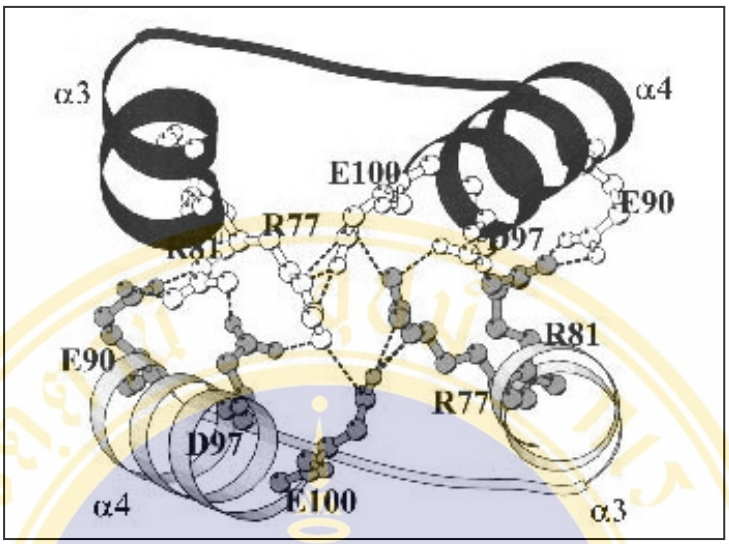

Figure 1.9 Ball and stick representation of the amino acid residues in the charge cluster at the subunit interface of rat mu class GST.

Normally there are many probes to monitor structural changes during the unfolding/refolding of the GSTs. The first probe is the enzyme activity. It provides an indication of the conformation of domain I and the subunit interface due to the involvement of some residues from the adjacent subunit in forming a fully functional active site. The second technique is intrinsic tryptophan fluorescence spectroscopy. Each subunit of GSTs has one or two tryptophan residues which are located in close proximity to the active site and are involved in the subunit interface, as well as, sequestering the substrate glutathione. This features make it a sensitive fluorescence probe to monitor conformational changes at/near the active site and the inter-subunit area (see details in chapter 3.5.3). The third probe is the binding of the amphipathic dye, 8-anilino-1-naphthalenesulfonate, ANS. This technique is used to determine the exposure of hydrophobic regions and formation of compact hydrophobic states during unfolding. For example, the enhanced ANS binding and the blue shift in the emission maximum during the unfolding process demonstrate that the binding environment becomes more hydrophobic (see details in chapter 3.5.4). The fourth probe is far UV circular dichroism (CD) which is sensitive to secondary structure of proteins and was used to investigate the folded CD spectrum of enzymes in unfolding solution to monitor the disruption of protein structure (see details in chapter 6.4). The last

technique is size-exclusion chromatography. This method can be employed to study protein unfolding due to its ability to resolve changes in the hydrodynamic properties of structures along an unfolding pathway and to detect the presence of intermediate states provided they are kinetically stable within the time scale of the chromatographic run.

1.6 Comparison Studies of the GSTs variant forms.

The molecular basis for catalytic differences between closely related GSTs from the same class which have nucleotide and amino acid sequence similarities was investigated. In GST Pi class, the two proteins encoded by two genes, GSTp-1 and GSTp-2, exhibit profoundly different catalytic activities (60). The proteins share 97% sequence identity which differ in only six amino acids. This difference was concentrated in just two secondary structural elements located at the bottom and the inner wall of the active site. To establish the basis for the difference between these highly similar proteins, mutants were generated where specific amino acids were exchanged. Kinetic analysis of the wild type and mutant enzymes revealed that the amino acid differences occurring at positions 10 (Val/Ser), 11 (Arg/Pro) and 104 (Val/Gly) were responsible for the reduced enzymatic activity of GSTp-2. In GST Alpha class, the two proteins, which differ in their primary structures by 10 amino acids, mGSTA1-1 and mGSTA2-2, also showed differences in catalytic efficiency. Chimeric enzymes of these two showed that position 207 (Met/Leu) and 221(Ile/Phe) are critical for high activity (61). Moreover, in an other mammalian GST, Mu class, there are two proteins which share a 78% sequence identity but display differences in stability, rGSTM1-1 and rGSTM2-2. M1-1 is more stable at the secondary and tertiary structure levels, whereas its quaternary structure is less stable. The chimeric subunit variants M(12), which has domain I of M1-1 and domain II of M2-2, and its complement M(21), demonstrated that although the equilibrium unfolding mechanism is not altered, domain exchange impacts significantly on the conformational stability of the native dimers and monomeric intermediates. Therefore interactions involving Arg77, topologically conserved in GSTs, appear to play an important role in the stability of both dimeric and monomeric intermediates (58).

1.7 Insect GSTS and *Anopheles Dirus* GST

The insect GSTs are of interest because of their potential role in insecticide resistance (62). The resistance to pesticides in insects has been shown to correlate with elevated levels of GST activity (63-66). Although not as well characterized as the mammalian GSTs, insect GSTs have been identified and reported in multiple forms from house fly (67;68), gress grub (69), *Drosophila melanogaster (70;71)*, and mosquito (33;65;72-78). Previously, insect GSTs have been divided into two broad classes; class I (Delta class) and class II, based on their amino acid sequence homology (> 40% identity to other members within the class) and immunological properties (79-81). Several class I sequences have been studied while only a few class II sequences have been reported. The genomic DNA of class I alternative spicing gene organization is highly conserved in *Anopheles dirus* and *Anopheles gambiae*. The 5' terminus is highly conserved, however the 3' terminus involved in the determination of substrate specificity is variable and specific for the individual GSTs.

The *Anopheles dirus* mosquito is an important malaria vector in South East Asia. From an *An. dirus* genomic library, a 7.5 kb fragment containing the adgst1AS1 gene (*Anopheles dirus* alternatively spliced GST gene) was identified (82). This gene contains six exons that encodes four Delta class GSTs (insect class I), adGSTD1-1, 2-2, 3-3 and 4-4, which possess 61-77% amino acid identity compared among themselves (**Figures 1.10**).

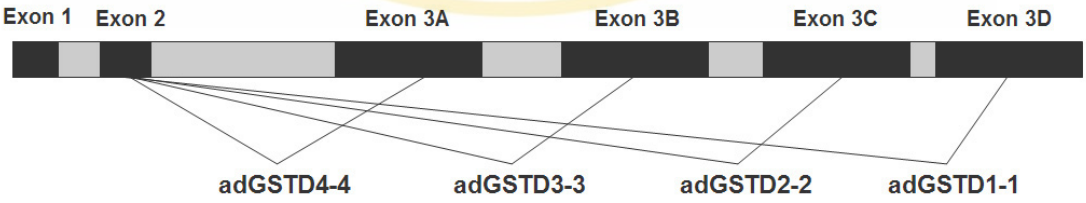

Figure 1.10 AdGST1AS1 gene organization. The double number of the enzyme; 1-1, 2-2, 3-3 and 4-4, represent homodimerization.

These four GSTs share an untranslated exon 1 and a translated exon 2 coding for 45 amino acids at the N-terminus but vary between four different exon 3 sequences (exon 3A-3D). The arrangement of each exon is similar to aggst1α gene

from *An. gambiae,* a malaria vector in Africa, with approximately 79% nucleotide identity. Although the four splice products were encoded from the same gene, the enzymes possess distinct enzyme kinetic properties for substrates, inhibitors including insecticides as well as stability (77;83).

1.8 AdGSTD3-3 and adGSTD4-4

AdGSTD3-3 and adGSTD4-4 are of interest because their crystal structures, tools to guide the structure-function relationship study, are available. These two isozymes have 68% amino acid identity and are very similar when tertiary structures are aligned (**Figure 1.11**).

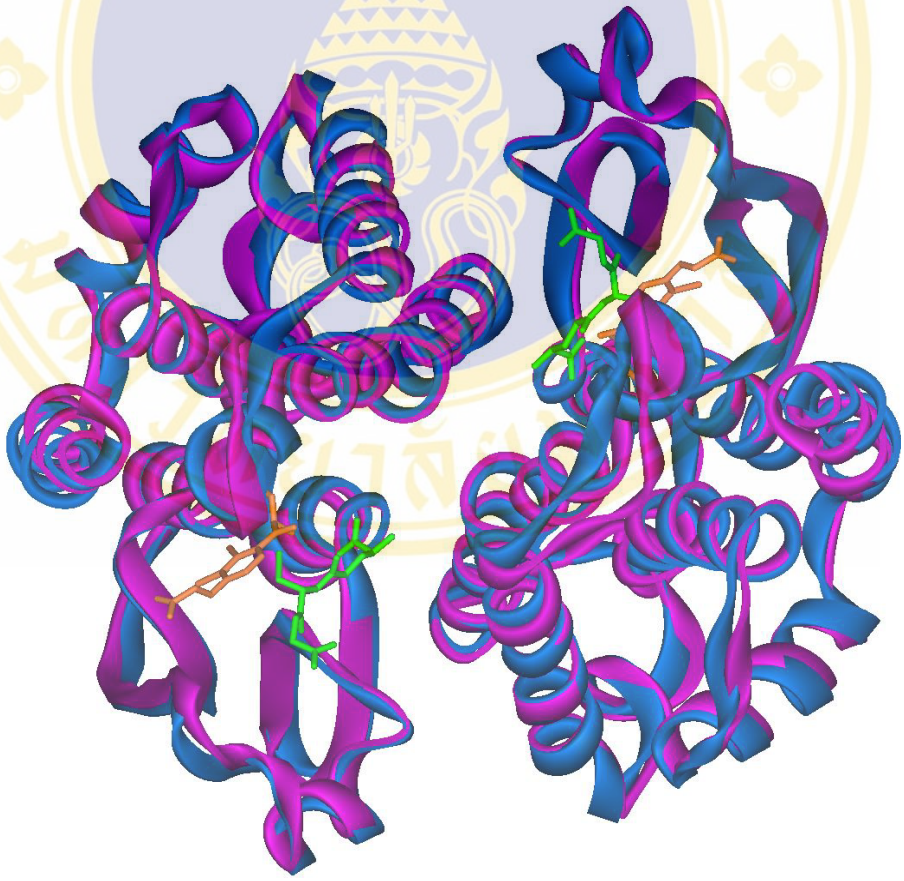

Figure 1.11 Tertiary structure alignment of adGSTD3-3 (blue) and adGSTD4-4 (pink) (33). The sticks represent the substrates, the green is GSH and the orange is EA.

Although the tertiary structures of both isozymes are similar, adGSTD3-3 shows 2-fold more activity but 7-fold less in stability when compared with adGSTD4-4 (83-85). Moreover these splicing products also showed different effects on JNK activity (unpublished result). Therefore to understand the functional diversity of the GST splice forms, site-direct mutagenesis and enzymatic characterization were performed. Among 77 different amino acid residues in these two isozymes, the amino acid at an equivalent position, Met101 of adGSTD3-3 and Val107 of adGSTD4-4, was selected. This equivalent position is the one of nine residues at the subunit interface where the same residue position from both subunits fold to interact with each other. Moreover this equivalent position is not only located at the middle of the subunit interface which may have a role in dimerization (**Figure 1.12 A**), it is also involved in the active site (**Figure 1.12 B**). After being changed to the same amino acid, the mutants showed differing results. The adGSTD3-3 mutant, Met101Ala, dramatically affected to the catalytic property while adGSTD4-4 mutant, Val107Ala, had no effect. However, in a physical property study of the thermal stability, the adGSTD4-4 mutant demonstrated a striking effect with an increase of approximately 17-fold in the half-life when compared to the wild type while the adGSTD3-3 mutant showed only a slight effect (**Table 1.1**). Based upon this data a further study of the subunit interface residues of both isozymes was performed.

Table 1.1 The specific activity and half-life of the adGSTD3-3 and adGSTD4-4 wild types and the alanine mutants at the equivalent position.

Enzymes	Specific activity (mmol/min/mg)	Half-life (min)
adGSTD3-Wild type	98.34 ± 0.47	2.71 ± 0.35
adGSTD3-Met101Ala	158.75 ± 3.03	4.13 ± 0.41
adGSTD4-Wild type	53.95 ± 1.30	14.01 ± 1.70
adGSTD4-Val107Ala	51.19 ± 1.68	254.43 ± 9.85

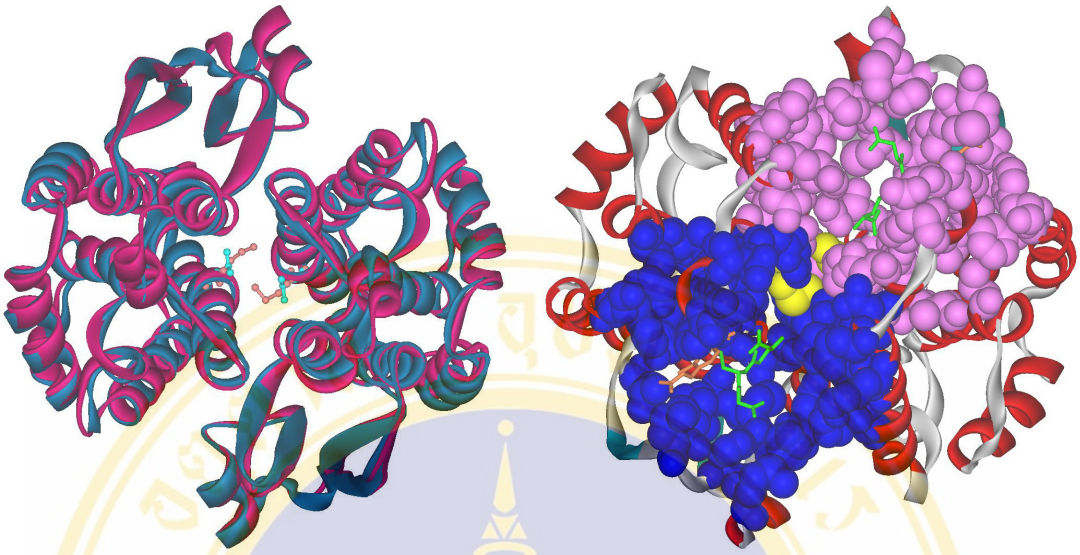

(A) (B)

Figure 1.12 Tertiary structures demonstrate the location of adGSTD3-Met101 and adGSTD4-Val107. (A) The ribbon representation of AdGSTD3-3 and adGSTD4-4, different color refers to different isoform, Met101 and Val107 are represented by ball and stick; pink and blue color respectively. (B) Active site pocket residues of the enzyme are shown by CPK, pink and blue color represents the active site pocket of different subunit. The yellow CPK is the position of Met101. The sticks represent substrates, the green is GSH and the orange is EA.

1.8.1 Subunit Interface of the adGSTD3-3 and adGSTD4-4

The dimer interfaces of both isozymes feature extensive hydrophobic and hydrogen bonding interaction however lack the ball-and-socket motif. There are two areas of the subunit interactions of these isozymes; the hydrophobic interactions at both sides of the interface (**Figure 1.13; Circle A**) and the interactions at the middle of the interface (**Figure 1.13; Circle B**).

The former area is the equivalent location of the ball-and-socket motif in the α/μ/π/Sj26 subunit type. However, in adGSTD3-3 and adGSTD4-4, the position of the ball is not an aromatic ring residue but a proline instead. The only possible interaction at this region is the interaction between the proline residue and a threonine from an opposite subunit (**Figure 1.14**). The later area is the region that equivalent amino acid residues, which are the same number of each monomer and folded to interact each

others in the same place (**Figure 1.15**). According to the interactions in this area, there are nine amino acids which can be separated into three parts: the conserve electrostatic interaction at the top (**Figure 1.16**), the hydrophobic interactions at the middle, which Met101 of adGSTD3-3 and Val107 of adGSTD4-4 in previous study are located in, (**Figure 1.17**) and the ionic network at the edge of the subunit interface (**Figure 1.18**).

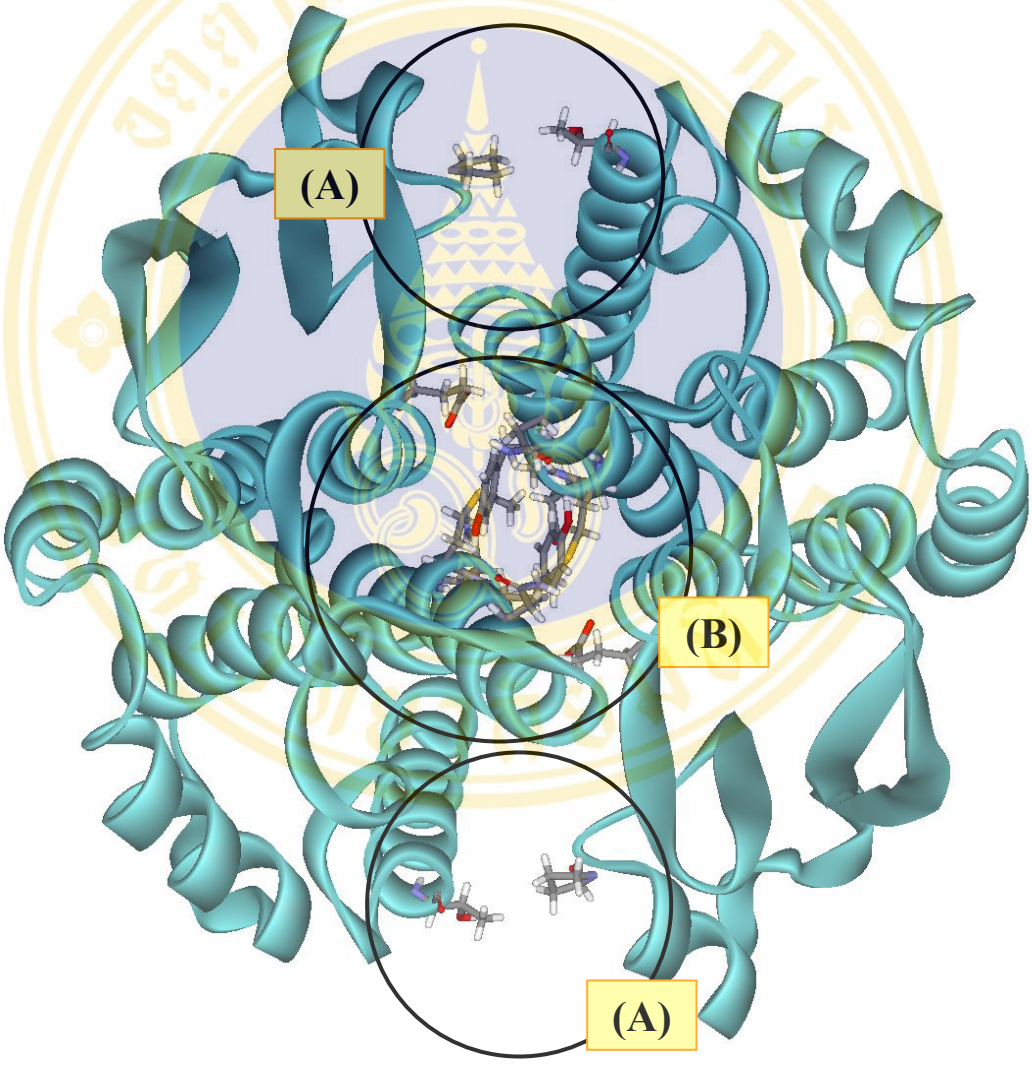

Figure 1.13 The subunit interactions of the adGSTD3-3.

Circle (A) is the hydrophobic interactions at both sides of the interface.

Circle (B) is the interactions at the middle of the interface which are the same number residue of each monomer folded to interact each others in the same place.

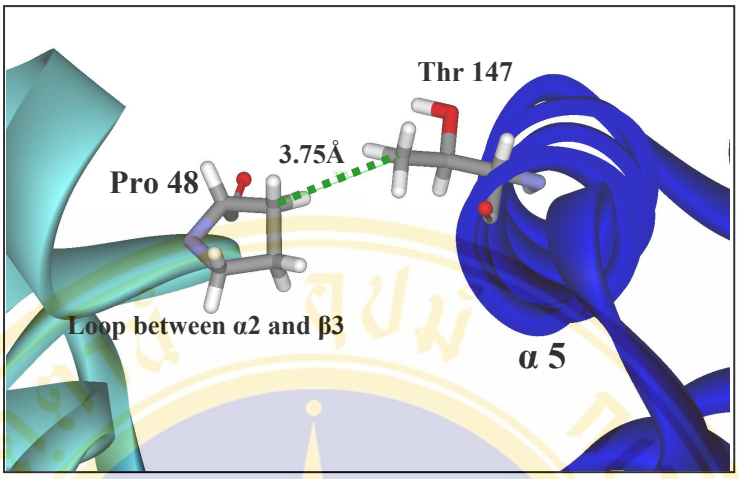

Figure 1.14 The interaction between proline 48 and threonine 139 of adGSTD3-3.
The proline 48 and the threonine 139 were showed as stick forms. The different color ribbon represents the different subunit.

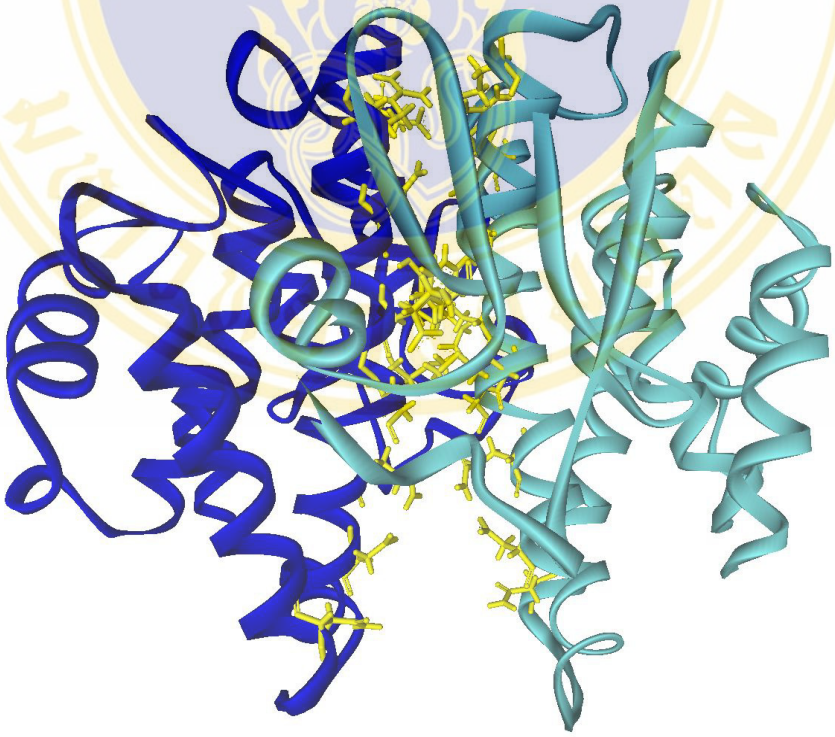

Figure 1.15 The overall residues involved in the interactions at the middle of the subunit interface of adGSTD3-3.
The subunit interface residues are represented by yellow stick models and the different color ribbon represents the different subunit.

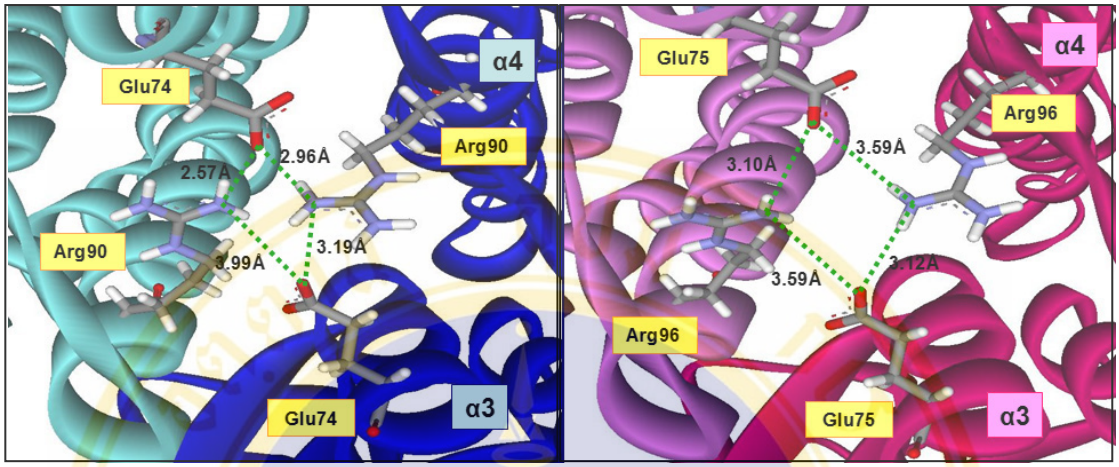

(A) (B)

Figure 1.16 The conserved electrostatic interaction at the top of subunit interface. The conserved arginines and glutamates are shown by stick models. The different color ribbons represent the different subunit, the helix number and residues are shown in boxes. (A) adGSTD3-3 and (B) adGSTD4-4.

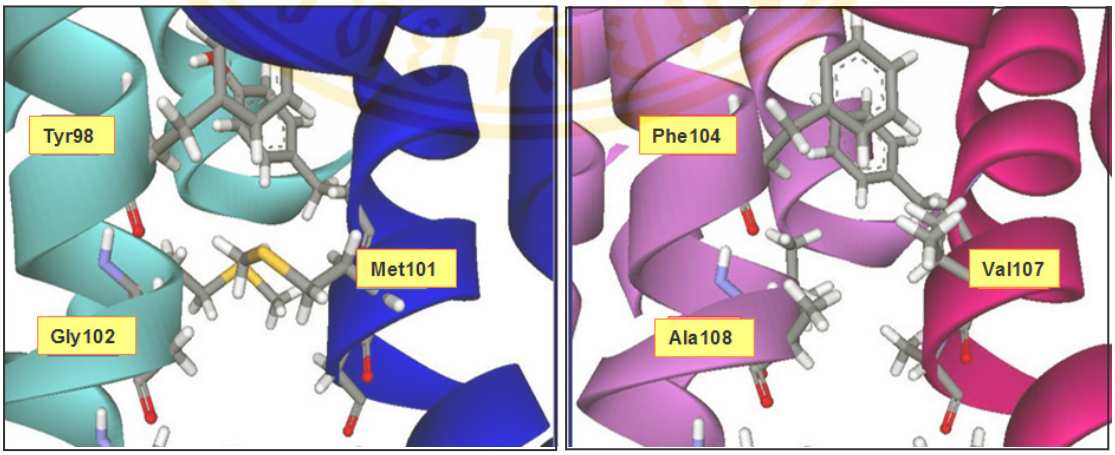

(A) (B))

Figure 1.17 The hydrophobic interactions at the middle of the subunit interface. The hydrophobic interface residues are shown by stick models. The different color ribbons represent the different subunit. (A) adGSTD3-3 and (B) adGSTD4-4.

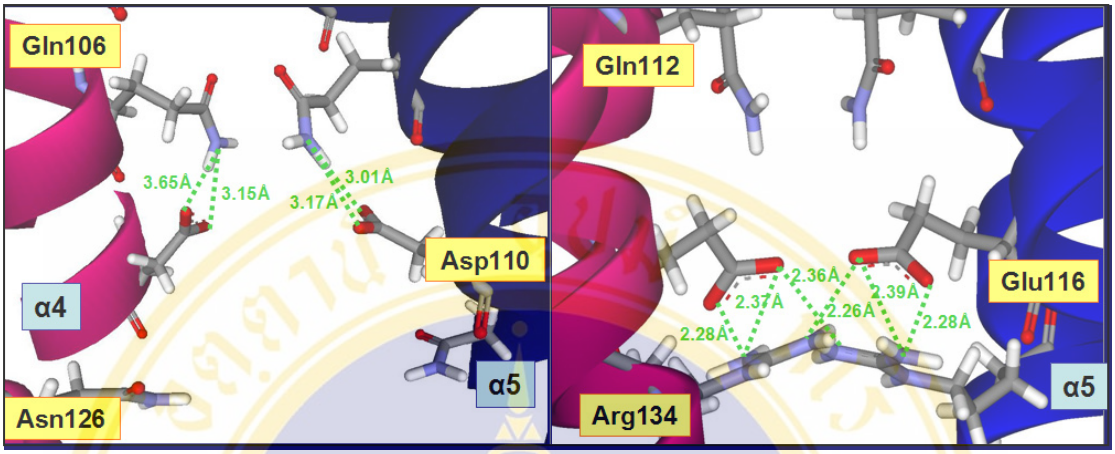

(A) **(B)**

Figure 1.18 The ionic network at the edge of the subunit interface.
The interface residues are shown by stick models. The different color ribbons represent the different subunit, the helix number and residues are shown in boxes. (A) adGSTD3-3 and (B) adGSTD4-4.

1.8 Objectives

To characterize the contributions of amino acids at the subunit interface of adGSTD3-3 and adGSTD4-4 in effecting the enzyme properties, my thesis project was separated into four parts.

1.8.1 The influence of the conserve electrostatic interactions at the top of the interface.

There are two conserved residues from different helices (Glu in α3 and Arg in α4) among GST delta, theta and sigma class that form a conserved charge-charge interaction at the top of subunit interface (**Figure 1.16**). This interaction may be important for stabilizing and folding of the enzymes. Therefore, it was planned determine if the inter- and intra-subunit electrostatic interactions of these residues are important interactions that help to maintain tertiary and quaternary structures of both

isozymes. To break these electrostatic interactions, mutants were generated; Glu75Ala and Arg96Ala of adGSTD4-4.

1.8.2 The effect of the different hydrophobic amino acids at the equivalent positions at the middle of subunit interface of adGSTD3-3 and adGSTD4-4.

This subunit interface region shows the most variation in amino acid residues at equivalent positions between the two isozymes (**Figure 1.17**). Therefore, to study the role of hydrophobic residues at the dimeric interface of these isozymes, disruption of the amino acid side chain packing by switching the amino acid side chain of the isozymes were performed with these mutations; Tyr98Phe, Met101Val, Gly102Ala and Tyr98Phe/Met101Val/Gly102Ala of adGSTD3-3 and Phe104Tyr, Val107Met, Ala108Gly and Phe104Tyr/Val107Met/ Ala108Gly of adGSTD4-4.

1.8.3 The influence of the charge-charge networks at the edge of the subunit interface.

The different residues in the bottom edge of subunit interface, Asp110 and Asn126 of adGSTD3-3 and Glu116 and Arg134 of adGSTD4-4, were studied. AdGSTD4-4, Glu116 and Arg134 can form hydrogen bonds network both inter- and intra-subunit which help to maintain tertiary and quaternary structures of this isozyme. However, these interactions do not appear in adGSTD3-3. For adGSTD3-3, there are hydrogen bonds only in the same subunit between Asp110 and the highly conserved residue, Glu106 (**Figure 1.18**). To study the influence of the ionic networks in the bottom edge of subunit interface whether they affect the catalytic activity and stability of enzymes, the mutations at the equivalent positions of these two isozymes were generated, Asp110Ala of adGSTD3-3 and Glu116Ala of adGSTD4-4.

1.8.4 Study unfolding pathway of adGSTD3-3 and adGSTD4-4.

Due to the different amino acid sequence and the enzymatic properties, the unfolding pathway was studied to determine whether these two spicing products show the same or different unfolding pathway.

From these investigations, we can gain knowledge about the diversity of the GST splice forms in the term of dimerization and the roles of the subunit interface residues. This knowledge can utilize not only for GSTs but also the other multimeric proteins. Moreover, we will know the unfolding pathway of the insect delta class GST which can help us to understand more about the folding pathway of multimeric proteins in general. In addition, exploring the structure and function of insect GSTs can help to gain an understanding of resistance mechanisms to important pesticides and other applications for the other functions of GSTs.

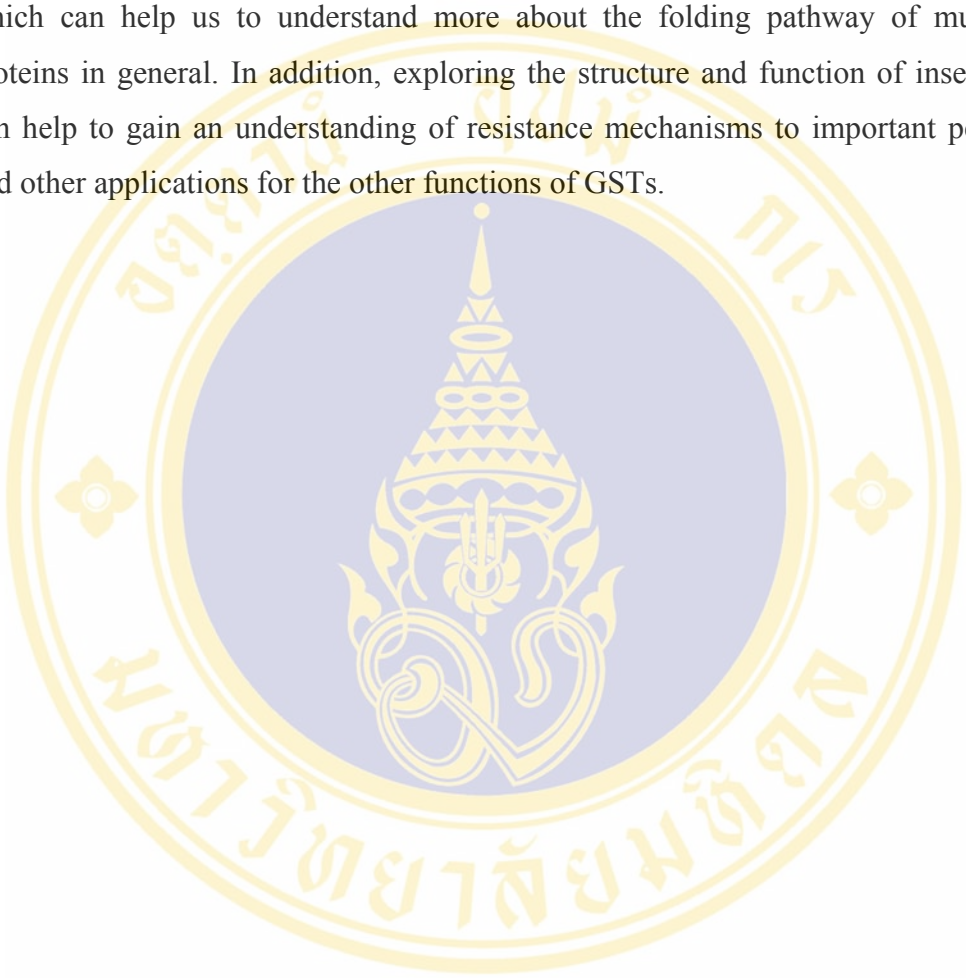

CHAPTER 2
MATERIALS and METHODS

2.1 Construction of Mutant Plasmids

2.1.1 Preparation of Double Stranded Plasmid DNA Template

The AdGSTD3-3 and AdGSTD4-4 plasmid DNA templates were prepared from the previous construct (83) which consisted of pET3a containing an insert of AdGSTD3-3 and AdGSTD4-4 coding sequence. The plasmid constructs are shown in **Figure 2.1**. Plasmid extraction was performed by using cetyl ammonium bromide (CTAB) method. A single colony of *E.coli* was incubated in 3 ml LB broth containing 100 µg/ml ampicillin and incubated at 37ºC with 200 rpm shaking overnight. The *E.coli* culture was transferred to a 1.5 ml microtube and the pellet was collected by centrifugation at 10,000 rpm for 10 seconds, resuspended in 200 µl of STET buffer (8% sucrose, 0.1% Triton X-100, 50 mM EDTA, 50 mM Tris-HCl, pH 8.0) and mixed by vortexing 5 µl of freshly prepared lysozyme solution (5 mg/ml) was added to the suspension and incubated for 10 minutes at room temperature. The mixture was boiled at 100ºC for 45 seconds and centrifuged at 12,000 rpm for 15 minutes at room temperature. The cell pellet (cell debris and chromosomal DNA) was removed by using a sterile toothpick.

Plasmid and low molecular weight residual DNA were recovered by adding 20 µl of 5% CTAB to the supernatant, mixing and let stand for 30 minutes. The contents were centrifuged at 12,000 rpm for 5 minutes at room temperature and the supernatant was discarded. The pellet was resuspended in 300 µl of 1.2 M NaCl by vigorous mixing. To remove RNA, 10µl of RNaseA (10 mg/ml) was added and incubated at 37ºC for 30 minutes. An equal volume of chloroform was added, mixed by inversion and centrifuged at 12,000 rpm for 5 minutes. The supernatant was transferred to a new 1.5 ml micro tube and 2 volumes of absolute ethanol was added. After incubation at -80ºC for 15 minutes, the mixture was centrifuged at 12,000 rpm for 15 minutes at

room temperature. The final DNA pellet was washed with 70% ethanol and the supernatant was discarded. The DNA was briefly air-dried at room temperature, resuspended in 20 µl of sterile water and stored at -20ºC.

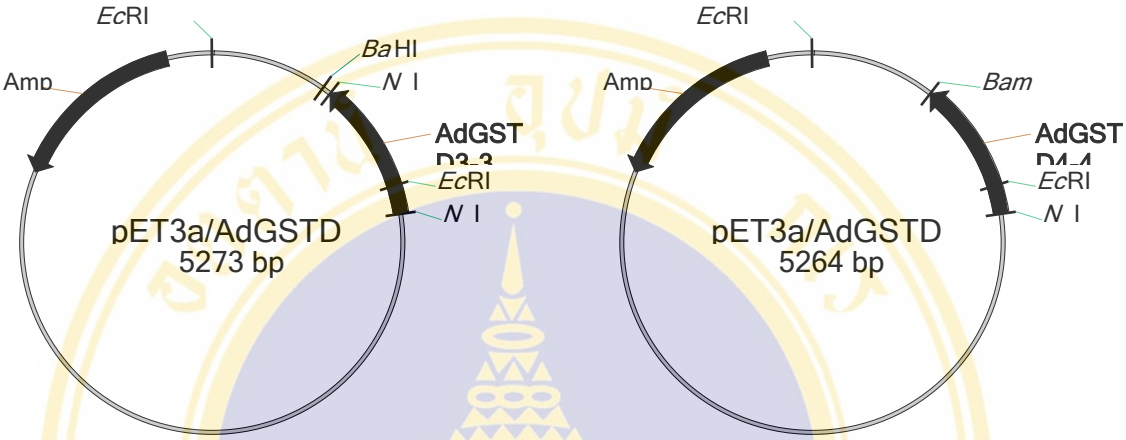

Figure 2.1 Construction of the adGSTD3-3 and adGSTD4-4 sequence in the pET3a vectors containing the ampicillin resistant gene for screening and T_7 promoter for expression.

2.1.2 Visualizing DNA Molecules in Agarose Gel

One percent agarose was prepared in 1X TBE buffer (0.09 M Tris-Borate and 2 mM EDTA, pH 8.0). The agarose was melted and poured into a gel tray and allowed to set 30 minutes. The plasmid DNA was mixed with loading buffer (0.25% bromophenol blue and 30% glycerol in water) before being loaded into the wells. Then the DNA was run on the gel along with the marker either *λHind*III or *λBste*II DNA. Electrophoresis was performed at 100 volt for 60 minutes. The gel was removed and stained with 0.5 mg/ml of ethidium bromide solution in water for 10 minutes followed by destaining with distilled water for 10 minutes. The DNA bands were visualized by ultraviolet irradiation and photographed.

2.1.3 Site Directed Mutagenesis of AdGSTD3-3 and AdGSTD4-4

The method used was based on Stratagene's Quick Change TM site-directed mutagenesis kit by using *pfu* DNA polymerase which replicates both plasmid strands

with high fidelity and without displacing the mutant oligonucleotide primers. The basic procedure (**Figure 2.2**) utilized a double stranded DNA vector with an insert and two synthetic oligonucleotide primers containing the desired change. On incorporation of the oligonucleotide primers, a mutated plasmid containing staggered nicks is generated. After the amplification step, the PCR product is treated with *Dpn*I endonuclease (Target sequence: 5'-Gm6ATC-3') which specific for methylated and hemimethylated DNA. The *Dpn*I endonuclease was used to digest the parental DNA template and to select for mutations containing synthesized DNA. DNA isolated from *E.coli* is *dam* methylated therefore susceptible to *Dpn*I digestion. The nicked vector DNA of pET3A incorporating the desired mutations were then transferred into *E.coli* BL21(DE3)pLysS.

2.1.4 Primer Design

All primers were designed using Vector NTI suite6 software. Both changed nucleotide and amino acid residues above the forward primer sequences are shown in bold letters. The recognition sites for restriction endonucleases are underlined.

M D F **F** L R Q N V V A
D3: Y98F-f:* 5' CCATGTCGAA**GAA**CAGTCGCTGATTGACGACGG 3'

D3: Y98F-r: 5' CCGTCGTCAATCAGCGACTGTTCTTCGACATGG 3'

Q Y L T G **V** D F Y L R
D3: M101V-f: 5' GCTGGTACAGGGTACC**GAC**GTCGAAGTACAGTCG 3'
*Kpn*I
D3: M101V-r: 5' CGACTGTACTTCGACGTCGGTACCCTGTACCAGC 3'

R Q Y L T **A** M D F Y L
D3: G102A-f: 5' CGCTGGTACAGAGT**C**GC**C**ATGTCGAAGTACAG 3'
*Hinf*I
D3: G102A-r: 5' CTGTACTTCGACATGGCGACTCTGTACCAGCG 3'

P Y Y Y **A** A F R Q Y L T
D3: D110A-f:** 5' GGGTAGTAGTA**GGC**GGCAAAACGCTGGTACAGCG 3'

D3: D110A-r: 5' CGCTGTACCAGCGTTTTGCCGCCTACTACTACCC 3'

L T **A** **V** D F F L R Q N V V
D3:Y98F/M101V/G102A-f: 'CAGCGT**GGCCAC**GTCGAAGAACAGTCGCTGGTTGACGACG3'
*Hinc*II
D3: Y98F/M101V/G102A-r: 'CGTCGTCAACCAGCGACTGTTCTTCGACGTGGCCACGCTG3'

A G Y K **A** V L Y I Q
D4: E75A-f: 5' GCGCCGTACTT**CGC**GACCAGGTAGATCTGG 3'
*Nru*I
D4: E75A-r: 5' CCAGATCTACCTGGTCGCGAAGTACGGCGC 3'

H V V A **A** R R P D S
D4: R96A-f: 5' GGTGGACGACGGC**AGC**GCGCCGCGGATCGC 3'
*Sac*II
D4: R96A-r: 5' GCGATCCGCGGCGCGCTGCCGTCGTCCACC 3'

E A F R Q Y L V A **M** D F F
D4: V107M-f: 5' CTCGGCGAATCTCTGGTACAGGACGGC**CAT**ATCGAAGAAC 3'
*Hinf*I
D4: V107M-r: 5' GTTCTTCGATATGGCCGTCCTGTACCAGAGATTCGCCGAG 3'

Y E A F R Q Y L V **G** V D F
D4: A108G-f: 5' GTACTCGGCGAATCTCTGGTACAGGAC**GCC**CACATCGAAG 3'
*Hinf*I
D4: A108G-r: 5' CTTCGATGTGGGCGTCCTGTACCAGAGATTCGCCGAGTAC 3'

P Y Y Y **A** A F R Q Y L V
D4: E116A-f:** 5' GGATAGTAGTA**CGC**GGCGAAACGCTGGTACAGGACG 3'

D4: E116A-r: 5' CGTCCTGTACCAGCGTTTCGCCGCGTACTACTATCC 3'

A F R Q Y L V **G** **M** D F Y
D4: F104Y/V107M/A108G-f:** 5' GGCGAAGCGTTGGTACAGGAC**GCCCAT**ATCGAAGTAG3'

D4: F104Y/V107M/A108G-f: 5' CTACTTCGATATGGGCGTCCTGTACCAACGCTTCGCC 3'

Note: The triple mutants, AdGSTD3-3: Y98F/M101V/G102A and AdGSTD4-4: F104Y/V107M/A108G, were generated by using the PCR products of AdGSTD3-3: Y98F and AdGSTD4-4: F104Y as a template, respectively.

* *Hinc*II site removed. ** *Hae*II site removed.

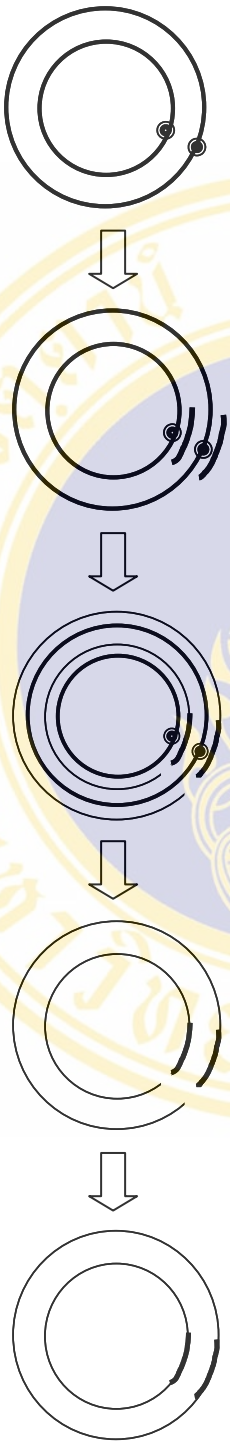

AdGSTD3-3 and adGSTD4-4 gene pET3a with target site for mutation.

Denature the plasmid and anneal the mutagenic primers containing the desired mutation.

Using the nonstrand-displacing action of *Pfu* DNA polymerase, extend and incorporate the primers resulting in nicked circular strands.

Digest the methylated, nonmutated parentalDNA template with *Dpn*I.

Transform the circular, nicked dsDNA into *E.coli* DH5α competent cells. After transformation, the *E.coli* cells repair the nicks in the mutated plasmid.

Figure 2.2 Overview of the Quick Change site-directed mutagenesis method.

2.1.5 Conditions for the PCR Reactions

The sample reactions were prepared as indicated in **Table 2.1**. And the temperature cycling parameters for the site-direct mutagenesis were performed by the conditions shown in **Table 2.2**.

Table 2.1 Master mix reaction for PCR

Reagent	Volume (µl)
10X reaction buffer (*pfu* DNA polymerase buffer)	5
10 pmol/µl of oligonucleotide primer 1 (forward)	1
10 pmol/µl of oligonucleotide primer 2 (reverse)	1
10 mM dNTP mix (2.5 mM each NTP)	1
100-200 ng of dsDNA template	x
Native *pfu* DNA polymerase (2.5 U/µl)	0.5
Sterile distilled water	41.5-x
Total volume	50

Table 2.2 Temperature cycling parameters for site-directed mutagenesis

Temperature (ºC)	Time (min: sec)	Cycles
95	0:30	1
95	0:30	16
55	1:00	
68	11:00	
4	HOLD	

After the amplification reaction was completed, the PCR products were analyzed on 0.7 % agarose gel electrophoresis.

2.1.6 Restriction Preparation of PCR Products

To remove the parental template DNA, 1 µl of *Dpn*I was added into the 50 µl PCR reaction and incubated in a 37 ºC water bath for 3 hour. Then 2 µl of *Dpn*I-treated DNA was transformed into *E.coli* DH5α competent cells prepared by the $CaCl_2$ method.

2.1.7 Transformation of PCR Products into *E.coli*

2.1.7.1 Propagation of Bacteria

E.coli DH5α was inoculated from a single cell colony into 3 ml of LB medium and grown at 37ºC overnight in a shaking incubator.

2.1.7.2 Preparation of Competent *E.coli* Cells (Calcium Chloride Method)

To prepare bacterial competent cells for transformation, 2 ml of the overnight culture was transferred into 200 ml of LB. The culture was incubated at 37ºC with vigorous agitation, monitoring the growth of the culture until OD_{600} reached 0.3-0.5. The bacterial cells were divided into two sterile disposable ice-cold 100 ml polypropylene tubes. The culture was cooled to 4ºC by storing the tubes on ice for 10 minutes. The cells were recovered by centrifugation at 4000 rpm for 10 minutes at 4ºC. The medium was decanted from the cell pellet. The tubes were inverted on a pad of paper towels for 1 minute to allow the last traces of media to drain away. Each pellet was resuspended by gentle vortexing in 10 ml of ice-cold 0.1 M $CaCl_2$ solution. The cells were recovered by centrifugation at 4000 rpm for 10 minutes at 4ºC. The medium was decanted from the cell pellets. The tubes were inverted on a pad of paper towels for 1 minute. The pellet was resuspended by gentle vortexing in 5 ml of ice-cold 0.1 M $CaCl_2$ for each 50 ml of original culture. The cells were recovered by centrifugation and the medium was decanted. The pellet was resuspended in 8 ml 0.1 M $CaCl_2$ in 15% glycerol. The cell mixture was dispensed into 200 µl aliquots and frozen at -80ºC. The efficiency of the prepared competent cells was determined by transforming 10 ng of pUC18 DNA into 200 µl of the competent cells.

2.1.7.3 Transformation of Competent Cells

100 ng of DNA was added to 200 µl of competent cells and incubated on ice for 1 hour. The tube was transferred to a 42ºC water bath for exactly 90 seconds to heat-

shock the cells and then rapidly transferred to ice for 5 minutes. 800 µl of LB broth was added to the transformed cells and incubated for 1 hr in a shaking incubator at 37ºC. Then 200 µl of transformed competent cells were spread onto an agar medium plate containing an appropriate antibiotic. The plate was incubated at 37ºC for 12-16 hours.

2.1.8 Restriction Analysis

Three to five colonies of each mutant were randomly selected for restriction analysis. Digestion reactions were prepared as indicated in **Table 2.3**. The reaction tubes were incubated for 3 hours at an appropriate temperature depending on the enzyme used. Then the digested DNA was run on 1-1.5 % agarose gel as described in section 2.2. The desired plasmid DNA clone was stored at -20ºC.

Table 2.3 Digestion reaction for restriction analysis

Reagent	Volume(µl)
Restriction enzyme: correspond to the restriction recognition site introduced in the mutagenic primers.	0.5
10X buffer: corresponding to the enzyme used.	2
BSA	0.2
Plasmid DNA	x
Sterile distilled water	17.3-x
Total volume	20

2.1.9 DNA Sequencing

To verify the correct sequence in both directions with T7 promoter universal primers, DNA sequencing was conducted using ABI PRISM Bigdye^{TM} Terminator or

Cycle Sequencing Ready Reaction Kit (Perkin Elmer), following the manufacturer's instructions. The reaction mixtures were prepared in thin wall 0.5 ml PCR tube as in **Table 2.4**. The tubes were placed in a PCR machine (GeneAmp960, Perkin Elmer). The PCR cycling parameters are shown in **Table 2.5**.

Table 2.4 PCR reaction for sequencing

Reagent	Volume (µl)
2.5X buffer	4
Big dye kit (dNTP + ddNTP + enzyme)	4
Universal T7 promoter or terminator: depend on direction of reaction.	0.5
200 ng DNA	x
Sterile distilled water	11.5-x
Total volume	20

Table 2.5 Temperature cycling parameters for DNA sequencing

Temperature (ºC)	Time (min: sec)	Cycles
96	3:00	1
96	0:10	28
50	0:05	
60	4:00	
60	7:00	
4	HOLD	

2.1.10 DNA Precipitation

The PCR products were transferred to a new 1.5 ml tube with 10 µl of 3 M NaOAc and 250 µl of absolute EtOH. The mixture was incubated at 4ºC for 30 minutes and centrifuged at 13,000 rpm for 15 minutes. The pellet was washed with

70% ethanol and allowed to dry. Then the DNA samples were analyzed by an automated DNA sequencer ABI Prism 377 (Perkin Elmer).

2.2 Expression and Purification of the Enzymes

2.2.1 Expression of Recombinant Clones

E.coli BL21(DE3)pLysS containing a recombinant plasmid was grown in 3 ml LB broth containing 100 µg/ml ampicillin and 34 µg/ml chloramphenicol at 37ºC overnight. The overnight culture was transferred into a new flask containing LB broth, 100 µg/ml ampicillin and 34 µg/ml chloramphenicol to make up 1% of the final concentration. The culture was incubated at 37ºC with shaking until the OD_{600} reached 0.6. An expression was induced by adding IPTG to a final concentration of 0.1 mM for 3 hours. Then the culture was placed on ice for 20 minutes, transferred to a 200 ml-centrifuge bottle and spun at 7000 rpm, 4ºC for 10 minutes. The LB broth was decanted and the cell pellet was resuspended in 10 ml of LB, transferred to a new 50 ml centrifuge tube and spun at 7000 rpm, 4ºC for 10 minutes. The pellet was collected and stored at -20ºC until used.

2.2.2 Enzyme Purification

2.2.2.1 Preparation of Cell Lysate

The pellet from 200 µl culture was resuspened with 19.2 ml of phosphate buffer pH 7.3 (140 mM NaCl, 2.7 mM KCl, 10 mM Na_2HPO_4, 1.8 mM KH_2PO_4 pH 7.3), 800 µl of 100 mg/ml lysozyme, 14.4 µl of 1.4 M β-mercaptoethanol and 200µl of 1 M DTT. The mixture was gently vortexed and placed on ice for 30 minutes. Then the cell suspension was lysed by French Press at 1000 psi and centrifuged at 10,000 rpm, 4ºC for 20 minutes. The supernatant was collected and placed on ice for affinity chromatography.

2.2.2.2 Protein Purification

The soluble recombinant GST in the supernatant of total lysate was purified by using GSTrap affinity chromatography according to the manufacturer's instructions. The column was equilibrated with 5 bed volumes of the binding buffer, PBS pH 7.3,

then the resulting supernatant was subjected to GSTrap affinity column. The non-specific binding proteins were eluted by 5 bed volumes of elution buffer (10 mM GSH in 1.5 M Tris-HCl pH 8.0, and 10 mM DTT). Only the fractions containing recombinant GST were pooled in the centriprep-10 (Amicon) then centrifuged at 2500 xg at 4ºC in a SORVALL 26S, SH-300 rotor. The final volume of the concentrated GST was less than 1.5 ml. Then the GSH was eliminated by HiTrap desalting column (Amersham Phamacia Biotech), equilibrated with 5 column volumes of 50 mM phosphate buffer pH 6.5. The concentrated GST was adjusted in volume to 1.5 ml and applied to the column and eluted with 2 ml of the same buffer containing 10 mM DTT (85). The protein was concentrated until the final volume was less than 1 ml. Sterile glycerol was added to a final concentration of 50%. The purified GSTs were stored at -20ºC. All the above steps were performed at 4ºC.

2.2.3 SDS-PAGE Analysis

2.2.3.1 Protein Sample Preparation

The OD_{600} of the bacterial cell culture was measured. Then the cells corresponding to 0.1 OD were collected by centrifugation at 5,000 rpm for 2 minutes. The cell pellet was resuspended by vortexing in 60 µl sterile distilled water and 20 µl of 4X gel sample buffer (4 mM EDTA, 4% SDS, 40% glycerol, 100 mM DTT, 1.45 mM bromophenol blue, 200 mM Tris-HCl, pH 7.5) and heated in 95ºC for 10 minutes in a heating block to denature the proteins and stored in the refrigerator until the SDS-PAGE had been set up.

2.2.3.2 Separation of Protein Samples

An SDS-PAGE gel was prepared as described in **Table 2.6**. After the gel was polymerized for approximately 30 minutes the well comb was removed. The wells were washed with water to remove unpolymerized acrylamide solution. The electrophoresis apparatus was assembled. The samples were loaded, approximately 0.05 OD, including 4 µl of a protein standard marker. The separation was started in descending direction at a constant current of 25 mA until the bromophenol marker was run to the bottom of the gel. The electrophoresis equipment was disassembled and the gel was stained in Coomassie staining solution for 2 hours at room

temperature. Then the gel was destained overnight in destaining solution, dried and made a permanent record by scanning the gel.

Table 2.6 Preparation of SDS-PAGE (0.75 mm x 2 gels)

Solution	6% Stacking gel	15% Separating gel
Acrylamide solution (ml) (30% acrylamide+0.3% bis-acrylamide)	O.6	5
1.5 M Tris-HCl pH 8.8 (ml)	-	2.5
0.5 M Tris-HCl pH 6.8 (ml)	0.75	-
Distilled water (ml)	1.6	2.3
10% SDS (µl)	30	100
10% (w/v) Ammonium persulphate (µl)	20	50
TEMED(µl)	10	10
Total volume (ml)	3	10

2.2.4 Protein Quantification (Protein Assay)

The method of Bradford (86), with BSA as a standard, was used for the determination of protein quantity. The Biorad protein reagent (Bio-Rad) was diluted 1:5 with sterile distilled water and filtered through Whatman N0.1 filter paper to remove the insoluble dye. 300 µl of the reagent was added to 10 µl of protein sample in a microtiter plate. The mixture was incubated at room temperature and absorbance measured at 595 nm after 5 minutes. A protein standard curve was generated by using seven different concentration of bovine serum albumin; 0-0.6 mg/ml. Then the unknown protein concentration was calculated from the standard curve.

2.3 Enzymatic Characterization

2.3.1 Determination of GST Activity

GST activity was measured by monitoring the formation of the conjugate of glutathione (10 mM) and CDNB (1mM for AdGSTD3-3 and 3mM for AdGSTD4-4) at 340 nm ($\Delta\varepsilon = 9.6\ mM^{-1}cm^{-1}$) in 0.1 M phosphate buffer pH 6.5 at 25ºC according to the method of Habig et al (87). The substrate was prepared by adding 25µl of CDNB (42 mM for AdGSTD3-3 and 126 mM for AdGSTD4-4) in absolute ethanol and 450 µl of 21 mM GSH in 0.1 M phosphate buffer into 25 µl of 0.1 M phosphate buffer pH 6.5. The reaction was stared by adding 100µl of 0.1 M phosphate buffer with 10 µl of diluted enzyme sample into a well of a microtiter plate and then quickly adding 100µl of the prepared substrate. The rate of conjugation between GSH and CDNB was monitored by measuring change in absorbance at 340 nm for 1 minute using a SpectraMax 250.

2.3.2 Determination of Substrate Specificities

Specific activity toward different substrates; 1-chloro-2,4-dinitrobenzene (CDNB), 1,2-dichloro-4-nitrobenzene (DCNB), p-nitrophenethyl bromide (PNPB), p-nitrobenzyl chloride (PNBC) and ethacrynic acid (EA) were performed as described in **Table 2.7** (88). GSH stock solution was prepared in 0.1 M phosphate buffer using the appropriate pH for each substrate. All the stock hydrophobic substrates were prepared in absolute ethanol and diluted into the assay buffer. All measurements were performed at 25-27ºC in 0.1 M phosphate buffer. Specific activities were calculated based on the molar extinction coefficient for each substrate (87). The specific activities reported are the mean ± standard deviation from at least three independent experiments.

2.3.3 Determination of Kinetic Parameters

Kinetic parameters of the enzymes were determined by varying concentrations of CDNB from 0.02-3 mM with GSH concentration constant at 10 mM. The reaction was performed in 0.1 M phosphate buffer pH 6.5. The kinetic parameters were also established by varying the GSH concentration from 0.008 to 20 mM with constant

CDNB concentration; 1mM for AdGSTD3-3 and 3mM for AdGSTD4-4. The maximal velocity (V_{max}) and the Michaelis constant (K_m) were analyzed by non-linear regression using the software package GraphPad Prism (GraphPad Software, Inc. San Diego, CA). The catalytic constant (k_{cat}) and the catalytic efficiency (k_{cat}/K_m) were calculated on an active-site basis using the subunit molecular mass of each enzyme. The kinetic constants are the the mean ± standard deviation from at least three independent experiments.

Table 2.7 The conditions for the determination of substrate specificities

Substrates	Concentration (mM)	pH buffer	λ max (nm)	Absorbance coefficient ($mM^{-1} cm^{-1}$)
CDNB	1 (for D3-3) 3 (for D4-4)	6.5	340	9.6
DCNB	1	7.5	345	8.5
EA	0.2	6.5	270	5.0
PNBC	0.1	6.5	310	1.2
PNPB	0.1	6.5	310	1.9

2.3.4 Calculation of Kinetic Parameters for the Cooperativity of Substrate Binding.

The cooperativity upon substrate binding was found in some mutants suggesting that the induce-fit mechanism was altered by the mutation thereby generating subunit communication between two active sites (89). Therefore, the kinetic parameters were determined by fitting the 1:1 Michaelis-Menten equation to the experimental data. Hill coefficient was calculated from the slope of Hill plot according to the Hill equation (90):

$$Y = v_i / V_{max} = [S]^h/(K_m+[S]^h)$$

Where v_i is the initial velocity at nonsaturating substrate concentration, V_{max} is the maximum velocity at saturating substrate concentration, [S] is the substrate concentration, K is the substrate concentration corresponding to the half enzyme saturation and *h* is the Hill coefficient.

2.4 Structural Characterization

2.4.1 Stability Assay

The enzymes at a 0.1 mg/ml final concentration were incubated in 0.1 M phosphate buffer contraining 1 mM EDTA and 5 mM DTT at 45ºC. The remaining activity was measured by withdrawing an appropriate volume at different time points until the remaining activity was less than 50%. The half-life of each enzyme was calculated using the equations (88):

$$\text{Slope} = k/2.3$$

$$k = 0.693/t_{1/2}$$

The slope was obtained from the linear plot between the log of percentage of original activity and the time point of preincubation.

2.4.2 Intrinsic Tryptophan Fluorescence Spectroscopy

Intrinsic tryptophan fluorescence spectroscopy was used to investigate changing of the amino acid side chain around tryptophan in 0.1 M phosphate buffer pH 6.5. The fluorescence spectra of 0.2 mg/ml enzyme were monitored by a Shimadzu RF 5001PC. The scanning of protein sample was performed in a quartz cell (0.5 cm path length). The parameters used are shown in **Table 2.8**. The experiment was carried out at room temperature (24-26 ºC). After scanning, the background spectrum of 0.1 M phosphate buffer pH 6.5 was subtracted from the spectrum of the proteins and then the subtracted spectrum were normalized by the real protein concentration of each enzymes measured by UV absorption spectroscopy assay. A total of three scans each for background and protein were recorded and averaged. The fluorescence spectrum of each mutant was analyzed and compared to the wild type.

2.4.3 Protein Concentration Assay by UV Absorption Spectroscopy I

UV absorption of aromatic ring was used to determine a concentration of the proteins after Intrinsic Fluorescence Spectroscopy. The protein concentration was measured in a 0.5 cm path-length quartz cuvette at 280 nm using Hitachi U2000 UV-Visible spectrophotometer. The absorbance of 0.1 M phosphate buffer pH 6.5 was subtracted from the protein absorbance. The protein concentration was calculated in units of mg/ml by the equation.

Protein concentration (mg/ml) = Absorbance at 280 nm / 0.5 cm x ε*

* The extinction coefficient for each protein calculated by Vector NTI suite6 software.

Table 2.8 The parameters for the intrinsic tryptophan fluorescence spectroscopy

Excitation wavelength (nm)	295*
Emission scan wavelength (nm)	300 to 450
Record range	0 - 500
Scanning speed	medium
Sampling interval (nm)	1.0
Slit width for excitation (nm)	3
Slit width for emission (nm)	3
Sensitivity	high
Response time (s)	auto

* An excitation wavelength of 295 nm was used to selectively excite tryptophans.

2.4.4 Refolding Assay

2.4.4.1 Refolding rate constants and % activity recovery measurement

The enzymes were first denatured in 4 M guanidinium chloride in renaturation buffer (0.2 M phosphate, 1 mM EDTA and 5 mM DTT, pH 6.5) at room temperature for 1 hr and then rapidly diluted (defining time 0) 1:40 into renaturation buffer. Therefore, the final guanidinium chloride concentration was 0.1 M during refolding. Recovered activity was monitored as a function of time by withdrawal of appropriate aliquots of the renaturation mixture and immediately assaying for activity. Refolding

rate constants were determined by nonlinear regression using a single exponential equation (91).

2.4.4.2 Intrinsic tryptophan fluorescence spectroscopy

The fluorescence spectra of 0.5 μM of enzyme in 0.1 M phosphate buffer pH 6.5 (native enzyme), in 4 M GuHCl solution (unfolded enzyme) and in renaturation buffer after refolded 1 hr (refolded enzymes) were monitored by a Shimadzu RF 5001PC. The scanning of protein sample was performed in a quartz cell (0.5 cm path length). The parameters used are shown in **Table 2.8**. For other steps used the standard reaction assay as showed in section 2.4.2.

2.4.5 ANS Binding Assay

2.4.5.1 ANS Binding Spectra Measurement

200 μM ANS in 0.1 M sodium phosphate buffer pH 6.5 was added to a final concentration of 2 μM enzyme in 400 μl reaction (49). The binding of ligand was monitored by a Perkin Elmer Luminescence spectrometer LS50B. Scanning of the protein sample was performed in a quartz cell (1 cm path length). The parameters used are shown in **Table 2.9**. The experiment was carried out at room temperature (24-26 ºC). The spectrum of ANS in phosphate buffer pH 6.5 was subtracted from the spectra of the protein binding ANS. A total of three scans each for blank and sample were recorded and averaged for each enzyme. The fluorescence spectrum of each mutant was analyzed and compared to the wild type.

Table 2.9 The parameters for the ANS binding assay

Excitation wavelength (nm)	395*
Emission scan wavelength (nm)	400 to 600
Scanning speed (nm/min)	50
Sampling interval (nm)	1.0
Slit width for excitation (nm)	10
Slit width for emission (nm)	5

* An excitation wavelength of 395 nm was used to excite ANS dye.

2.4.5.2 Remaining Activity Measurement of ANS bound protein

Enzyme activity measurements in the presence of ANS were assessed immediately after adding ANS by using the standard reaction assay (section 2.15).

2.5 Unfolding Pathway Investigation

Protein samples (0.1 mg/ml for remaining activity measurement, intrinsic fluorescence spectroscopy, and ANS binding assay, 0.4 mg/ml for far-UV **c**ircular dichroism spectroscopy and 1 mg/ml for size-exclusion chromatography) were incubated with guanidinium chloride (0 to 5 M) in unfolding buffer (20 mM Na_2HPO_4, 5 mM DTT, 1 mM EDTA, pH 6.5) at room temperature overnight (~16 hr) to achieve equilibrium prior to measurements.

2.5.1 Remaining Activity Measurement

Enzyme activity measurements in the presence of denaturant were assessed using the standard reaction assay (section 2.15)(55)

2.5.2 ANS Binding Assay

The binding of ligand was monitored by a Shimadzu RF 5001PC. Scanning of the protein sample was performed in a quartz cell (0.5 cm path length). The parameters used are shown in **Table 2.10**. The experiment was performed at room temperature (24-26 ºC). The spectrum of ANS in phosphate buffer pH 6.5 was subtracted from the spectra of the protein binding ANS. A total of three scans each for blank and sample were recorded and averaged for each enzyme. An unfolding curve was determined by plotting fluorescence intensity at 471 nm (maximum intensity of the enzymes in 0 M guanidinium chloride) against guanidinium chloride concentration(92).

2.5.3 Intrinsic Fluorescence Spectroscopy

Fluorescence spectroscopy was used as a probe to obtain unfolding curves. The fluorescence intensity was monitored by a Shimadzu RF 5001PC. The scanning of protein sample was performed in a quartz cell (0.5 cm path length). The parameters used are shown in **Table 2.10**. The experiment was performed at room temperature (24-26 ºC). The background spectrum of unfolding buffer was subtracted from the spectrum of protein. A total of three scans each for background and protein were recorded and averaged. An unfolding curve was determined by plotting fluorescence intensity ratio of 350nm (for unfolded protein) and 330 nm (for folded protein) against guanidinium chloride concentration(92).

2.5.4 Circular Dichroism Spectroscopy

Far-UV circular dichroism (CD) spectroscopy (200-260 nm) which is sensitive to secondary structure of proteins was used to investigate the folded CD spectrum of enzymes in unfolding solution. The CD spectra were measured by a JASCO J-715 spectrophotometer. The machine was purged with nitrogen gas (151 L/min) during operation and was calibrated with a known concentration (1 mg/ml) of (+)-10-camphorsulphonic acid (CSA). This compound has a well-known CD spectrum, with a negative band at 192 nm and a positive band at 290.5 nm. Scanning of the protein sample was performed in a quartz cell (0.02 cm path length). The parameters used are shown in **Table 2.11**. The experiment was performed at room temperature (24-26 ºC). CD of unfolding buffer pH 6.5 was subtracted from the spectra of proteins. Absorption base line was corrected using average intensity at 250-260 nm.

2.5.5 Protein Concentration Assay by UV Absorption Spectroscopy II

UV absorption of peptide bond (OD at 215 nm and 225 nm) was used to determine a concentration of the proteins after the circular dichroism analysis. The protein concentration was measured in a 0.02 cm path length quartz cuvette using Hitachi U2000 UV-Visible spectrophotometer. The absorbance of unfolding buffer pH 6.5 was subtracted from the protein absorbance. The protein concentration was calculated in units of mg/ml by the equation.

$$\text{Protein concentration (mg/ml)} = 0.144 \times 50\ (OD_{215}\text{-}OD_{255})$$

Table 2.10 The parameters of ANS binding assay and the fluorescence spectroscopy for unfolding pathway study

Parameters	ANS binding assay	Intrinsic fluorescence
Excitation wavelength (nm)	395*	280*
Emission scan wavelength (nm)	400 to 600	300 to 450
Record range	0 - 200	0 - 1000
Scanning speed	medium	medium
Sampling interval (nm)	1.0	1.0
Slit width for excitation (nm)	3	3
Slit width for emission (nm)	3	3
Sensitivity	high	high
Response time (s)	auto	auto

* An excitation wavelength of 395 nm and 280 nm was used to excite ANS dye and all aromatic ring residues, respectively.

Table 2.11 The parameters for circular dichroism spectroscopy for unfolding pathway study

scan wavelength (nm)	200 to 260
Resolution (nm)	1
Band width (nm)	2.0
Sensitivity (mdeg)	50
Response (sec)	1
Speed (nm/min)	50
Accumulation (time)	3

2.5.6 Size-Exclusion Chromatography

The proteins were separated by FPLC system (Amersham Pharmacia Biotech, USA) with a superdex 75 column. The column was equilibrated with phosphate buffer or unfolding buffer at varing guanidinium chloride concentrations for 2 column volumes at a flow rate 0.4 ml/min and the elution profile was monitored at 280 nm. The buffer and protein samples were filtered through 0.2 μm membrane filter before being applied to the column. The peaks were collected at 1 ml per tube and then analyzed on SDS-PAGE.

CHAPTER 3
RESULTS: THE CONSERVED ELECTROSTATIC INTERACTIONS AT THE TOP OF THE SUBUNIT INTERFACE

This chapter reports the results of the study of the conserved charge-charge interaction at the top of subunit interface among GST delta, theta and sigma class (**Figure 1.16**). For this study the following electrostatic interaction mutants were generated; Glu75Ala and Arg96Ala of adGSTD4-4.

3.1 Expression and Purification of the enzymes in *E.coli*

The obtained expression constructs of recombinant plasmid were sequenced and transformed into *E.coli* BL21DE3plysS. All the wild type and mutants were purified from the lysate by affinity chromatography using immobilized GSH. The yields are shown in **Table 3.1**. The purity of the enzymes was determined by SDS-PAGE as shown in **Figures 3.1-3.3**. The expected band of 23 kDa, which corresponds to the calculated molecular weight of the GST subunits, appears as a single band as observed in the purified fractions. The protein concentrations of GSTs were measured in *E.coli* lysate and purified proteins (elution fraction) by using Bradford reagent.

Table 3.1 Purification of the enzymes

Enzymes	Fraction	Total protein (mg)	% Yield (%)
D4-wild type	Lysate	58.2*	
	Elution	35.65	61.25
D4-Glu75Ala	Lysate	244.6**	
	Elution	13.5	5.52
D4-Arg96Ala	Lysate	220.7**	
	Elution	3.0	1.36

* Expressed in 200 µL LB media. ** Expressed in 1 L LB media.

From the mutant enzyme purifications, approximately 1-5 % of total GST proteins from the bacterial lysate were obtained from the glutathione affinity column. This lower yield may result from reduction in binding affinity to the GSH on the gel matrix of the GSTrap column. The crystal structure of adGSTD4-4 demonstrated that Glu75 and Arg96 are not in the active site but located in the edge of helix 3 and helix 4, respectively which are in a hydrophilic environment in subunit interface exposed to the aqueous environment. It appears that the alteration of these positions disrupted the contributions of amino acids in the active site as shown below.

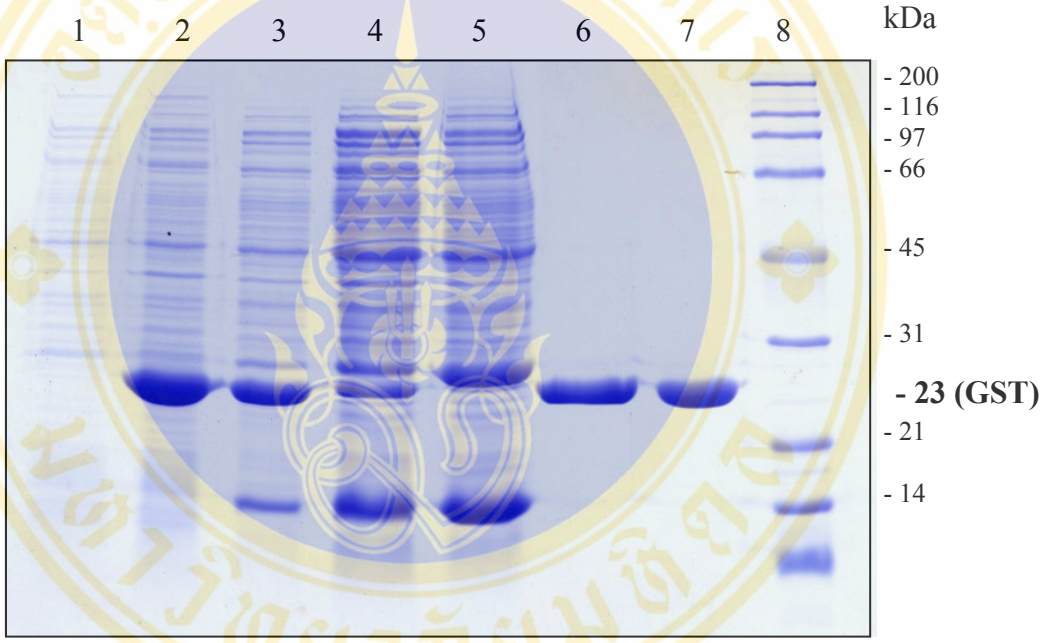

Figure 3.1 The SDS-PAGE of crude extract and purified wild type adGSTD4-4.

SDS-polyacrylamide gel showing the expressed wild type adGSTD4-4 eluted from a GSTrap affinity column. The 23-kDa band is indicated with a bold label.
Lane 1 : 0.05 O.D. of *E.coli* extract before induction by IPTG
Lane 2 : 0.05 O.D. of *E.coli* extract after induction by IPTG
Lane 3 : 25 µg of lysate
Lane 4 : 25 µg of flow through fraction
Lane 5 : 25 µg of wash fraction
Lane 6 : 5 µg of purified enzyme
Lane 7 : 5 µg of purified enzyme (after desalted and concentrated)
Lane 8 : Broad-range marker

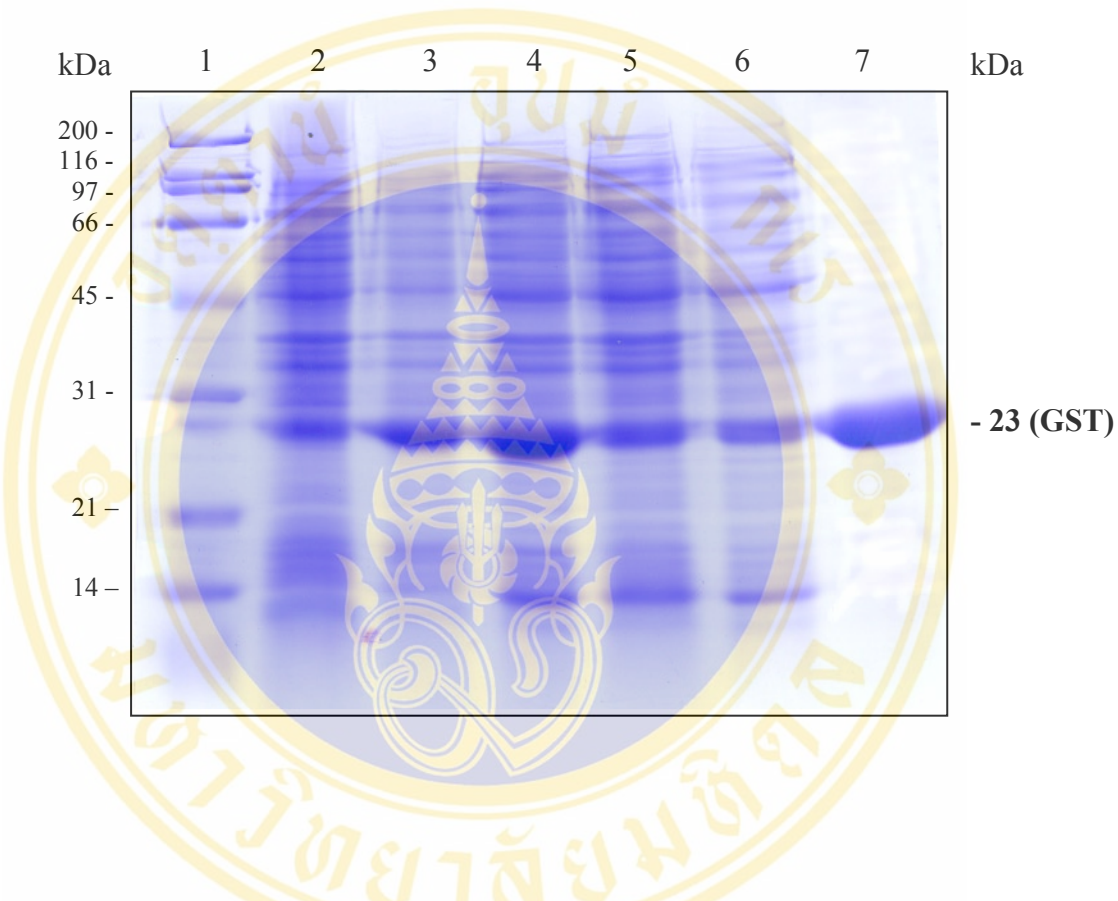

Figure 3.2 The SDS-PAGE of crude extract and purified adGSTD4-Glu75Ala.

SDS-polyacrylamide gel showing the expressed adGSTD4-Glu75Ala eluted from a GSTrap affinity column. The 23-kDa band is indicated with a bold label.

Lane 1 : Broad-range marker

Lane 2 : 0.05 O.D. of *E.coli* extract before induction by IPTG

Lane 3 : 0.05 O.D. of *E.coli* extract after induction by IPTG

Lane 4 : 25 µg of lysate

Lane 5 : 25 µg of flow through fraction

Lane 6 : 25 µg of wash fraction

Lane 7 : 5 µg of purified enzyme

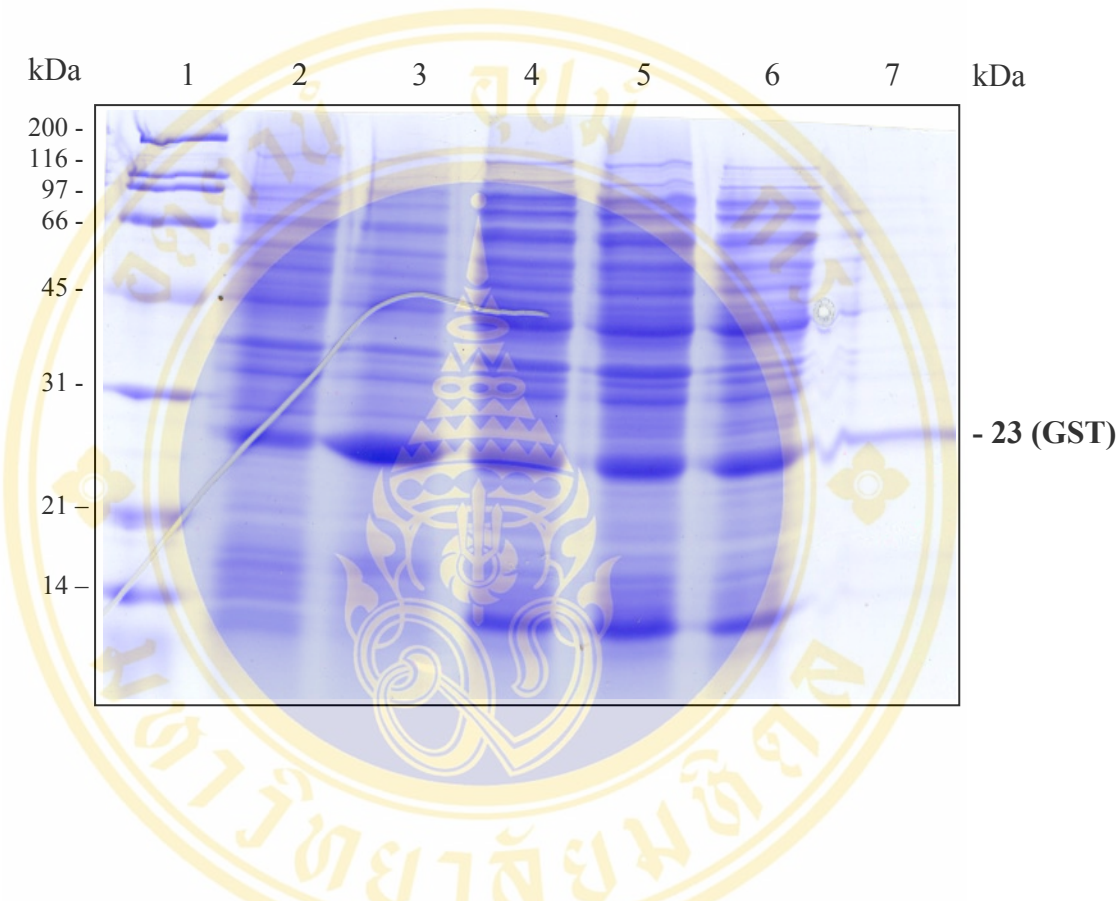

Figure 3.3 The SDS-PAGE of crude extract and purified adGSTD4-Arg96Ala. SDS-polyacrylamide gel showing the expressed adGSTD4-Arg96Ala eluted from a GSTrap affinity column. The 23-kDa band is indicated with a bold label.

Lane 1 : Broad-range marker

Lane 2 : 0.05 O.D. of *E.coli* extract before induction by IPTG

Lane 3 : 0.05 O.D. of *E.coli* extract after induction by IPTG

Lane 4 : 25 μg of lysate

Lane 5 : 25 μg of flow through fraction

Lane 6 : 25 μg of wash fraction

Lane 7 : 5 μg of purified enzyme

3..2 Enzymatic Characterization

3.2.1 Determination of Substrate Specificities

Specific activities toward several GST substrates were determined and demonstrated that the change of single residues resulted in a change of enzyme specificity (**Table 3.2)**. The activity was measured with glutathione and 5 different substrates at the appropriate pH and λ_{max}. CDNB, a general substrate for GSTs, is the substrate that yielded decreasing conjugating activity with both mutants, 1.3-fold for Glu75Ala and 1.8-fold for Arg96Ala. The conjugating activity of the mutants towards DCNB, the mu class substrate, was increased, especially Arg96Ala the activity increased approximately 8-fold. EA, pi class substrate, the mutants yielded about 5-fold more than wild type. Glu75Ala mutant decreased activity toward PNBC, rat theta substrate, approximately 0.3-fold while that of Arg96Ala was increased approximately 3.7-fold. For PNPB, human theta substrate, Glu75Ala possessed higher activity about 1.6-fold. However, the activity toward PNPB of Arg96Ala could not be detected. The results indicated that substitution by alanine at both positions affected the active site conformation by changing specific activity toward five substrates even though the mutant residues are not in the active site pockets.

Table 3.2 Specific activity of the enzymes toward five different substrates.

Enzymes	Specific Activity (µmol/min/mg)				
	CDNB	DCNB	EA	PNPB	PNBC
D4-WT	48.04 ± 1.98	0.03 ± 0.00	0.03 ± 0.02	0.06 ± 0.01	0.03 ± 0.01
D4-Glu75Ala	36.58 ± 5.03	0.06 ± 0.01	0.12 ± 0.01	0.02 ± 0.01	0.06 ± 0.00
D4-Arg96Ala	25.96 ± 0.13	0.27± 0.04	0.18 ± 0.01	0.23 ± 0.02	nd*

* nd = not detectable. The data are mean ± standard deviation from at least 3 independent experiments. The substrate concentrations used were 3 mM 1-chloro-2,4-dinitrobenzene (CDNB), 1 mM 1,2-dichloro-4-nitrobenzene (DCNB), 0.1 mM p-nitrobenzyl chloride (PNBC), 0.1 mM p-nitrophenethyl bromide (PNPB) and 0.2 mM ethacrynic acid (EA).

3.2.2 Determination of Kinetic Parameters

The kinetic parameters were studied by varying concentrations of both GSH and CDNB substrates. The reactions followed Michaelis-Menten kinetics except for Glu75Ala mutant which had a positive cooperativity upon CDNB binding that altered the induced-fit mechanism of the enzymes (93). Kinetic parameters were determined by non-linear regression analysis using Graphpad prism software except Glu75Ala mutant which the parameters were calculated by the Hill equation (see section 2.3.4). Comparison of the kinetic parameters of the mutants with the wild type values showed that the residue changes affected enzymatic properties (**Table 3.3**). Glu75Ala had the same maximal velocity (V_{max}) as the wild type but the replacement of Arg-96 with the non-polar residue, alanine, caused a decrease of 27.4% in the V_{max}. The K_m value of Glu75Ala, which is referred to the affinity binding constant of the substrate, for CDNB was increased approximately 13-fold while the K_m value for GSH was decreased approximately 1.2-fold. This shows that the Glu75 mutant had dramatically affected the active site architecture especially the H-site, the site that provides the structural element for recognition of the broad range of hydrophobic co-substrate. For the Arg96Ala mutant, the active site conformation was also affected; there were approximately 1.3-fold and 1.6-fold increase in the K_m values for CDNB and GSH. The k_{cat}/K_m value, which reflects the catalytic efficiency of the enzyme, for Glu75Ala mutant possesses about a 1.3-fold greater catalytic efficiency for GSH but with a 12.7-fold lower efficiency for CDNB compared to the wild type enzyme. Arg96Ala had a lower efficiency for both CDNB and GSH about 1.6- and 2.2-fold, respectively.

Table 3.3 Michaelis-Menten parameters for adGSTD4-4 and the mutants.

Enzymes	V_{max}	k_{cat}	CDNB		GSH	
			K_m	k_{cat}/K_m	K_m	k_{cat}/K_m
D4-Wild type	53.95 ± 1.30	22.5	0.63 ± 0.09	35.71	0.67 ± 0.05	33.58
D4-Glu75Ala	55.99 ± 0.89	23.26	8.26 ± 2.63	2.82	0.54 ± 0.06	43
D4-Arg96Ala	39.15 ± 0.93	16.24	0.80 ± 0.06	21.95	1.08 ± 0.02	15.02

The data are mean ± standard deviation from at least 3 independent experiments. The units are: V_{max} : µmole/min/mg, K_m : mM, k_{cat} : s-1, k_{cat}/K_m : mM^{-1} s^{-1}.

3.3 Structural Characterization

3.3.1 Stability Assay

All enzymes were prepared at the same concentration (0.1 mg/ml). The remaining activity was measured by withdrawing an appropriate volume at different time points until the remaining activity was less than 50% and the results are shown in **Table 3.4**. The results indicated that the electrostatic interaction networks between two glutamate residues and two arginine residues from helix 3 and helix 4 of both subunits contribute to structural stabilization. The half-life of the mutants showed significantly decreased stability of the enzymes, 7.4-fold for Glu75Ala and 15-fold for Arg96Ala.

Table 3.4 The half-life of the enzymes.

Enzymes	Half-life (min)
D4-Wild type	14.01 ± 1.70
D4-Glu75Ala	1.89 ± 0.13
D4-Arg96Ala	0.91 ± 0.07

The data are mean ± standard deviation from at least 3 independent experiments.

3.3.3 Intrinsic Tryptophan Fluorescence Spectroscopy

Fluorescence spectroscopy is the most extensively used optical spectroscopic method in analytical measurement and scientific investigation (94). Our research area that has benefited from extensive fluorescence investigations is the field of protein structure-function studies. In adGSTs, each subunit has two tryptophan residues which are located in β-sheet 4 in domain I and α-helix 7 in domain II (**Figure 3.4**). The one located in β-sheet 4 in domain I (Trp 63) is in close proximity to the active site, with an involvement in sequestering the substrate glutathione as well as the subunit interface which make it a sensitive fluorescence probe to monitor conformational changes at/near the active site and the inter-subunit area.

The fluorescence spectra of 0.2 mg/ml enzyme were monitored by a Shimadzu RF 5001PC to investigate changes of the amino acid side chains around the

tryptophan residues. The normalized fluorescence spectrum of each mutant was analyzed and compared to the wild type in **Figure 3.5**. The λ_{max} values of the mutants were similar to the wild type, indicating that a similar polarity characterizes the environment of the tryptophan residues present in all enzyme variants. However, the normalized intensities of fluorescence of the Arg96 mutants were approximately 66% decreased. This finding suggests that there are significant conformational changes in the environment of the tryptophan residues located near the subunit interface and the mutation site.

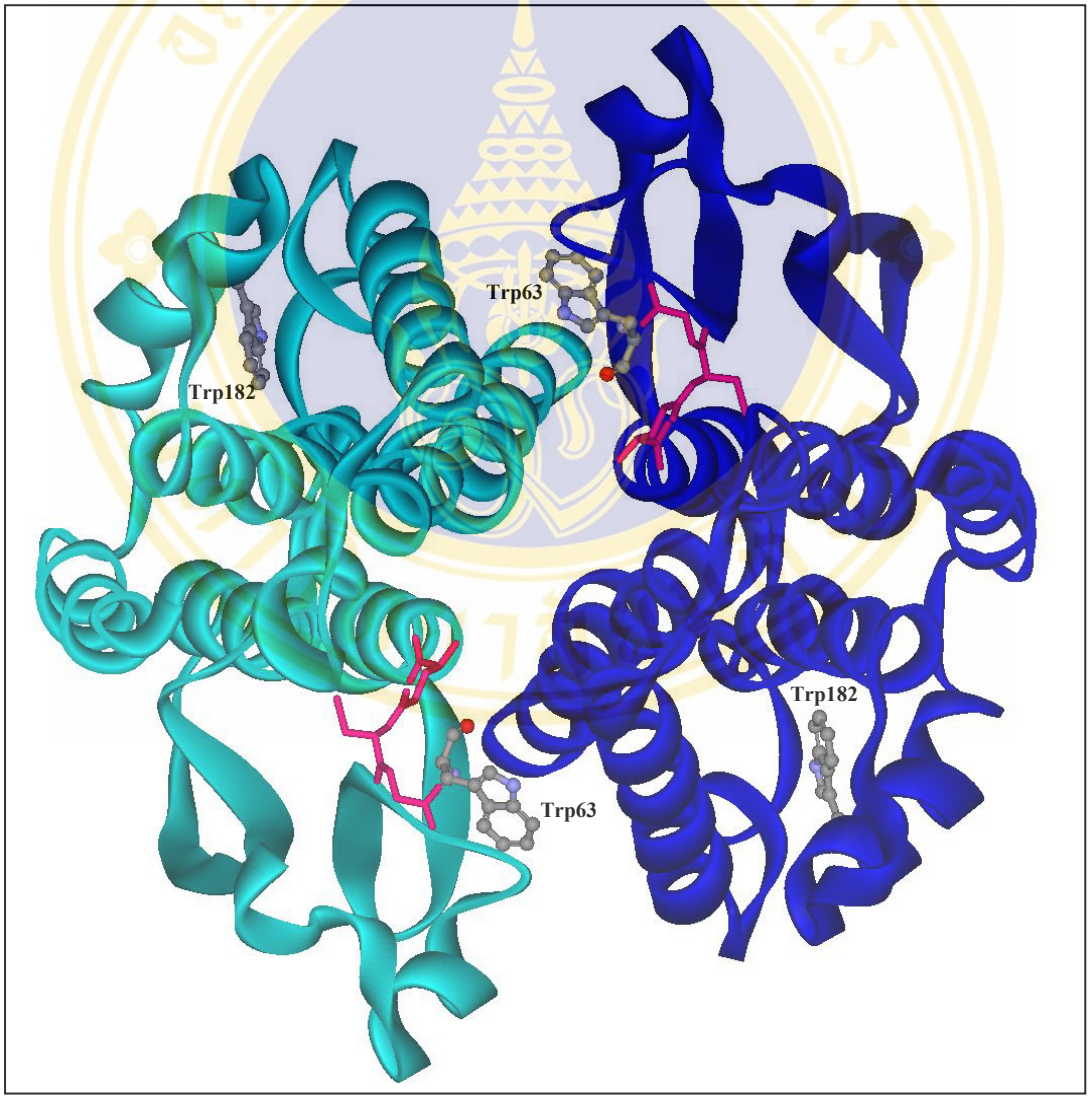

Figure 3.4 Ribbon representation of the adGSTD3-3 with the tryptophan residues. The active site ligands are represented as stick models.

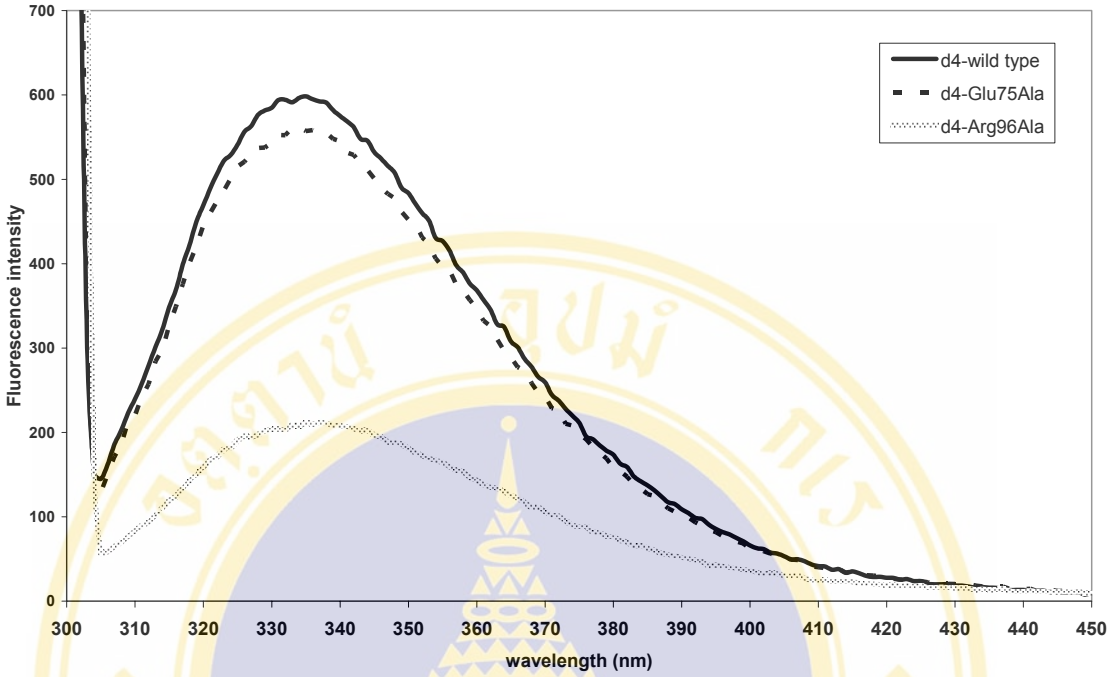

Figure 3.5 The normalized intrinsic tryptophan fluorescence spectra of the wild type adGSTD4-4 and the electrostatic interaction mutants. The data are mean from 3 independent experiments.

3.3.2 Refolding Assay

3.3.2.1 Refolding rate constants and % activity recovery measurement

After rapid dilution into renaturation buffer, the unfolded proteins were monitored for recovered activity as a function of time by withdrawal of appropriate aliquots of the renaturation mixture and immediately assaying for activity. Refolding rate constants were determined by nonlinear regression using a single exponential equation.

Not only do these residues influence the protein stability, they also affect the recovery of the active conformation. Both mutants did not recover the specific activity after being unfolded by 4 M GuHCl (**Table 3.5**). This implies that these residues play a critical role in the folding pathway of the enzymes. The crystal structure shows that the interactions of all four residues, two Glu75 from helix3 and two Arg96 from helix4, consist of both intra- and inter-subunit interactions (**Figure 1.16**). Therefore, a further experiment was performed, intrinsic tryptophan fluorescence spectroscopy. This was to determine whether the loss of these interactions affects tertiary folding of

each subunit or the dimerization of the two subunits, both of which are important to form the complete active site pocket of the enzymes.

Table 3.5 Refolding rate constants and % activity recovery of the enzymes.

Enzymes	Refolding rate constant	% Activity Recovery
D4-WT	0.59 ± 0.03	19.70 ± 0.70
D4-Glu75Ala	nd*	0.00
D4-Arg96Ala	nd*	0.00

*nd is not detectable. The data are mean ± standard deviation from at least 3 independent experiments.

3.3.2.2 Intrinsic tryptophan fluorescence spectroscopy

The different λ_{max} values of the native (335 nm) and the unfolded form (355 nm) of the protein, the fluorescence spectra of native, unfolded and refolded enzymes were monitored by a Shimadzu RF 5001PC to compare the tertiary structure of the protein in each state (**Figure 3.6**).

The results demonstrated that all enzymes can be refolded back to the same back bone architecture as the native form as showed by the similar λ_{max} values. However, the normalized intensities fluorescence spectra were different which suggested that there were conformational changes of the amino acid side chains surrounding the tryptophan residues.

From the refolding assay in terms of both catalytic and structural experiments, the data suggested that loss of the conserved electrostatic interactions had a dramatic effect on the dimerization process of the enzymes, which is important to form the complete active site pocket.

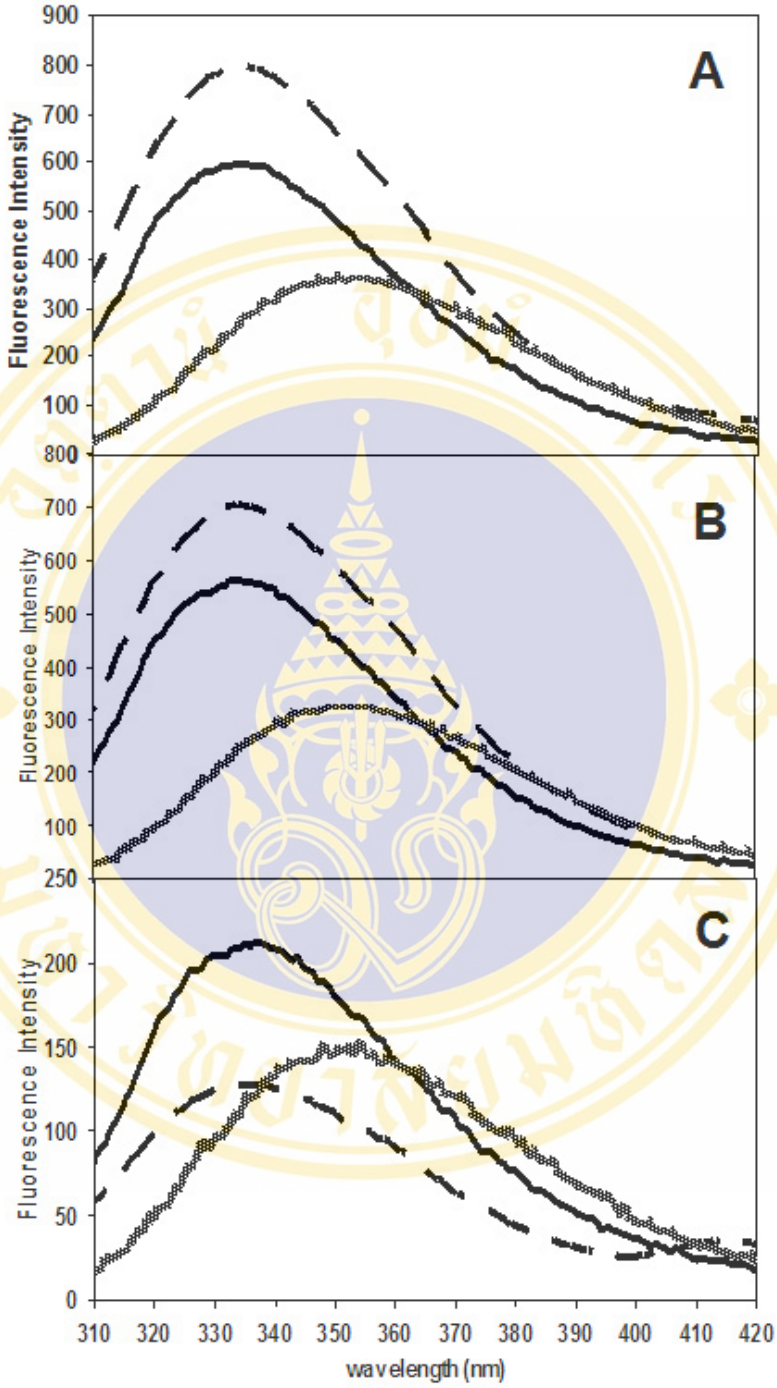

Figure 3.6 The normalized intrinsic tryptophan fluorescence spectra compared among the native, refolded and unfolded form of adGSTD4-4 and the electrostatic interaction mutants.

(A) adGSTD4-4 wild type, (B) adGSTD4-Glu75Ala and (C) adGSTD4-Arg96Ala. The data are mean from at least 3 independent experiments.

(▬ : a native form, ▪▪▪ : a refolded form and ▬ : an unfolded form of the enzyme)

3.3.4 ANS Binding Assay

3.3.4.1 ANS Binding Spectra Measurement

The anionic dye ANS (8-anilino-1-naphthalenesulfonate) is a much used fluorescent “hydrophobic probe” for examining the nonpolar character of proteins such as the dimer interface of the multimeric enzymes. Binding of ANS to proteins comes from both its nonpolar anilinonapthalene and the negatively charged sulfonate group. It is important to realize that ANS fluorescence may not require immersion of the anilinonapthalene group in the hydrophobic environment inside the protein. It requires only removal of the ANS organic moiety from water, an effective quencher of ANS fluorescence (95;96). For GSTs, the anionic dye ANS can bind to a site at the dimer interface (97). Therefore, the dye can be utilized as a probe to monitor the appearance/disappearance of hydrophobic patches or surfaces on proteins that are undergoing structural changes.

When ANS binds adGSTD4-4, its fluorescence was enhanced accompanied by a blue shift in its emission maximum from 514 nm (free ANS in buffer) to 482 nm for both wild type and mutants (**Figure 3.7**), indicating that the polarity of the binding site has become more hydrophobic. The spectrum of ANS in phosphate buffer pH 6.5 was subtracted from the spectra of the protein binding ANS. A total of three scans each for blank and sample were recorded and averaged for each enzyme. When compared with the wild type, there was no change in the emission maximum wavelength of ANS bound to both mutants **(Figure 3.8)**. For the ANS fluorescence intensity, Arg96Ala appeared to exhibit a significantly lower capacity to bind ANS as suggested by the 5-fold decrease in ANS fluorescence intensity while Glu75Ala mutant show a similar intensity as the wild type.

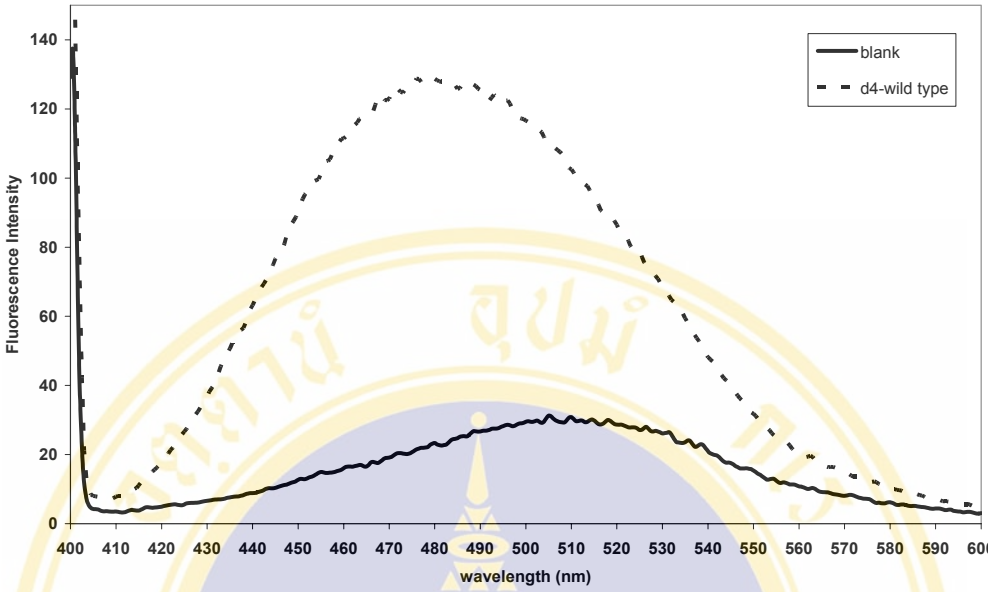

Figure 3.7 Fluorescence emission spectra of ANS bound to the adGSTD4-4. The data are mean from at least 3 independent experiments.

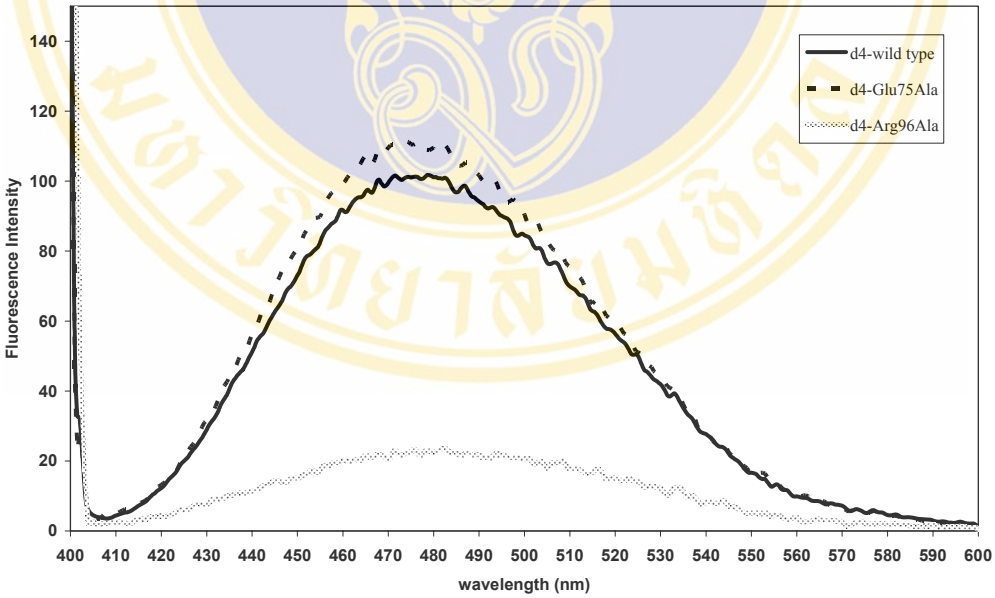

Figure 3.8 ANS binding spectra of the wide type adGSTD4-4 and the electrostatic interaction mutants. The spectra were measured immediately after addition of ANS. As ANS fluorescence is quenched by water, alteration of the fluorescence intensity of protein-bound ANS is highly dependent upon its accessibility to water. The data are mean from at least 3 independent experiments.

3.3.4.2 Remaining Activity Measurement

To study the impact of ANS on the enzyme conformation, the enzyme activity in presence and absence of ANS was measured as an indirect probe by using the standard reaction assay. The results showed that in the reaction with ANS present the specific activity of all enzymes was decreased to a similar ratio which is shown in terms of percent inhibition (**Table 3.6)**. It indicated that ANS spectra changes in **Figure 3.8** did not occur from conformation changes of the enzymes induced by the ANS dye.

Table 3.6 The effect of ANS on specific activity of the enzymes.

Enzymes	% inhibition
D4-wild type	18.37 ± 1.20
D4-Glu75Ala	22.52 ± 0.82
D4-Arg96Ala	18.82 ± 3.89

The data are mean ± standard deviation from at least 3 independent experiments.

CHAPTER 4
RESULTS: THE HYDROPHOBIC INTERACTIONS AT THE CENTER OF THE SUBUNIT INTERFACE

This subunit interface region shows the most difference in amino acid residues at the equivalent positions between adGSTD3-3 and adGSTD4-4 (**Figure 1.17**). Therefore, to study the affect of the different hydrophobic amino acid at the equivalent positions in the center of the subunit interface of the two isozymes, disruption of the amino acid side chain packing by switching the amino acid side chain of the isozymes was performed by these mutations; Tyr98Phe, Met101Val, Gly102Ala and Tyr98Phe/Met101Val/Gly102Ala of adGSTD3-3 and Phe104Tyr, Val107Met, Ala108Gly and Phe104Tyr/Val107Met/ Ala108Gly of adGSTD4-4.

4.1 Expression and Purification of the enzymes in *E.coli*

The expression constructs of recombinant plasmid were sequenced and transformed into *E.coli* BL21DE3plysS. The expression of the 23 kDa GST in *E.coli* was controlled by the T_7 promoter therefore the plasmids encoding the wild type or mutant were highly expressed in *E.coli* BL21DE3plysS upon IPTG induction. All the wild type and mutant were purified from the lysate by affinity chromatography on immobilized GSH. The purity of the enzymes was determined by SDS-PAGE as shown in **Figures 4.1-4.10**. The protein concentrations of GSTs were measured in *E.coli* lysate and purified proteins (elution fraction) by using Bradford reagent. The yields are shown in **Table 4.1**.

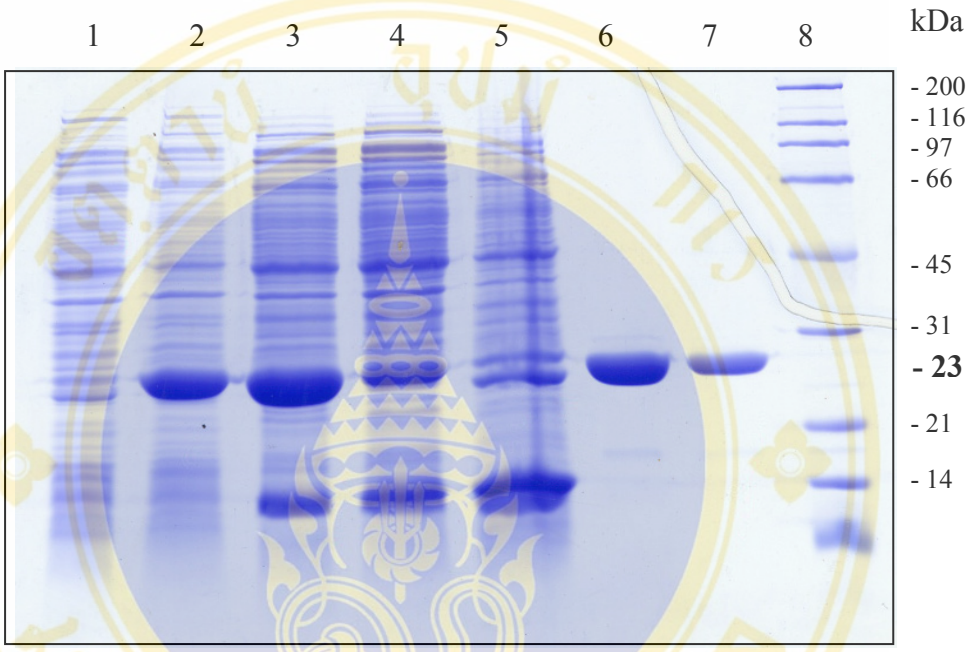

Figure 4.1 The SDS-PAGE of crude extract and purified wild type adGSTD3-3.

SDS-polyacrylamide gel showing the expressed wild type adGSTD3-3 eluted from a GSTrap affinity column. The 23-kDa band is indicated with a bold label.

Lane 1 : 0.05 O.D. of *E.coli* extract before induction by IPTG

Lane 2 : 0.05 O.D. of *E.coli* extract after induction by IPTG

Lane 3 : 25 µg of lysate

Lane 4 : 25 µg of flow through fraction

Lane 5 : 25 µg of wash fraction

Lane 6 : 5 µg of purified enzyme

Lane 7 : 5 µg of purified enzyme (after desalted and concentrated)

Lane 8 : Broad-range marker

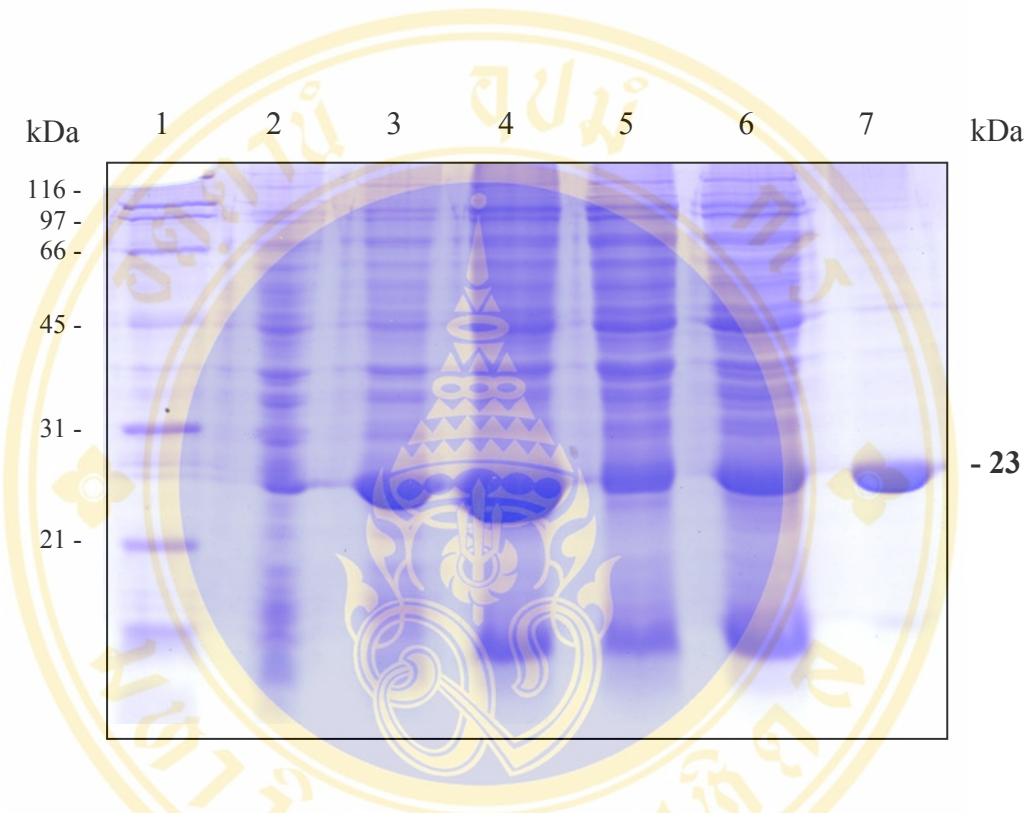

Figure 4.2 The SDS-PAGE of crude extract and purified adGSTD3-Tyr98Phe.

SDS-polyacrylamide gel showing the expressed adGSTD3-Tyr98Phe eluted from a GSTrap affinity column. The 23-kDa band is indicated with a bold label.

Lane 1 : Broad-range marker

Lane 2 : 0.05 O.D. of *E.coli* extract before induction by IPTG

Lane 3 : 0.05 O.D. of *E.coli* extract after induction by IPTG

Lane 4 : 25 µg of lysate

Lane 5 : 25 µg of flow through fraction

Lane 6 : 25 µg of wash fraction

Lane 7 : 5 µg of purified enzyme

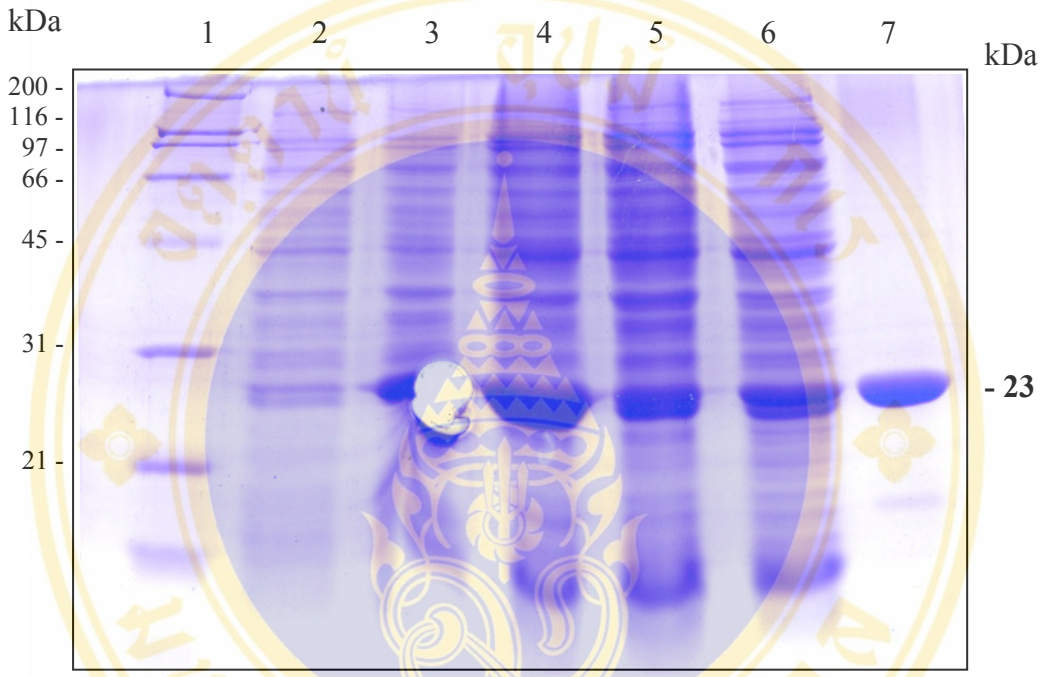

Figure 4.3 The SDS-PAGE of crude extract and purified adGSTD3-Met101Val.

SDS-polyacrylamide gel showing the expressed adGSTD3-Met101Ala eluted from a GSTrap affinity column. The 23-kDa band is indicated with a bold label.

Lane 1 : Broad-range marker

Lane 2 : 0.05 O.D. of *E.coli* extract before induction by IPTG

Lane 3 : 0.05 O.D. of *E.coli* extract after induction by IPTG

Lane 4 : 25 µg of lysate

Lane 5 : 25 µg of flow through fraction

Lane 6 : 25 µg of wash fraction

Lane 7 : 5 µg of purified enzyme

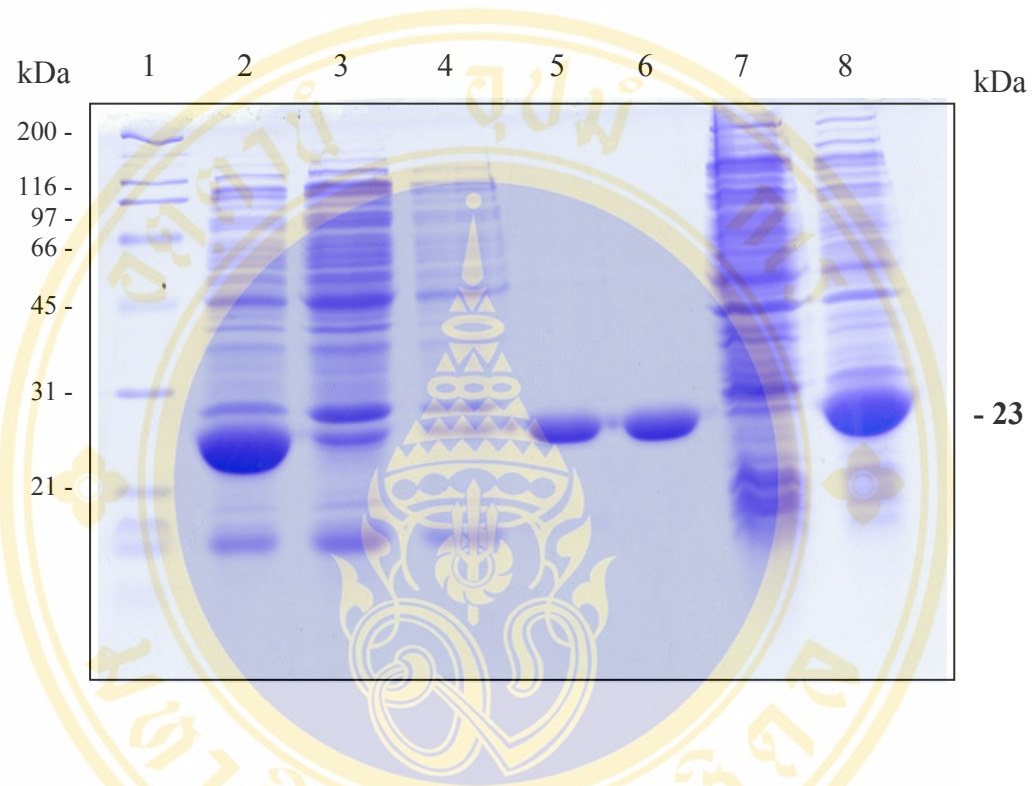

Figure 4.4 The SDS-PAGE of crude extract and purified adGSTD3-Gly102Ala.

SDS-polyacrylamide gel showing the expressed adGSTD3-Gly102Ala eluted from a GSTrap affinity column. The 23-kDa band is indicated with a bold label.

Lane 1 : Broad-range marker

Lane 2 : 25 µg of lysate

Lane 3 : 25 µg of flow through fraction

Lane 4 : 25 µg of wash fraction

Lane 5 : 5 µg of purified enzyme

Lane 6 : 5 µg of purified enzyme (after desalted and concentrated)

Lane 7 : 0.05 O.D. of *E.coli* extract before induction by IPTG

Lane 8 : 0.05 O.D. of *E.coli* extract after induction by IPTG

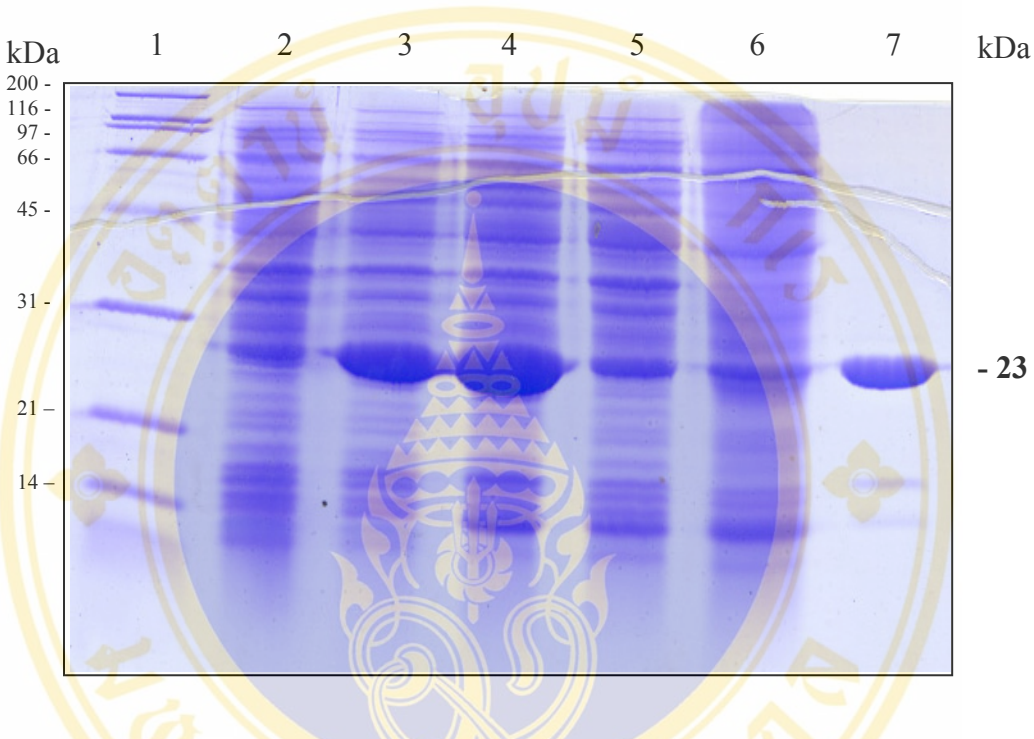

Figure 4.5 The SDS-PAGE of crude extract and purified adGSTD3-Tyr98Phe/Met101Val/Gly102Ala.

SDS-polyacrylamide gel showing the expressed adGSTD3- Tyr98Phe/Met101Val/ Gly102Ala eluted from a GSTrap affinity column. The 23-kDa band is indicated with a bold label.

Lane 1 : Broad-range marker

Lane 2 : 0.05 O.D. of *E.coli* extract before induction by IPTG

Lane 3 : 0.05 O.D. of *E.coli* extract after induction by IPTG

Lane 4 : 25 µg of lysate

Lane 5 : 25 µg of flow through fraction

Lane 6 : 25 µg of wash fraction

Lane 7 : 5 µg of purified enzyme

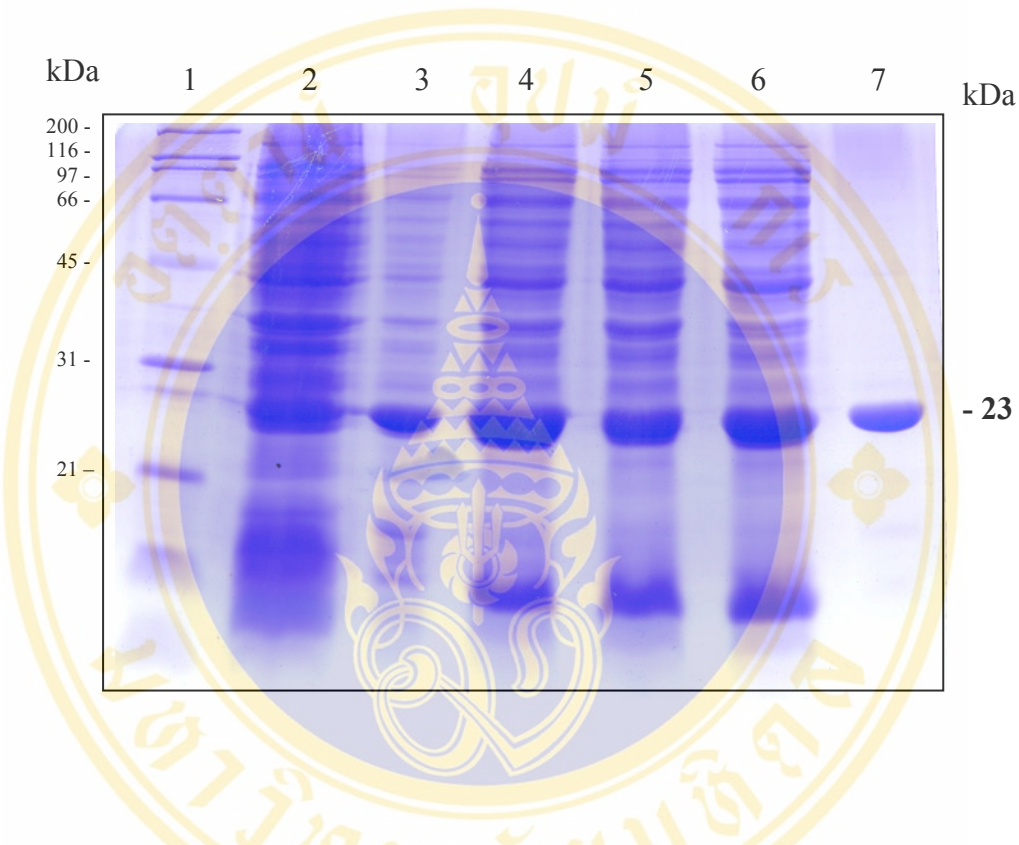

Figure 4.6 The SDS-PAGE of crude extract and purified adGSTD4-Phe104Tyr.

SDS-polyacrylamide gel showing the expressed adGSTD4-Phe104Tyr eluted from a GSTrap affinity column. The 23-kDa band is indicated with a bold label.

Lane 1 : Broad-range marker

Lane 2 : 0.05 O.D. of *E.coli* extract before induction by IPTG

Lane 3 : 0.05 O.D. of *E.coli* extract after induction by IPTG

Lane 4 : 25 μg of lysate

Lane 5 : 25 μg of flow through fraction

Lane 6 : 25 μg of wash fraction

Lane 7 : 5 μg of purified enzyme

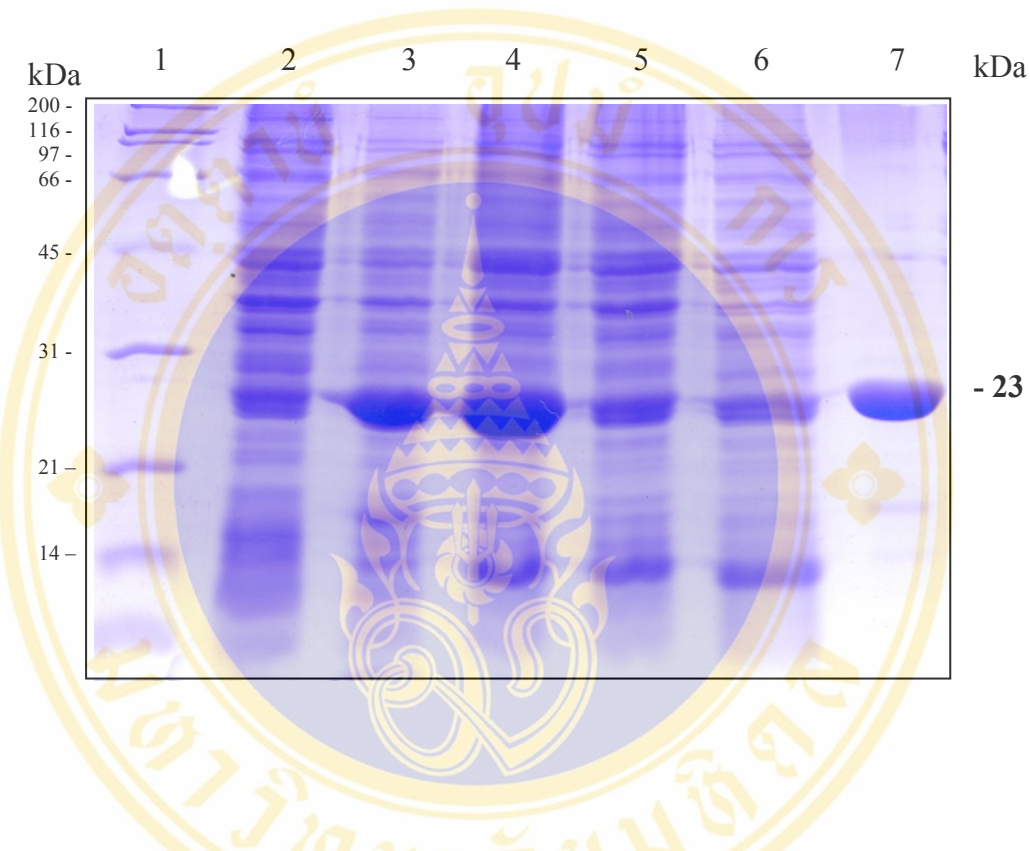

Figure 4.7 The SDS-PAGE of crude extract and purified adGSTD4-Val107Ala.

SDS-polyacrylamide gel showing the expressed adGSTD4-Val107Ala eluted from a GSTrap affinity column. The 23-kDa band is indicated with a bold label.

Lane 1 : Broad-range marker

Lane 2 : 0.05 O.D. of *E.coli* extract before induction by IPTG

Lane 3 : 0.05 O.D. of *E.coli* extract after induction by IPTG

Lane 4 : 25 µg of lysate

Lane 5 : 25 µg of flow through fraction

Lane 6 : 25 µg of wash fraction

Lane 7 : 5 µg of purified enzyme

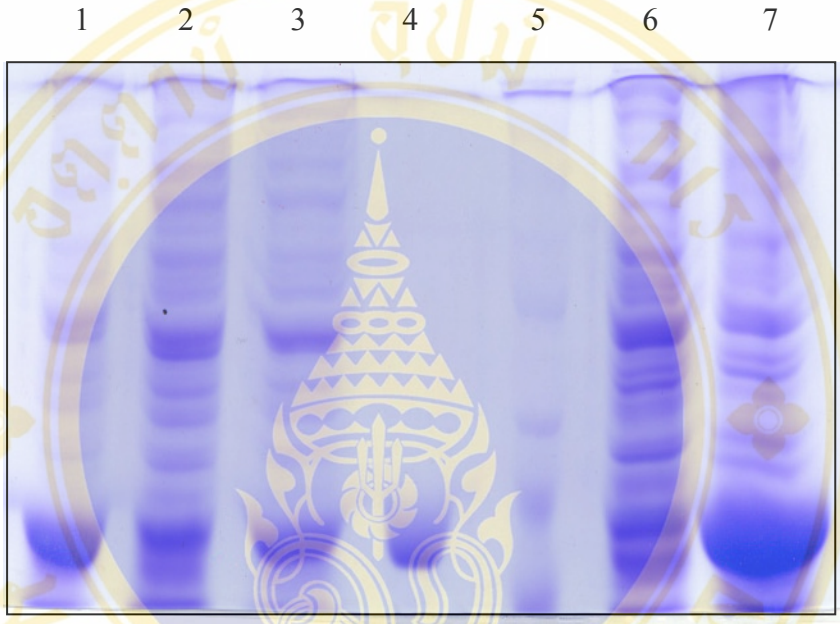

Figure 4.8 The SDS-PAGE of crude extract and purified adGSTD4-Val107Met. SDS-polyacrylamide gel showing the expressed adGSTD4-Val107Met eluted from a GSTrap affinity column. The 23-kDa band is indicated with a bold label.

Lane 1 : 25 μg of lysate

Lane 2 : 25 μg of flow through fraction

Lane 3 : 25 μg of wash fraction

Lane 4 : 5 μg of purified enzyme

Lane 5 : Broad-range marker

Lane 6 : 0.05 O.D. of *E.coli* extract before induction by IPTG

Lane 7 : 0.05 O.D. of *E.coli* extract after induction by IPTG

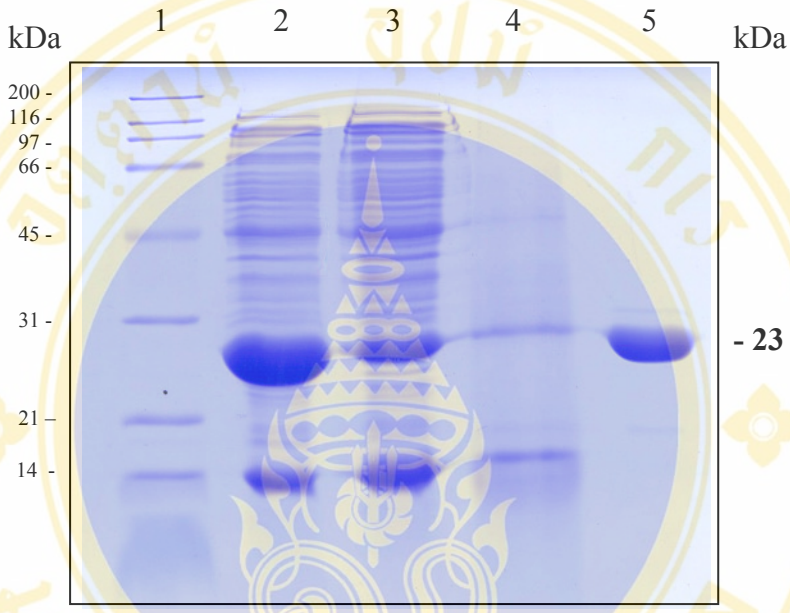

Figure 4.9 The SDS-PAGE of crude extract and purified adGSTD4-Ala108Gly.

SDS-polyacrylamide gel showing the expressed adGSTD4-Ala108Gly eluted from a GSTrap affinity column. The 23-kDa band is indicated with a bold label.

Lane 1 : Broad-range marker

Lane 2 : 25 µg of lysate

Lane 3 : 25 µg of flow through fraction

Lane 4 : 25 µg of wash fraction

Lane 5 : 5 µg of purified enzyme

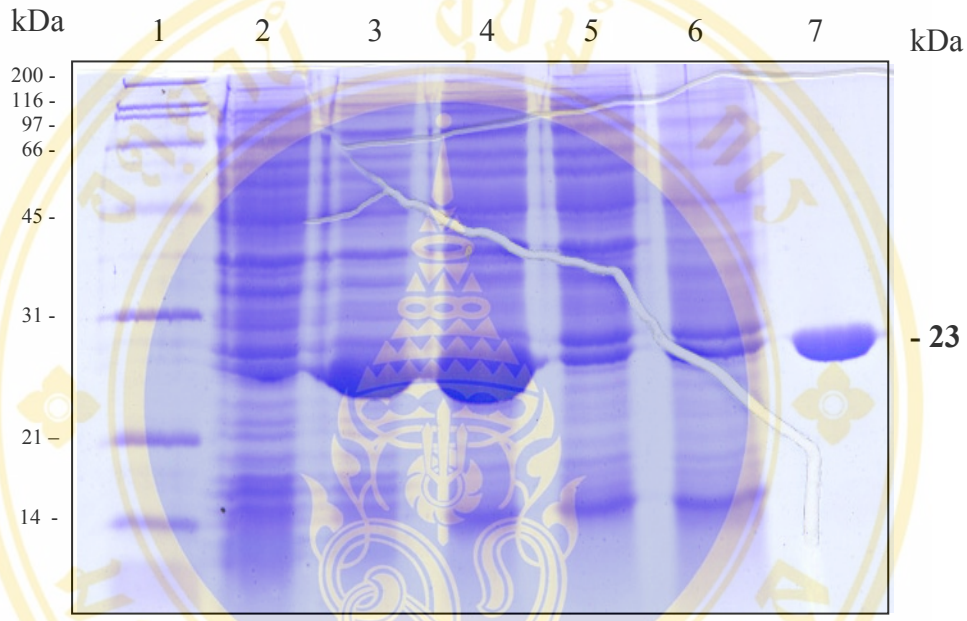

Figure 4.10 The SDS-PAGE of crude extract and purified adGSTD4-Phe104Tyr/Val107Met/Ala108Gly.

SDS-polyacrylamide gel showing the expressed adGSTD4-Phe104Tyr/Val107Met/Ala108Gly eluted from a GSTrap affinity column. The 23-kDa band is indicated with a bold label.

Lane 1 : Broad-range marker

Lane 2 : 0.05 O.D. of *E.coli* extract before induction by IPTG

Lane 3 : 0.05 O.D. of *E.coli* extract after induction by IPTG

Lane 4 : 25 μg of lysate

Lane 5 : 25 μg of flow through fraction

Lane 6 : 25 μg of wash fraction

Lane 7 : 5 μg of purified enzyme

Table 4.1 Purification of the mutant enzymes

Enzymes	Fraction	Total protein (mg)	% Yield (%)
D3-wild type	Lysate	50.75	
	Elution	27.25	53.69
D3-Tyr98Phe	Lysate	91.83	
	Elution	45.15	49.17
D3-Met101Val	Lysate	124.20	
	Elution	74.50	59.98
D3-Gly102Ala	Lysate	77.71	
	Elution	37.01	47.63
D3-Tyr98Phe/Met101Val/Gly102Ala	Lysate	127.89	
	Elution	74.60	58.33
D4-wild type	Lysate	58.20	
	Elution	35.65	61.25
D4-Phe104Tyr	Lysate	98.00	
	Elution	41.35	42.19
D4-Val107Met	Lysate	112.45	
	Elution	67.50	60.03
D4-Ala108Gly	Lysate	54.68	
	Elution	32.38	59.23
D4-Phe104Tyr/Val107Met/Ala108Gly	Lysate	92.86	
	Elution	73.05	78.67

From all enzyme purifications, approximately 40-80 % of total GST protein from the bacterial lysate was obtained from glutathione affinity column. All the purified enzymes were stored at -20˚C for further characterization.

4.2 Enzymatic Characterization

4.2.1 Determination of Substrate Specificities

Specific activities toward five GST substrates were determined and shown in **Table 4.2 and 4.3**. Specific activities toward CDNB of the equivalent mutations of adGSTD3-3 and adGSTD4-4 yielded approximately 2-fold less than that of the wild types except adGSTD4-Ala108Gly and the triple mutants which possessed the same activity as the wild types. The conjugating activity of the mutants towards DCNB was approximately the same as the wild type except Met101Val and Gly102Ala of adGSTD3-3 which had about 5- and 3-fold less than the wild type. The activity toward EA of the adGSTD3-3 mutants was approximately the same as the wild type while that of Gly102Ala was not detectable. For the adGSTD4-4 mutations, the conjugating activity toward EA showed various affects; the activity of Ala108Gly was the same as the wild type while that of Val107Met increased about 6.7-fold. In addition, the Phe104Tyr and triple mutant decreased the activity about 2- and 15-fold, respectively. Specific activities toward PNPB of several mutants did not change. However, for Val107Met, the activity toward PNPB was increased about 5-fold while the activity of Ala108Gly and the triple mutants was not detectable. With PNBC as a substrate, all mutations demonstrated that their activities were decreased. Especially, Val107Met, the activity was not detectable. The data demonstrated that the change of these equivalent residues resulted in a change of enzyme specificity and active site conformations.

Table 4.2 Specific activity of the adGSTD3-3 toward five substrates.

Enzymes	Specific Activity (µmol/min/mg)				
	CDNB	DCNB	EA	PNPB	PNBC
D3-Wild Type	85.27 ± 3.23	0.25 ± 0.01	0.10 ± 0.05	nd*	0.13 ± 0.01
D3-Tyr98Phe	46.94 ± 6.38	0.23 ± 0.03	0.03 ± 0.01	nd*	0.05 ± 0.00
D3-Met101Val	41.11 ± 0.81	0.05 ± 0.01	0.08 ± 0.02	nd*	0.09 ± 0.00
D3-Gly102Ala	46.82 ± 0.25	0.08 ± 0.01	nd*	nd*	0.05 ± 0.00
D3-Tyr98Phe/Met101Val/Gly102Ala	84.77 ± 5.47	0.21 ± 0.01	0.15 ± 0.01	nd*	0.08 ± 0.00

* nd = not detectable. The data are mean ± standard deviation from at least 3 independent experiments. The substrate concentrations used were 1 mM CDNB, 1 mM DCNB, 0.1 mM PNBC, 0.1 mM PNPB and 0.2 mM EA.

Table 4.3 Specific activity of the adGSTD4-4 toward five substrates.

Enzymes	Specific Activity (µmol/min/mg)				
	CDNB	DCNB	EA	PNPB	PNBC
D4-Wild Type	56.77 ± 3.24	0.04 ± 0.01	0.31 ± 0.01	0.06 ± 0.01	0.19 ± 0.01
D4-Phe104Tyr	28.49 ± 2.24	0.06 ± 0.01	0.14 ± 0.01	0.05 ± 0.01	0.11 ± 0.05
D4-Val107Met	21.99 ± 2.29	0.08± 0.004	2.06 ± 0.29	0.31 ± 0.08	nd*
D4-Ala108Gly	55.31 ± 2.07	0.06 ± 0.02	0.32 ± 0.01	nd*	0.08 ±0.02
D4-Phe104Tyr/Val107Met/Ala108Gly	53.76 ± 1.43	0.05 ± 0.01	0.02 ± 0.00	nd*	0.04 ± 0.01

* nd = not detectable. The data are mean ± standard deviation from at least 3 independent experiments. The substrate concentrations used were 3 mM CDNB, 1 mM DCNB, 0.1 mM PNBC, 0.1 mM PNPB and 0.2 mM EA.

4.2.2 Determination of Kinetic Parameters

The kinetic parameters were studied by varying concentrations of both GSH and CDNB substrates. Comparison of the kinetic parameters showed that the residue changes affected enzymatic properties. (**Tables 4.4 and 4.5**)

Table 4.4 Michaelis-Menten parameters for adGSTD3-3 and the mutants.

Enzymes	Vmax	kcat	CDNB		GSH	
			Km	kcat/Km	Km	kcat/Km
D3-Wild type	98.34 ± 0.47	39.15	0.15 ± 0.01	258.04	0.29 ± 0.04	113.86
D3-Tyr98Phe	62.97± 0.58	24.94	0.12± 0.01	212.88	0.47± 0.05	53.06
D3-Met101Val	65.45 ± 1.67	26.03	0.72 ± 0.06	36.26	1.04 ± 0.06	25.03
D3-Gly102Ala	59.01 ± 2.35	23.51	0.37 ± 0.02	63.26	2.94 ± 0.38	7.99
D3- Tyr98Phe/Met101Val/Gly102Ala	102.8 ± 1.32	40.68	0.28 ± 0.03	146.81	1.12± 0.07	36.74

The data are mean ± standard deviation from at least 3 independent experiments. The units are: V_{max} : µmole/min/mg, K_m : mM, k_{cat} : s-1, k_{cat}/K_m : mM^{-1} s^{-1}.

Table 4.5 Michaelis-Menten parameters for adGST4-4 and the mutants.

Enzymes	Vmax	kcat	CDNB		GSH	
			Km	kcat/Km	Km	kcat/Km
D4-Wild type	53.95 ± 1.30	22.5	0.63 ± 0.09	35.71	0.67 ± 0.05	33.58
D4-Phe104Tyr	37.17 ± 0.14	15.5	0.52 ± 0.03	29.81	24.01 ± 2.94	0.65
D4-Val107Met	32.77 ± 0.89	13.69	1.6 ± 0.08	8.56	0.76 ± 0.11	17.96
D4-Ala108Gly	55.76 ± 2.03	26.77	0.87 ± 0.07	26.77	0.73 ± 0.12	36.67
D4- Phe104Tyr/Val107Met/Ala108Gly	78.03 ± 0.98	32.53	0.72 ± 0.04	45.18	0.25 ± 0.02	130.32

The data are mean ± standard deviation from at least 3 independent experiments. The units are: V_{max} : µmole/min/mg, K_m : mM, k_{cat} : s-1, k_{cat}/K_m : mM^{-1} s^{-1}.

All of the adGSTD3-3 single mutants had a significant decrease of 40% in the V_{max} but the replacement of three equivalent residues as a triple mutant caused the same maximal velocity (V_{max}) as the wild type. Whereas the V_{max} of adGSTD4-4 mutants showed a different trend; only Phe104Tyr and Val107Met had a significant decrease of 40% in the V_{max}. For the other equivalent position, Ala108, replacement by glycine did not affect the maximal velocity. However, the triple mutant of adGSTD4-4 caused an increase of approximately 50 % in the V_{max} value.

At the equivalent position mutations, adGSTD3-Tyr98Phe and adGSTD4-Phe104Tyr, affected the affinity toward glutathione (GSH) as shown by the K_m value. The K_m values of the mutants were increased approximately 1.6-fold and 35.8-fold for Tyr98Phe and Phe104Tyr, respectively. For Phe104Tyr mutant, there was a negative cooperativity upon GSH binding suggesting that the induced-fit mechanism was altered by the mutation (93). The Hill coefficient was calculated from the slope of the Hill plot according to the Hill equation (see section 2.3.4). For the second equivalent position, adGSTD3-Met101 and adGSTD4-Val107, the mutations caused approximately 4.8- and 2.5-fold increase in the K_m values for CDNB, respectively, and approximately 3.6-fold increase in the K_m values for GSH for Met101Val. However, replacement of Val107 by methionine did not affect the affinity toward GSH. For the third position, adGSTD3-Gly102 and adGSTD4-Ala108, the mutations affected the affinity toward both substrates like the second equivalent position where the mutations caused increases in the K_m values for CDNB of about 4- and 1.4-fold, respectively, and also an increase in the K_m values for GSH for Gly102Ala of about 10-fold. However, the Ala108Gly mutant did not affect the affinity toward GSH. The triple mutations, replacements of the three equivalent positions with the residue of the other isozyme, possessed a similar trend as the mutations at the second and the third equivalent position. The K_m values toward CDNB of both triple mutants increased by approximately 1.9-fold for adGSTD3-3 mutant and 1.2-fold for adGSTD4-4 mutant. For the co-substrate, GSH, the K_m value of the adGSTD3 triple mutant also increased about 3.9-fold however that of the adGSTD4 triple mutant decreased about 2.7-fold compared to the respective wild type enzyme.

For the catalytic efficiency of the enzyme, the k_{cat}/K_m value, the first and the second equivalent position mutants, Tyr98Phe and Met101Val of adGSTD3-3 and

Phe104Tyr and Val107Met of adGSTD4-4, had a lower efficiency toward both CDNB and GSH, especially the Phe104Tyr mutant, which had a negative cooperativity between the two active sites, the catalytic efficiency was decreased approximately 51.7-fold. At the third equivalent position, Gly102Ala of adGSTD3-3 and Ala108Gly of adGSTD4-4, the efficiency toward CDNB behaved in the same way by decreasing about 4.1- and 1.3-fold, respectively. However, the efficiency toward GSH of both mutants was different in that the efficiency of Gly102Ala decreased approximately 14.2-fold however that of Ala108Gly did not alter from the wild type. For the last mutations, the triple mutants, influenced the catalytic efficiency in an opposite trend, that was the catalytic efficiency of adGSTD3-triple mutant decreased approximately 1.8- and 3.1-fold toward CDNB and GSH, respectively while that of the adGSTD4-4 triple mutant increased about 1.2- and 3.9-fold toward CDNB and GSH, respectively.

The crystal structures of both isozymes showed that all selected equivalent positions located in the active site indicating that the whole electrostatic field in the active site pocket was disturbed by the mutations thereby altering the catalytic parameters of the enzymes. Moreover, their locations, the interface of two domains which provided different substrate binding sites for GSH and the hydrophobic substrate, gave these residues influence on both substrates binding as showed by the K_m values.

4.3 Structural Characterization

4.3.1 Stability Assay

After incubation at 45ºC, the remaining activity was measured by withdrawing an appropriate volume at different time points until the remaining activity was less than 50% and the results are shown in **Tables 4.6-4.7**. The haft-life of several mutants possessed similar stability as the wild type enzymes. However, there were four mutants which had thermal stability significantly changed. Two of them were the mutants at the same equivalent position, adGSTD3-Gly102 and adGSTD4-Ala108. Replacement of glycine by alanine in adGSTD3 at this position caused decreases of about 8-fold in half-life, whereas, glycine substitution of adGSTD4 showed an

increase of about 4.7-fold. The other two mutants that showed stability changes were the triple mutant of adGSTD3-3 and the adGST4-4 mutant with valine replaced by methionine. The former mutant had half-life of approximately 0.8-fold less than the wild type and the later had approximately 3-fold less than the wild type.

Table 4.6 The Half-life of the adGSTD3-3 and the mutants.

Enzymes	Half-life(min)
D3-Wild type	2.71 ± 0.35
D3-Tyr98Phe	3.12 ± 0.33
D3-Met101Val	2.77 ± 0.43
D3-Gly102Ala	0.34 ± 0.03
D3- Tyr98Phe/Met101Val/Gly102Ala	1.88 ± 0.01

Table 4.7 The Half-life of the adGSTD4-4 and the mutants.

Enzymes	Half-life(min)
D4-Wild type	14.01 ± 1.70
D4-Phe104Tyr	17.14 ± 1.76
D4-Val107Met	4.76 ± 0.15
D4-Ala108Gly	65.38 ± 1.45
D4- Phe104Tyr/Val107Met/Ala108Gly	16.68 ± 1.23

4.4.2 Intrinsic Tryptophan Fluorescence Spectroscopy

The fluorescence spectra of 0.2 mg/ml enzyme were monitored by a Shimadzu RF 5001PC to investigate changes of the amino acid side chain around the tryptophan residues. The normalized fluorescence spectra of adGSTD3-3 and adGSTD4-4 wild types are showed in **Figure 4.11**. Both isozymes have two tryptophan residues at the equivalent position. The same λ_{max} values (335 nm) indicate a similar polarity of the tryptophan environment. However, the normalized intensities of fluorescence of the two enzymes were different suggesting that there are conformational differences that characterize the environment of the tryptophan residues.

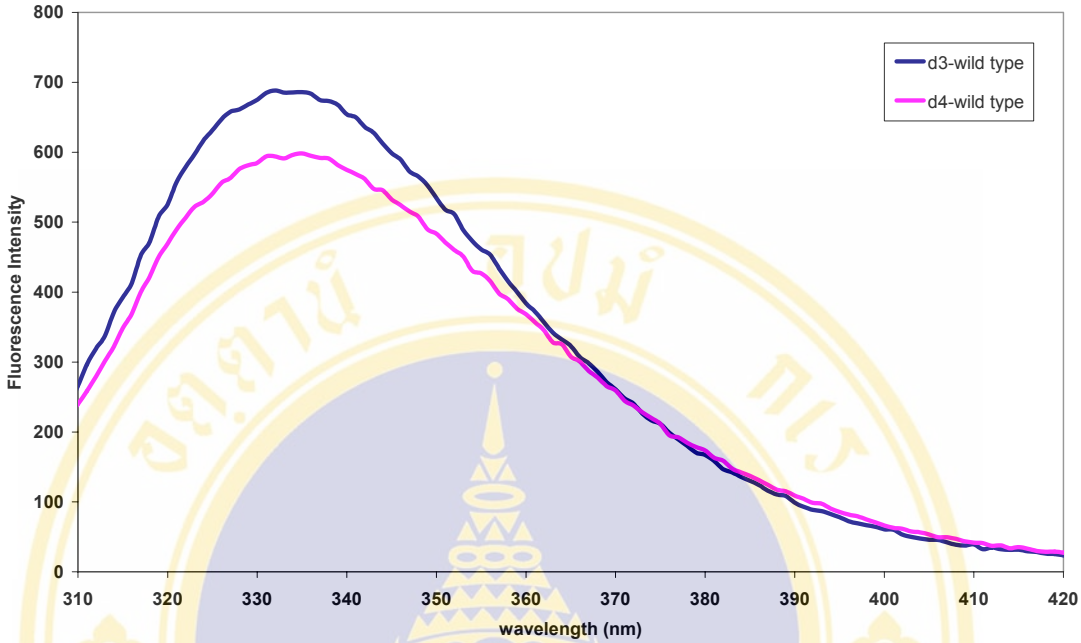

Figure 4.11 The normalized intrinsic tryptophan fluorescence spectra of the wide type adGSTD3-3 and adGSTD4-4. The data are mean from at least 3 independent experiments.

The normalized fluorescence spectra of adGSTD3-3 and adGSTD4-4 wild types compared to the mutants were obtained to study the effect of mutations on the enzyme tertiary structure **(Figures 4.12 and 4.13)**. The results showed that every mutant had the same λ_{max} as the wild types whereas several mutants presented differences in the normalized intensities of fluorescence implying that the mutations caused significant conformational changes in the environment of the tryptophan residues located near the subunit interface and the mutation site. For the adGSTD3-3 mutants, every mutant showed different fluorescence intensity when compared to the wild type. The adGSTD4-4 mutants also demonstrated different intensities except the Val107Met mutant which had a similar intensity as the wild type.

The effects on the fluorescence intensity of the mutants can be divided into three groups. The first group is the group which the mutation at the equivalent position of the two isozymes caused a similar effect. Both Gly102Ala of adgstd3-3 and Ala108Gly of adGSTD4-4 showed decreases of approximately 47.1% and 41.6% of the intensity. The second group is the group in which that the mutations gave the

opposite results. The substitution of tyrosine 98 by phenylalanine in adGSTD3-3 caused an increase of 28.6% whereas the equivalent position mutant of adGSTD4-4, Phe104Tyr, the intensity decreased approximately 46.7 %. For the triple mutants, the adGSTD3-triple mutant intensity decreased about 52.4 % whereas the adGSTD4-triple mutant increased about 41.7%. The last group is the group that one mutant affected the fluorescence intensity while the other had no effect. The mutations involved in this group were adGSTD3-Met101Val and adGSTD4-Val107Met. While the replacement of valine by methionine of adGSTD4-4 did not change fluorescence intensity, the adGSTD3 mutant at the equivalent position caused decreases of about 35.7% intensity.

The different intensities may be caused from the electron properties of the tryptophan excited state which is highly dependent on the nature of its environment. The intra-molecular interactions; an electrostatic exchange process of disulfide bonds, a proton transfer mechanism of histidine, the neutral amide of glutamine and asparagines as well as a short range electron transfer from the close proximity of the indole ring to the amide backbone of the protein, can lead to enhancement or quenching of the fluorescence. Moreover, the enhancement of fluorescence intensity can occur when the Trp residue is located in a hydrophobic environment.

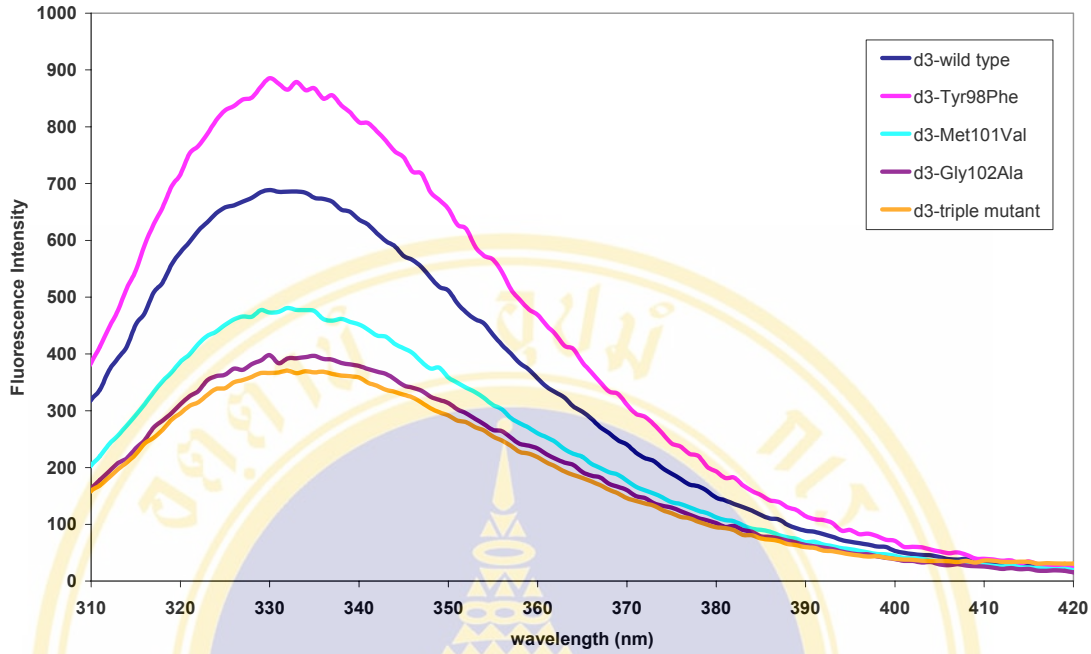

Figure 4.12 The normalized intrinsic tryptophan fluorescence spectra of adGSTD3-3 and the mutants of the hydrophobic residues at the center of the subunit interface. The data are mean from 3 independent experiments.

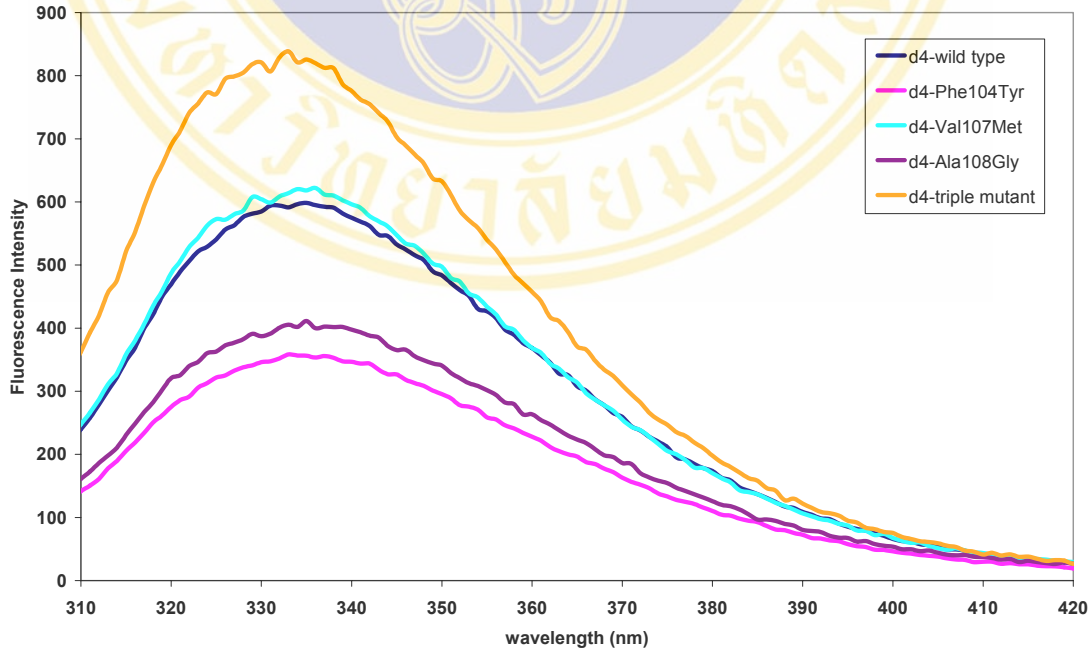

Figure 4.13 The normalized intrinsic tryptophan fluorescence spectra of adGSTD4-4 and the mutants of the hydrophobic residues at the center of the subunit interface. The data are mean from 3 independent experiments.

4.3.3 Refolding Assay

4.3.3.1 Refolding rate constants and % activity recovery measurements

After being rapidly diluted into phosphate buffer, the recovered activity and refolding rate constants were monitored as a function of time by withdrawal of appropriate aliquots of the renaturation mixture and immediately assaying for activity (**Tables 4.8-4.9**).

The refolding rate constant of adGSTD3 mutants were approximately 40-60% less than the wild type especially the triple mutant which had the lowest refolding rate constant. The mutations at the equivalent positions of adGSTD4 showed that only two mutations, Phe104Tyr and Ala108Gly, had the same result as the mutant of adGSTD3 which had a decrease of about 50% in the refolding rate constant. The triple substitution of adGSTD4 did not affect the refolding rate constant while the single mutation at Val107 increased 3.4-fold more than wild type. For adGSTD4-Val107, the mutant could not renature implying that this residue plays a critical role in the folding of the enzyme.

The % activity recovered is another factor which illustrates the ability of the enzymes to recover their appropriate active site conformation for catalytic activity. According to the results, the enzymes showed a range of % recovery from 19% to 94%. As stated above one mutant could not recovery any activity, the asGSTD4-Val107Met. To study the influence of mutations on the protein folding and whether the changes affect the tertiary folding of each subunit or the dimerization of the two subunits, the intrinsic tryptophan fluorescence spectroscopy was performed.

4.3.3.2 Intrinsic tryptophan fluorescence spectroscopy

The different λ_{max} values of the native (335 nm) and the unfolded form (355 nm) of the protein, the fluorescence spectra of native, unfolded and refolded enzymes were monitored by a Shimadzu RF 5001PC to compare the tertiary structure of the protein at these three states. The normalized intrinsic tryptophan fluorescence spectra compared among the native, refolded and unfolded form of adGSTD3-3 are shown in **Figure 4.14** and those of adGSTD4-4 are shown in **Figure 4.15**.

Table 4.8 Refolding rate constants and % activity recovered of adGSTD3-3 and the mutants.

Enzyme	Refolding rate constant	% Activity Recovery
D3-Wild type	0.87 ± 0.09	56.88 ± 0.23
D3-Tyr98Phe	0.58 ± 0.05	66.14 ± 2.83
D3-Met101Val	0.42 ± 0.05	40.52 ± 1.93
D3-Gly102Ala	0.38 ± 0.07	94.42 ± 5.77
D3- Tyr98Phe/Met101Val/Gly102Ala	0.31 ± 0.03	85.82 ± 4.39

The data are mean ± standard deviation from at least 3 independent experiments.

Table 4.9 Refolding rate constants and % activity recovery of adGSTD4-4 and the mutants.

Enzyme	Refolding rate constant	% Activity Recovery
D4-Wild type	0.59 ± 0.03	19.70 ± 0.70
D4-Phe104Tyr	0.28 ± 0.02	23.47 ± 0.51
D4-Val107Met	nd*	0.00
D4-Ala108Gly	0.32 ± 0.04	69.57 ± 7.55
D4- Phe104Tyr/Val107Met/Ala108Gly	0.60 ± 0.10	24.98 ± 0.18

* nd = not detectable. The data are mean ± standard deviation from at least 3 independent experiments.

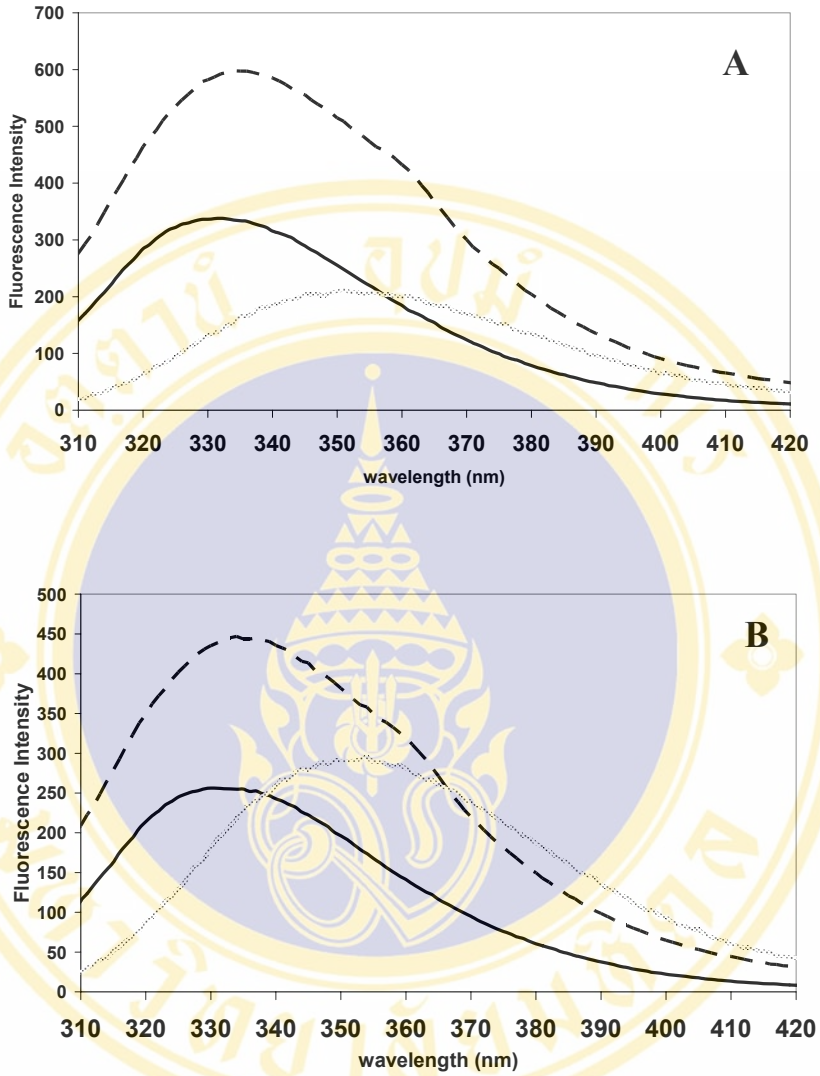

Figure 4.14 The normalized intrinsic tryptophan fluorescence spectra compared among the native, refolded and unfolded form of adGSTD3-3 and the mutants of the hydrophobic residues at the center of the subunit interface.

(A) adGSTD3-3 wild type, (B) adGSTD3-Tyr98Phe, (C) adGSTD3-Met101Val. (D) adGSTD3-Gly102Ala and (E) adGSTD3-Triple mutant.

The data are mean from at least 3 independent experiments.

(▬ : a native form, ▪▪▪ : a refolded form and ▒ : an unfolded form of the enzyme)

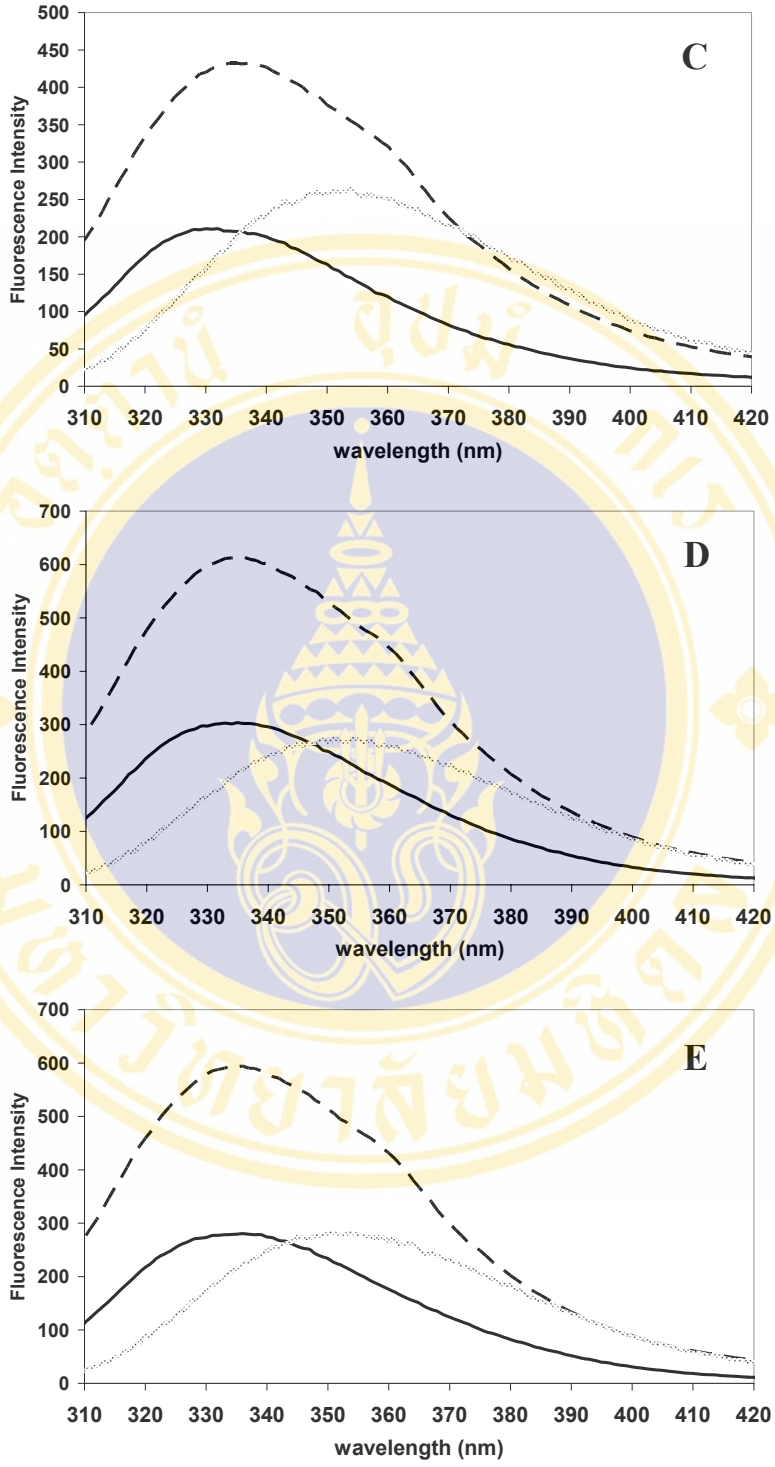

Figure 4.14 (Continued) The normalized intrinsic tryptophan fluorescence spectra compared among the native, refolded and unfolded form of adGSTD3-3 and the mutants of the hydrophobic residues at the center of the subunit interface.

(▬ : a native form, ▪▪▪ : a refolded form and ▒ : an unfolded form of the enzyme)

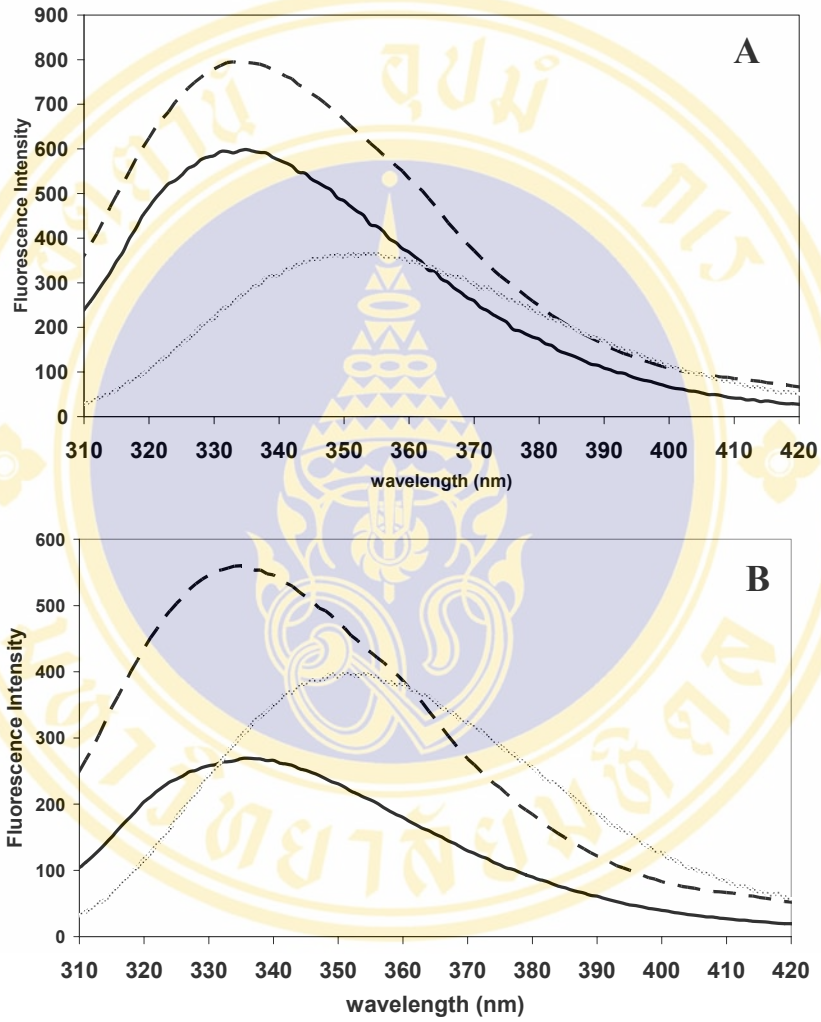

Figure 4.15 The normalized intrinsic tryptophan fluorescence spectra compared among the native, refolded and unfolded form of adGSTD4-4 and the mutants of the hydrophobic residues at the center of the subunit interface.

(A) adGSTD4-4 wild type, (B) adGSTD4-Phe104Tyr, (C) adGSTD4-Val107Met. (D) adGSTD4-Ala108Gly and (E) adGSTD4-Triple mutant.

The data are mean from at least 3 independent experiments.

(▬ : a native form, ▪▪▪ : a refolded form and ▒ : an unfolded form of the enzyme)

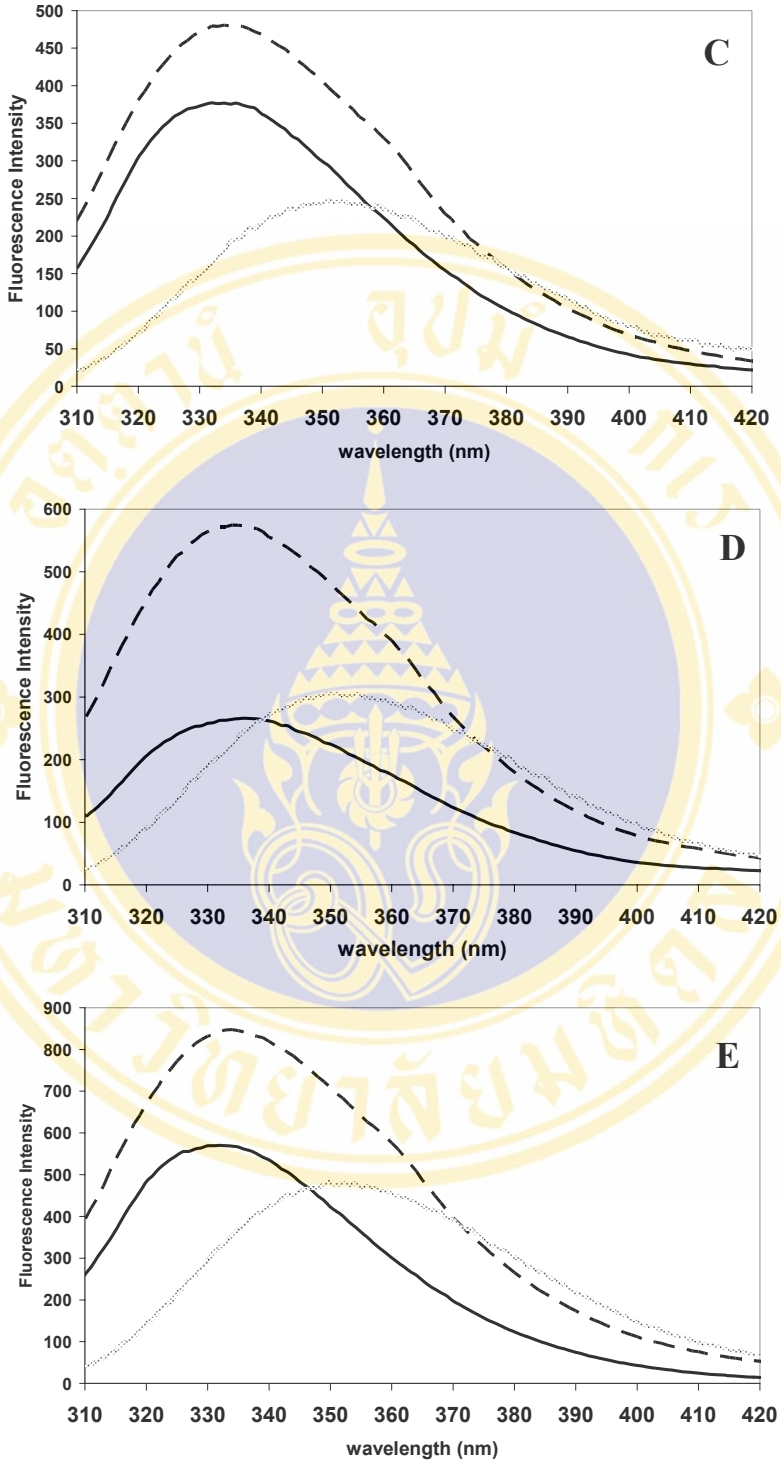

Figure 4.15 (Continued) The normalized intrinsic tryptophan fluorescence spectra compared among the native, refolded and unfolded form of adGSTD4-4 and the mutants of the hydrophobic residues at the center of the subunit interface.

(▬ : a native form, ▪▪▪ : a refolded form and ▪▪▪▪▪▪ : an unfolded form of the enzyme)

The results demonstrated that every enzyme could be refolded back to the same back bone architecture as the native form as showed by the similar λmax values including Val107Met mutant which could not recovery catalytic activity. However, there were shoulders in several refolded spectra around the λ_{max} of the unfolded proteins (355 nm). Therefore, the enhancement of the normalized intensity of the refolded state may be occurred by the integration between the native state form and the unfolded form.

From the similar patterns of the adGSTD3-3 mutant spectra, the mutations did not affect the tertiary structure folding of each subunit but had influence on the dimerization process which is necessary to achieve an appropriate active site conformation. Therefore, according to the refolding assay in terms of both catalytic and structural experiments the data suggests that the single mutation of glycine102 and the triple mutant had significant effects on the dimerization of the enzymes by increasing the % activity recovered from 56.9 % to approximately 94.4 % and 85.8 %, respectively (**Table 4.8**). The other two mutations, Tyr98Phe and Met101Val also had a slight effect on the dimerization.

On the contrary, the alterative pattern of the adGST4-4 mutant spectra indicated the mutations not only influenced the dimerization step, but also the packing of amino acid side chains around the tryptophan residues in each subunit. Except the Val107Met mutant which showed a similar pattern as the wild type although it could not recover the catalytic activity (**Table 4.9**).

4.3.4 ANS Binding Assay

4.3.4.1 ANS Binding Spectra Measurement

In this experiment, ANS was utilized as a probe to monitor the appearance/ disappearance of hydrophobic patches or surfaces on the proteins that were undergoing structural changes. When ANS binds to the proteins, the fluorescence was enhanced accompanied by a blue shift in its emission maximum from 514 nm (free ANS in buffer) to 498 nm for adGSTD3-3 and 482 nm for adGSTD4-4 wild type (**Figure 4.16**), indicating that the polarity of the binding site had become more hydrophobic with the lower the polarity, the greater the blue shift.

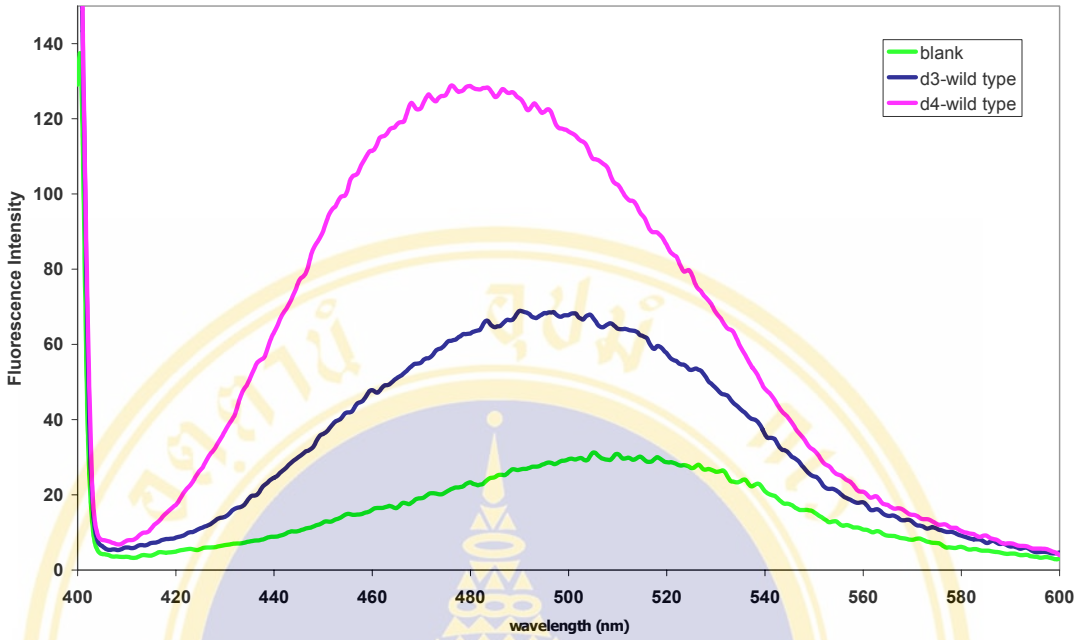

Figure 4.16 ANS binding spectra of the wild type adGSTD3-3 and adGSTD4-4. The data are mean from 3 independent experiments.

The spectrum of ANS in phosphate buffer pH 6.5 was subtracted from the spectra of the protein binding ANS. A total of three scans each for blank and sample were recorded and averaged for each enzyme. When compared with the wild types, there was no change in the emission maximum wavelength of ANS bound to all mutants **(Figure 4.17-4.18)**. The ANS fluorescence intensity, reflects the number of ANS bound to the protein. There was no intensity change for the glycine substitution and the triple mutant of adGSTD3-3. However, there was a slight effect in Tyr98Phe and Met101Val mutants with a decrease of about 23.8% and 25.8% (**Figure 4.17**). In contrast, every mutants of adGSTD4-4 showed a significant effect in the amount of ANS bound (**Figure 4.26**). The Phe104Tyr and Ala108Gly had a 40.9% decrease and the Val107Met and triple mutant had a 71.4% decrease. The results show that the amino acid substitutions of adGSTD4-4 with the adGSTD3-3 amino acid had a dramatic effect at the subunit interface much more than the amino acid replacements of adGSTD3-3.

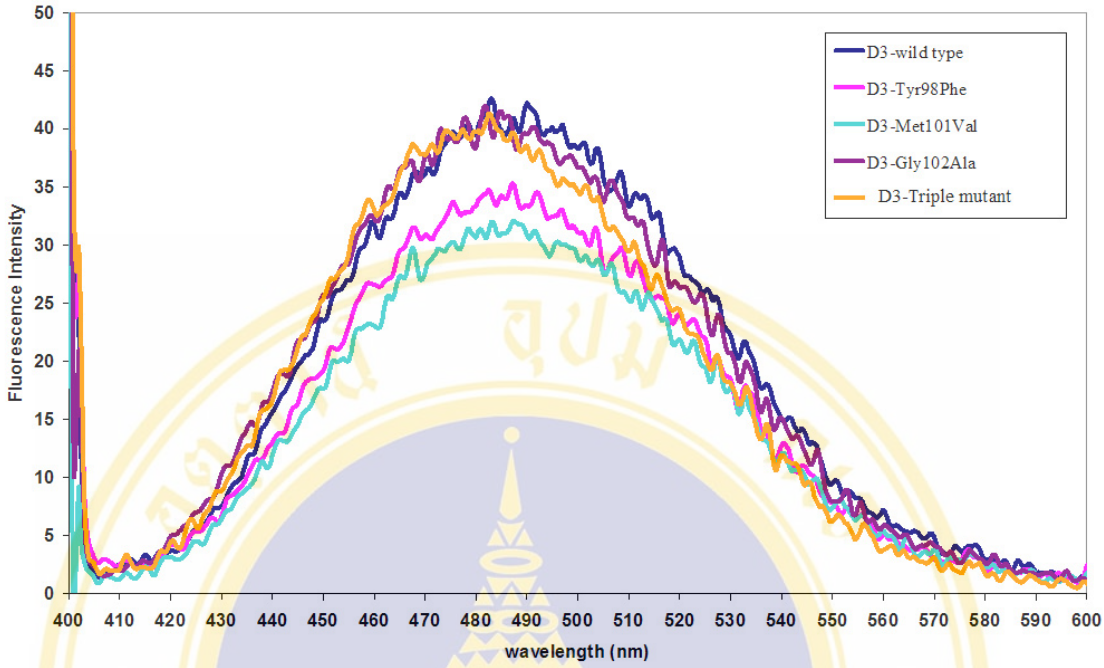

Figure 4.17 ANS binding spectra of the adGSTD3-3 and the hydrophobic interactions at the center of the subunit interface mutants. The data are mean from 3 independent experiments.

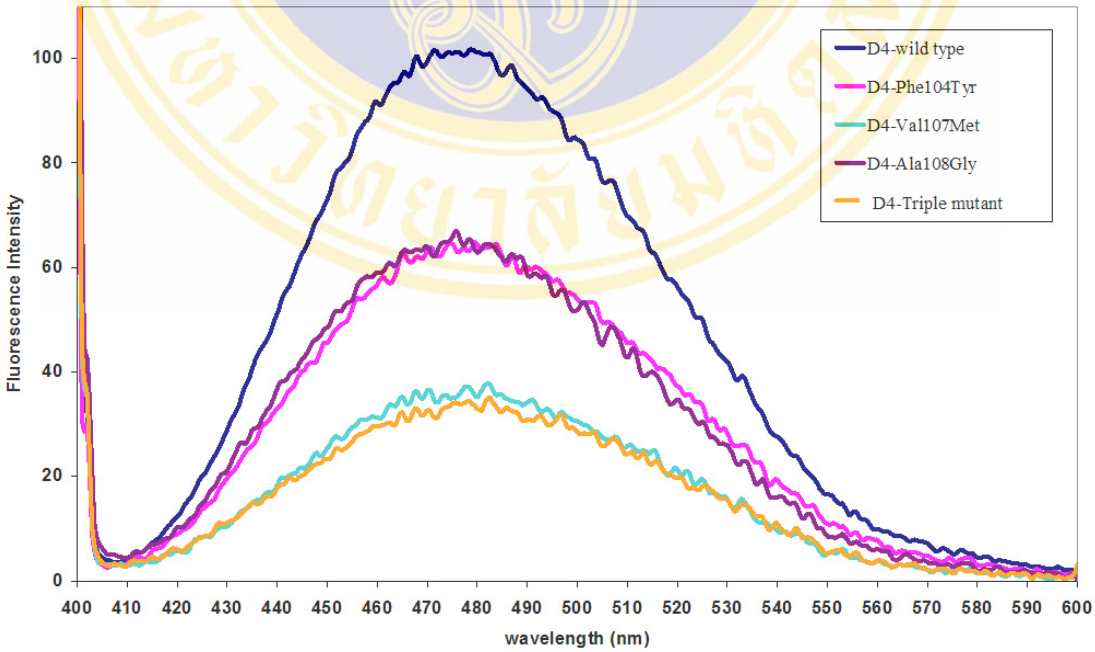

Figure 4.18 ANS binding spectra of the adGSTD4-4 and the hydrophobic interactions at the center of the subunit interface mutants. The data are mean from 3 independent experiments.

4.4.4.2 Remaining Activity Measurement

To study the impact of ANS on the protein conformation, the enzyme activity in the presence and absence of ANS was measured by using the standard reaction assay. The results showed that in the reaction with ANS present, the specific activity of the enzymes was decreased (**Tables 4.10-4.11)**. The data suggests that ANS can change the enzyme architecture or block the active site. However, the ratio of inhibition demonstrated that ANS dye affected the conformation of the two isozymes in the opposite way that was the adGSTD3-3 mutants had the effect from ANS less than the wild type by decrease the % inhibition about 50% for the single mutations and 25% for the triple mutant while ANS dye influenced the adGSTD4-4 mutant conformations more than the wild type by increase the % inhibition about 74.4%, 38.4%, 78.5% and 15.1% for Phe104Tyr, Val107Met, Ala108Gly and triple mutant, respectively.

Table 4.10 The effect of ANS to specific activity of adGSTD3-3.

Enzymes	% inhibition
D3-wild type	24.63 ± 1.41
D3-Tyr98Phe	13.13 ± 0.54
D3-Met101Val	11.86 ± 0.80
D3-Gly102Ala	13.69 ± 2.66
D3-Tyr98Phe/Met101Val/Gly102Ala	18.35 ± 0.65

The data are mean ± standard deviation from at least 3 independent experiments.

Table 4.11 The effect of ANS to specific activity of adGSTD4-4.

Enzymes	% inhibition
D4-wild type	18.37 ± 1.20
D4-Phe104Tyr	31.90 ± 1.96
D4-Val107Met	25.42 ± 1.41
D4-Ala108Gly	32.79 ± 1.03
D4- Phe104Tyr/Val107Met/Ala108Gly	21.14 ± 1.83

The data are mean ± standard deviation from at least 3 independent experiments.

CHAPTER 5
RESULTS: THE CHARGE- CHARGE NETWORK AT THE EDGE OF THE SUBUNIT INTERFACE

Several residues at the bottom edge of subunit interface, Asp110 and Asn126 of adGSTD3-3 and Glu116 and Arg134 of adGSTD4-4, were also studied. In adGSTD4-4, Glu116 and Arg134 can form a hydrogen bond network both inter- and intra-subunit which helps to maintain tertiary and quaternary structures of this isozyme. However, this network does not appear in adGSTD3-3. For adGSTD3-3, there are hydrogen bonds only in the same subunit between Asp110 and the highly conserved residue, Gln106 (**Figure 1.18**). To study the influence of the ionic network at the bottom edge of the subunit interface and whether it affects the catalytic activity and stability of the enzymes, mutations at the equivalent positions of these two isozymes were generated, Asp110Ala of adGSTD3-3 and Glu116Ala of adGSTD4-4.

5.1 Site-Directed Mutagenesis, Expression and Purification.

All the mutant enzymes were sequenced and transfromed into *E.coli* BL21DE3plysS. All the wild type and mutants were purified from the lysate by affinity chromatography using immobilized GSH. The yields are shown in **Table 5.1**. The purity of the enzymes was determined by SDS-PAGE as shown in **Figures 5.1 and 5.2**.

Table 5.1 Purification of adGSTD3-Asp110Ala and adGSTD4-Glu116Ala.

Enzymes	Fraction	Total protein (mg)	% Yield (%)
adGSTD3-Asp110Ala	Lysate	143.28*	
	Elution	49.11	34.27
adGSTD4-Glu116Ala	Lysate	158.71*	
	Elution	58.85	37.08

* Expressed in 400 µL LB media.

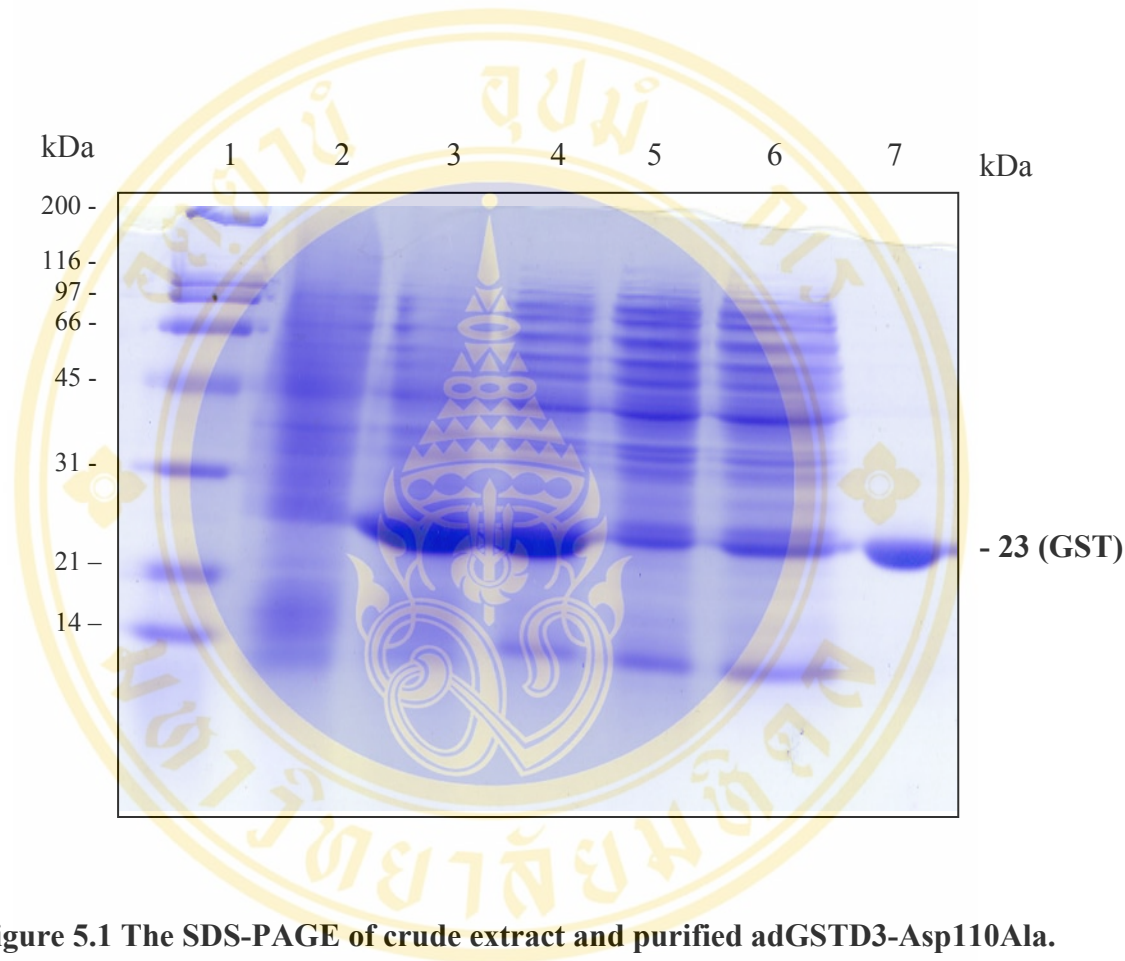

Figure 5.1 The SDS-PAGE of crude extract and purified adGSTD3-Asp110Ala.

SDS-polyacrylamide gel showing the expressed adGSTD3-Asp110Ala eluted from a GSTrap affinity column. The 23-kDa band is indicated with a bold label.

Lane 1 : Broad-range marker

Lane 2 : 0.05 O.D. of *E.coli* extract before induction by IPTG

Lane 3 : 0.05 O.D. of *E.coli* extract after induction by IPTG

Lane 4 : 25 µg of lysate

Lane 5 : 25 µg of flow through fraction

Lane 6 : 25 µg of wash fraction

Lane 7 : 5 µg of purified enzyme

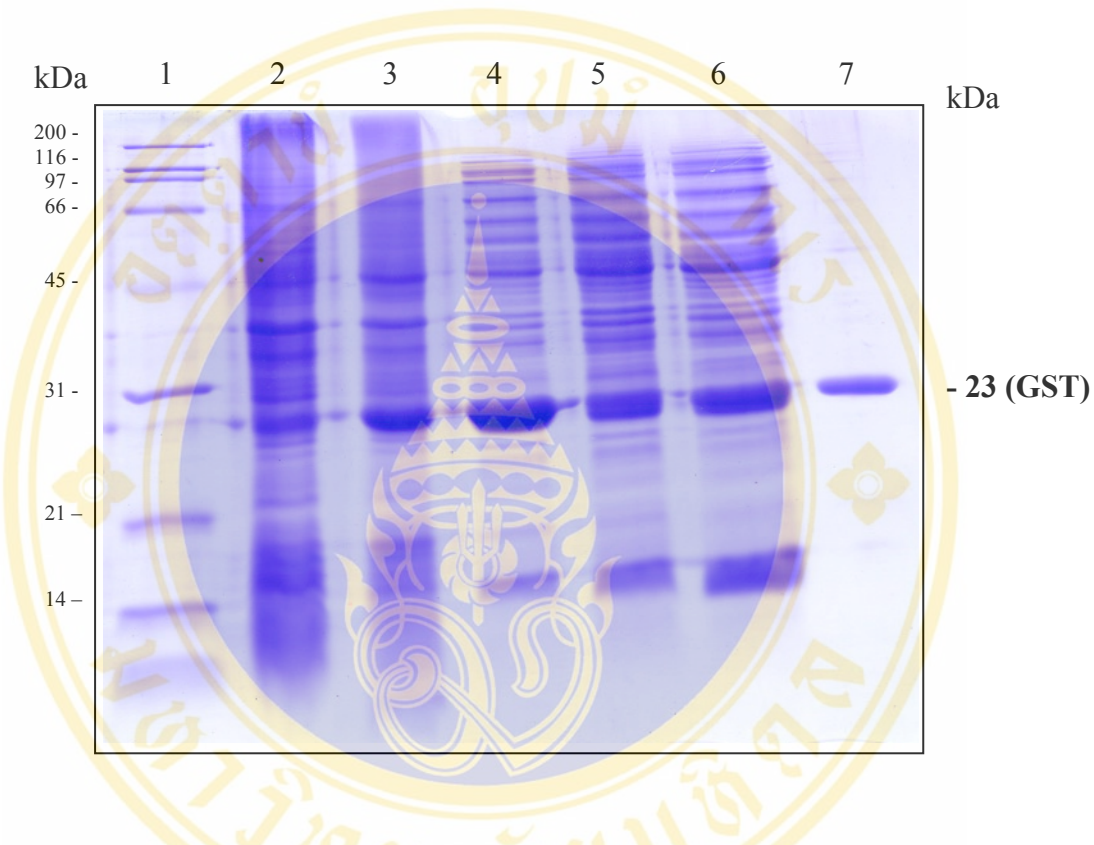

Figure 5.2 The SDS-PAGE of crude extract and purified adGSTD4-Glu116Ala.

SDS-polyacrylamide gel showing the expressed adGSTD4-Glu116Ala eluted from a GSTrap affinity column. The 23-kDa band is indicated with a bold label.

Lane 1 : Broad-range marker

Lane 2 : 0.05 O.D. of *E.coli* extract before induction by IPTG

Lane 3 : 0.05 O.D. of *E.coli* extract after induction by IPTG

Lane 4 : 25 μg of lysate

Lane 5 : 25 μg of flow through fraction

Lane 6 : 25 μg of wash fraction

Lane 7 : 5 μg of purified enzyme

5.2 Enzymatic Characterization

5.2.1 Determination of Substrate Specificities

To establish whether the mutant and the wild type enzymes have a similar or distinct catalytic specificity, their activities toward a panel of established GST substrates were determined (**Table 5.2**). The replacment of the positive charge residue by a small non-polar residue, alanine, at 110 adGSTD3, caused decreases of 1.2-, 1.6-, 14- and 1.9-fold in specific activity toward CDNB, DCNB, EA and PNBC, respectively. The specific activity toward PNPB of the mutant was detectable while that of the wild type could not be detected. In contrast, the alanine substitution of glutamate in adGSTD4 had no effect on the specific activity of the substrates except for DCNB as substrate, the mutant increased specific activity about 2-fold.

Table 5.2 Specific activity of the enzymes toward five different substrates.

Enzymes	Specific Activity (µmol/min/mg)				
	CDNB	DCNB	EA	PNPB	PNBC
D3-Wild type	85.27 ± 3.23	0.25 ± 0.01	0.14 ± 0.05	nd*	0.13 ± 0.02
D3-Asp110Ala	71.56 ± 2.69	0.16 ± 0.01	0.01 ± 0.01	0.03 ± 0.01	0.07 ± 0.01
D4-Wild type	48.04 ± 1.98	0.03 ± 0.01	0.03 ± 0.02	0.06 ± 0.02	0.03 ± 0.01
D4-Glu116Ala	56.27 ± 6.83	0.06 ± 0.01	0.01 ± 0.01	0.04 ± 0.01	0.04 ± 0.01

* nd = not detectable. The data are mean ± standard deviation from at least 3 independent experiments. The substrate concentrations used were 1 mM CDNB for adGSTD3-3, 3 mM CDNB for adGSTD4-4, 1 mM DCNB, 0.1 mM PNBC, 0.1 mM PNPB and 0.2 mM EA.

5.2.2 Determination of Kinetic Parameters

Comparison of the kinetic parameters of the mutants with the wild type values showed that the residue changes affected enzymatic properties although this position is not involved in the active site pocket (**Table 5.3**). The Glu116Ala mutant showed negative cooperativity upon CDNB binding suggesting that the induced-fit mechanism was altered by the mutation (93). Therefore, the parameters were calculated by the Hill equation. Both mutants affected the maximum velocity and the affinities toward the substrates in the same way. For V_{max} values the mutants increased approximately 32% and 107% for adGSTD3-Asp110Ala and adGSTD4-Glu116Ala, respectively. When CDNB was used as a substrate, the mutants demonstrated a greater K_m value than the wild types about 3.3- and 2.5-fold for Asp110Ala and Glu116Ala, respectively. Moreover, the co-substrate, GSH, the K_m value of both mutants increased approximately 1.8-fold. The catalytic efficiency of the enzyme, k_{cat}/K_m value, for the Asp110Ala mutant had a lower efficiency for both CDNB and GSH of 2.5- and 1.2-fold, respectively. Glu116Ala had a lower efficiency for CDNB of 1.2-fold but with a greater efficiency for GSH of about 1.1-fold.

Table 5.3 Michaelis-Menten parameters for the enzymes.

Enzymes	V_{max}	kcat	CDNB		GSH	
			K_m	kcat/K_m	K_m	kcat/K_m
D3-Wild type	98.34 ± 0.47	39.15	0.15 ± 0.007	258.04	0.29 ± 0.035	113.86
D3-Asp110Ala	130.8 ± 3.99	51.73	0.49 ± 0.07	105.57	0.54 ± 0.04	95.8
D4-Wild type	53.95 ± 1.30	22.5	0.63 ± 0.09	35.71	0.67 ± 0.05	33.58
D4-Glu116Ala	110.97 ± 2.31	46.09	1.55 ± 0.01	29.68	1.24 ± 0.06	37.13

The data are mean ± standard deviation from at least 3 independent experiments. The units are: V_{max} : µmole/min/mg, K_m : mM, k_{cat} : s-1, k_{cat}/K_m : mM^{-1} s^{-1}.

5.3 Structural Characterization

5.3.1 Stability Assay

The remaining activity after incubation at 45ºC of both mutants and the wild types are showed in **Table 5.4**. The half-life of the adGSTD3 mutants did not significantly change when compared to the wild type. On the other hand, the mutation of adGSTD4 at the equivalent position which disrupted the charge-charge network showed significantly decreased stability for the enzyme of approximately 64%. The results showed that the positively charged residue at the edge of subunit interface of adGSTD4 has an important role to stabilize the enzyme structure while the equivalent residue of adGSTD3-3 had only a slight effect.

Table 5.4 The half-life of the enzymes.

Enzymes	Half-life(min)
D3-Wild type	2.71 ± 0.35
D3-Asp110Ala	2.21 ± 0.24
D4-Wild type	14.01 ± 1.70
D4-Glu116Ala	5.16 ± 0.93

The data are mean ± standard deviation from at least 3 independent experiments.

5.3.2 Intrinsic Tryptophan Fluorescence Spectroscopy

To investigate whether the mutations caused changes in the environment around tryptophan residues, the fluorescence spectra of 0.2 mg/ml enzyme were monitored by a Shimadzu RF 5001PC. The normalized fluorescence spectrum of each mutant was analyzed and compared to the wild type in **Figures 5.3 and 5.4**. The results showed that the alanine substitution at this equivalent position of both isozymes had a slight effect on the environment of the tryptophan by decreasing fluorescence intensity approximately 25% and 9% for adGSTD3-Asp110Ala and adGSTD4-Glu116Ala, respectively.

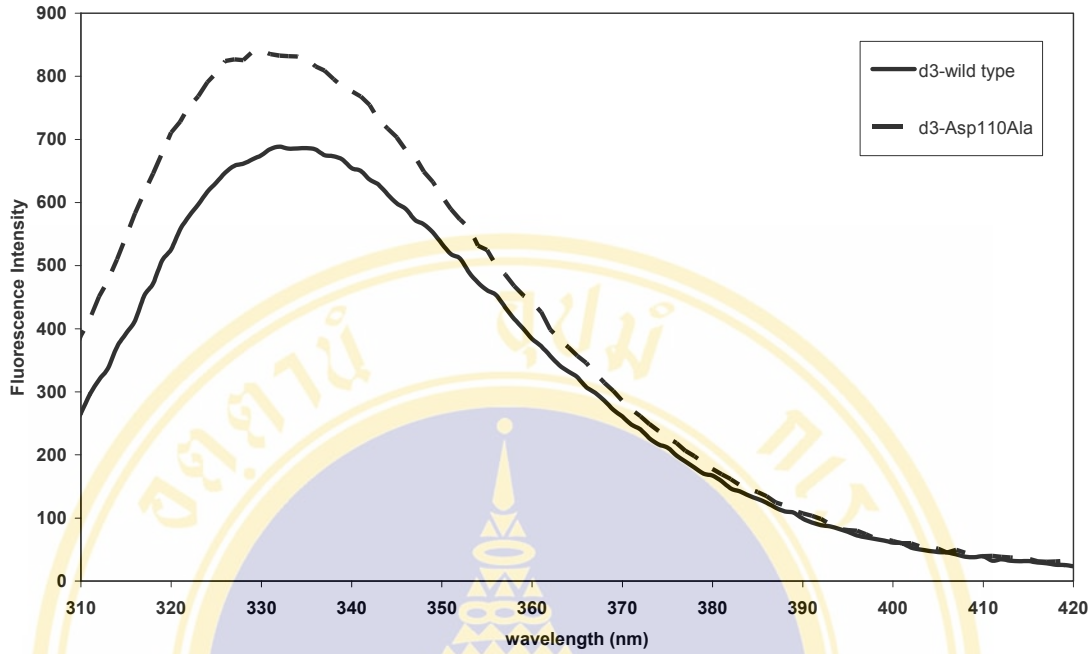

Figure 5.3 The normalized intrinsic tryptophan fluorescence spectra of the adGSTD3-3 and adGSTD3-Asp110Ala mutant. The data are mean from 3 independent experiments.

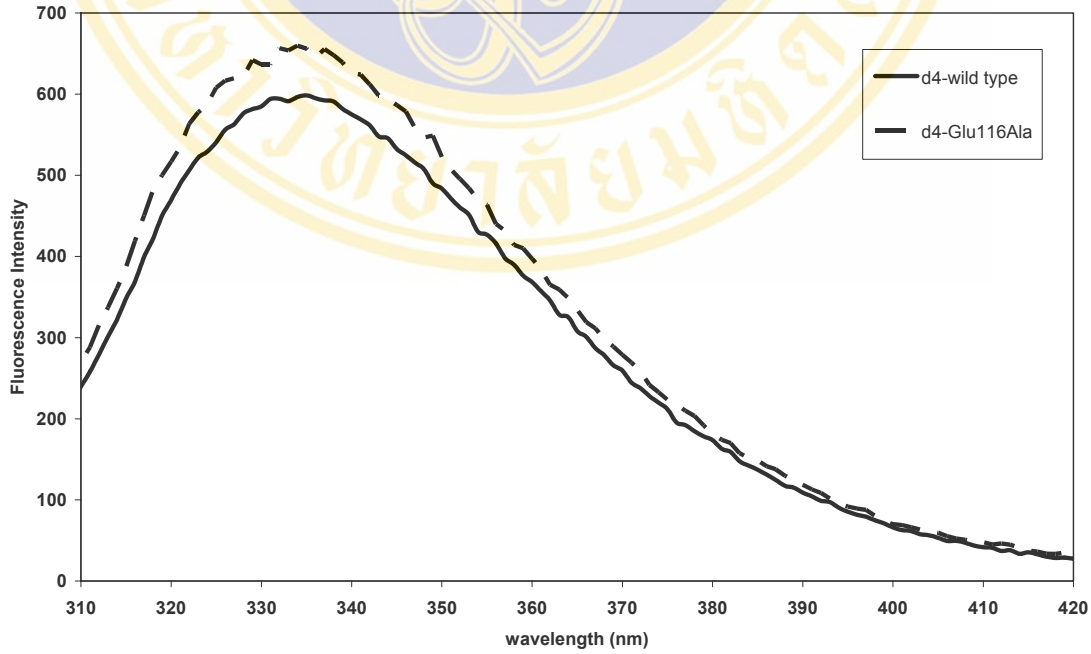

Figure 5.4 The normalized intrinsic tryptophan fluorescence spectra of the adGSTD4-4 and adGSTD4-Glu116Ala mutant. The data are mean from 3 independent experiments.

5.3.3 Refolding Assay

5.3.3.1 Refolding rate constants and % activity recovery measurement

After being rapidly diluted into renaturation buffer, the refolded proteins were measured for two parameters; the recovered activity and refolding rate constants. The results are showed in **Table 5.5.** Both mutants altered the rate of refolding and the % recovery of the enzyme activity implying that this position in both isozymes plays a role in the folding of the enzymes as well as in the process of renaturing the appropriate active site conformation.

Table 5.5 Refolding rate constants and % activity recovery of the enzymes.

Enzyme	Refolding rate constant	% Activity Recovery
D3-Wild type	0.87 ± 0.09	56.88 ± 0.23
D3-Asp110Ala	0.58 ± 0.11	80.51 ± 3.48
D4-Wild type	0.59 ± 0.03	19.70 ± 0.70
D4-Glu116Ala	0.68 ± 0.11	9.93 ± 0.68

The data are mean ± standard deviation from at least 3 independent experiments.

5.3.3.2 Intrinsic tryptophan fluorescence spectroscopy

The fluorescence spectra of native, unfolded and refolded enzymes were monitored by a Shimadzu RF 5001PC to compare the tertiary structure of the protein at the three states. The normalized intrinsic tryptophan fluorescence spectra compared among the native, refolded and unfolded from of adGSTD3-3 are shown in **Figure 5.5** and those of adGSTD4-4 are shown in **Figure 5.6**.

The results demonstrated that every enzyme could be refolded back to the same back bone architecture as the native form as showed by the similar pattern. The data suggests that the mutation did not alter the tertiary folding of the enzymes.

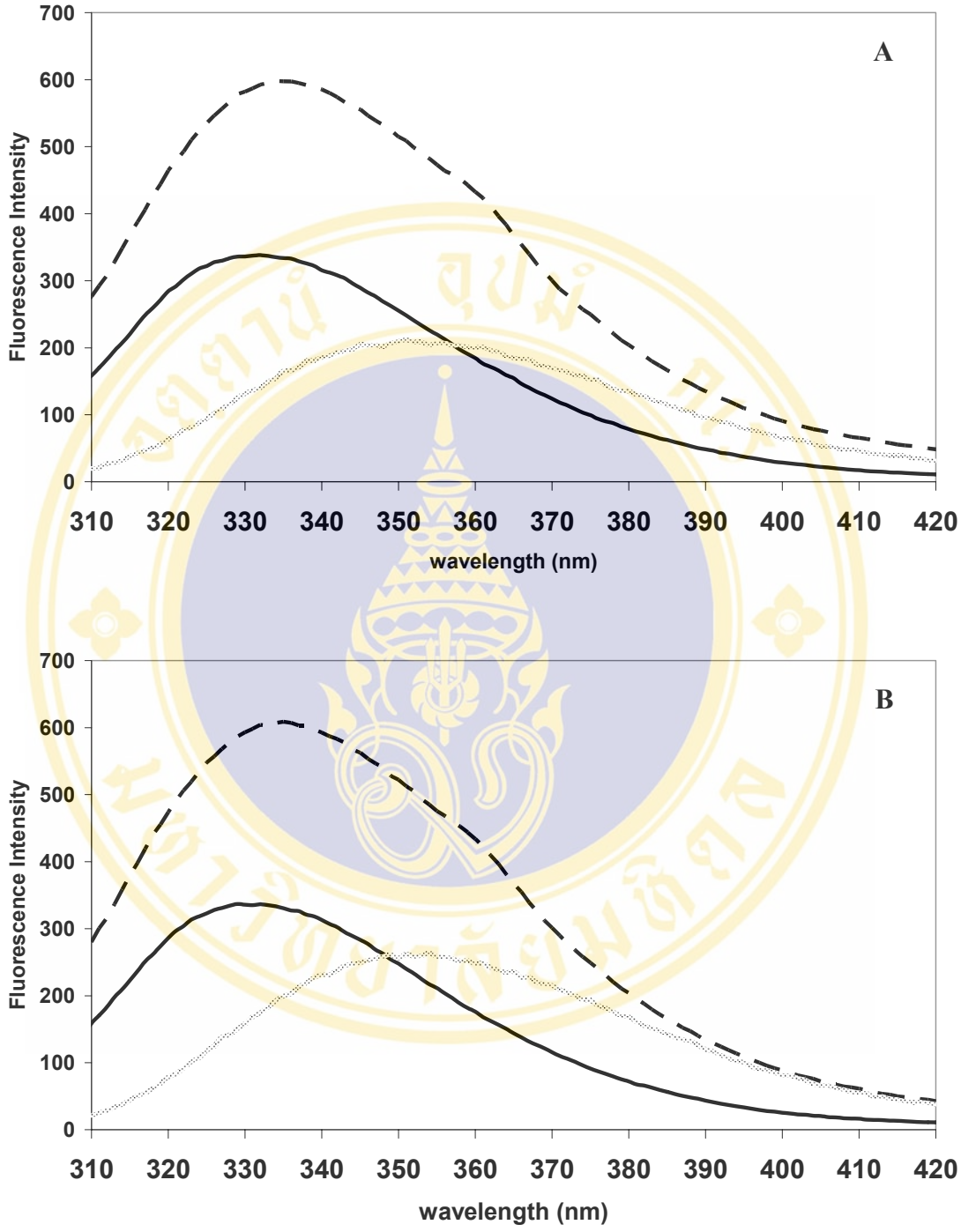

Figure 5.5 The normalized intrinsic tryptophan fluorescence spectra compared among the native, refolded and unfolded form adGSTD3-Asp110Ala mutants.
(A) adGSTD3-3 wild type and (B) adGSTD3-Asp110Ala. The data are mean from 3 independent experiments.
(▬ : a native form, ▪▪▪ : a refolded form and ▒ : an unfolded form of the enzyme)

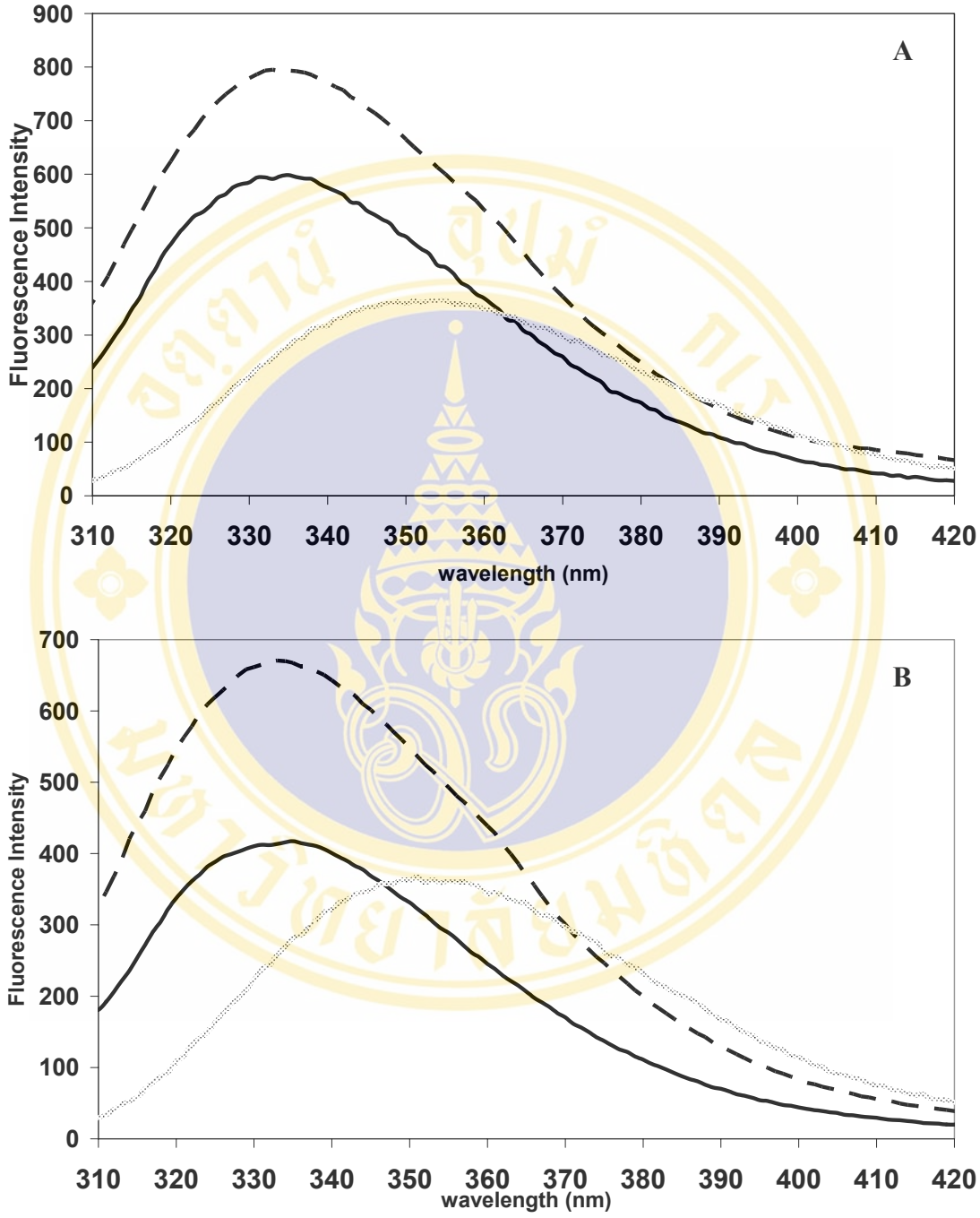

Figure 5.6 The normalized intrinsic tryptophan fluorescence spectra compared among the native, refolded and unfolded form adGSTD4-Glu116Ala mutants.

(A) adGSTD4-4 wild type and (B) adGSTD4-Glu116Ala. The data are mean from 3 independent experiments.

(▬ : a native form, ▪▪▪ : a refolded form and ▒ : an unfolded form of the enzyme)

5.3.4 ANS Binding Assay

5.3.4.1 ANS Binding Spectra Measurement

When compared with the wild type, there was no change in the emission maximum wavelength of ANS bound to both mutants **(Figures 5.7 and5.8)**. The ANS fluorescence intensity which reflects the number of ANS molecules bound to the protein, Glu116Ala appeared to significantly exhibit a lower capacity to bind ANS as showed by about a 57% decrease in ANS fluorescence intensity while the Asp110Ala mutant showed a similar intensity as the wild type.

5.3.4.2 Remaining Activity Measurement

To study the impact of ANS on the enzyme conformation, the enzyme activity in the presence and absence of ANS was measured as an indirect probe by using the standard reaction assay. The results showed that in the reaction with ANS present the specific activity of all enzymes was decreased to a similar ratio as the wild type (**Table 5.6**). This suggests that the ANS spectra changes in **Figures 5.7** and **5.8** did not occur from conformational changes of the enzymes induced by ANS dye.

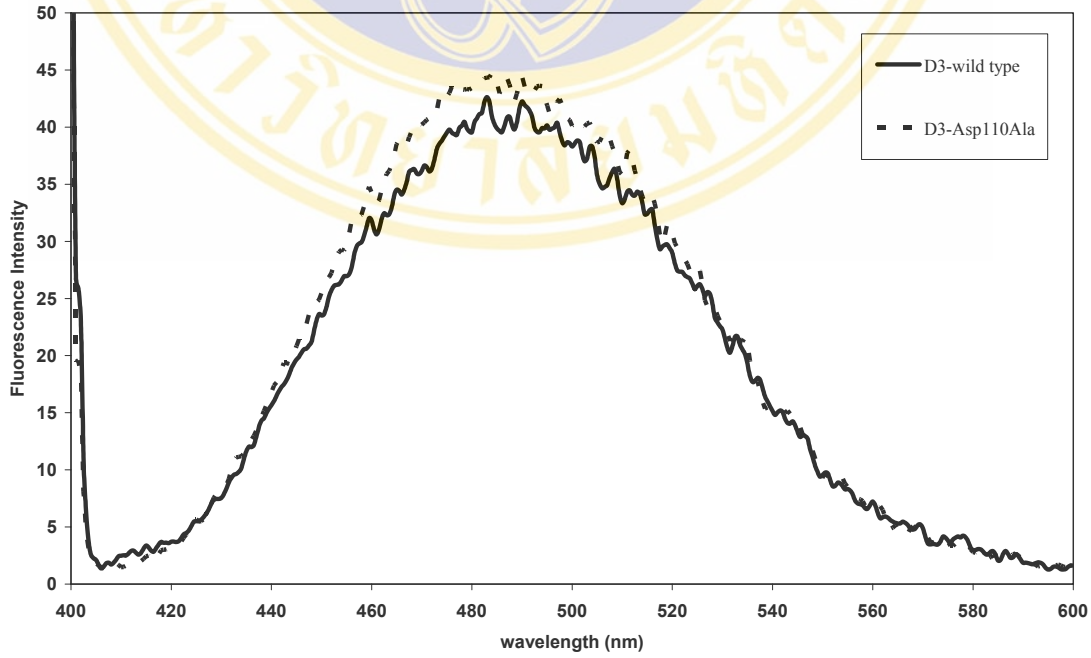

Figure 5.7 ANS binding spectra of the wide type adGSTD3-3 and adGSTD3-Asp110Ala mutants. The spectra were measured immediately after addition of ANS. The data are mean from 3 independent experiments.

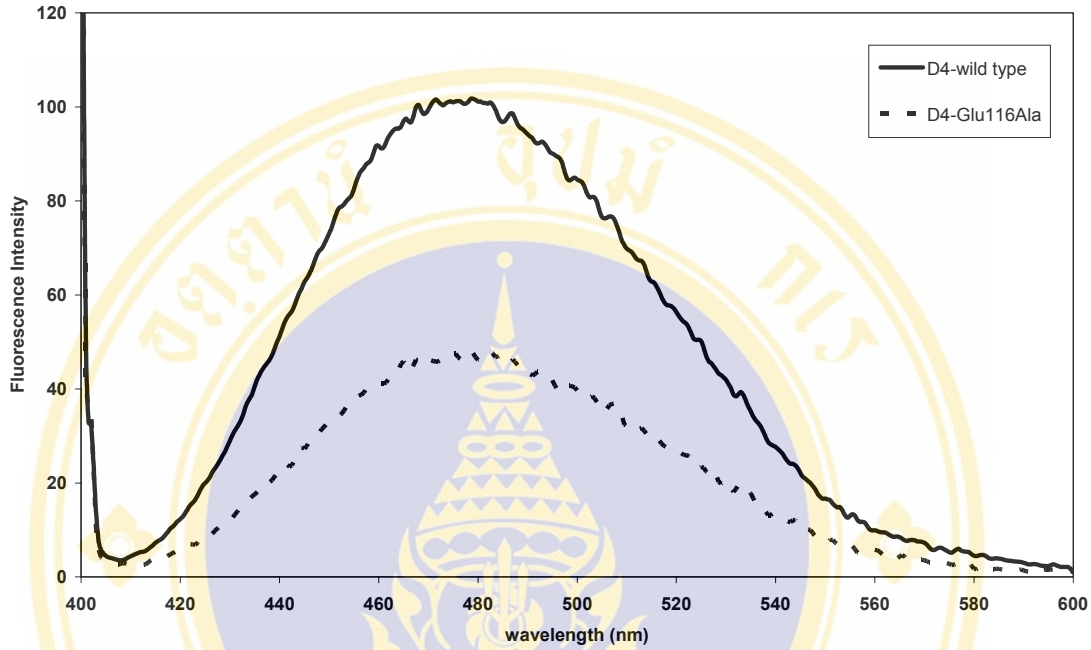

Figure 5.8 ANS binding spectra of the wide type adGSTD4-4 and adGSTD4-Glu116Ala mutants. The spectra were measured immediately after addition of ANS. The data are mean from 3 independent experiments.

Table 5.6 The effect of ANS to specific activity of the enzymes.

Enzymes	% inhibition
D3-wild type	24.63 ± 1.41
D3-Asp110Ala	23.41 ± 1.83
D4-wild type	18.37 ± 1.20
D4-Glu116Ala	17.30 ± 2.05

The data are mean ± standard deviation from 3 independent experiments.

CHAPTER 6
RESULTS: UNFOLDING PATHWAY INVESTIGATION

Although the two GSTs in this thesis are splicing products from the same gene, they are differences in the amino acid sequence and enzymatic properties. Therefore, an unfolding pathway study was performed to determine if the two proteins behaved in a similar manner. After being unfolded by guanidinium chloride (0 to 5 M) in unfolding buffer at room temperature overnight (~16 hr) to achieve equilibrium unfolding, adGSTD3-3 was soluble in the unfolding solution while adGSTD4-4 aggregated in the unfolding solutions from 0 M to 1.8 M GuHCl concentrations. Therefore, only adGSTD3-3 could be further studied. In this work we utilized five probes to monitor structural changes during the unfolding of the GSTs; the enzyme activity, the intrinsic tryptophan fluorescence spectroscopy, far UV circular dichroism (CD), ANS binding assay, and size-exclusion chromatography to observe quaternary structure, tertiary structure, secondary structure, subunit interface and overall component changes, respectively.

6.1 Remaining Activity Measurement

Enzyme activity measurements in the presence of denaturant were assessed using the standard reaction assay (section 2.15). The % remaining activity of the adGSTD3-3 enzyme in various guanidinium chloride concentration showed that the enzyme lost approximately 50% activity at 0.2 M GuHCl and lost 100% at 0.4 M GuHCl (**Figure 6.1**). The results indicate that at 0.4 M GuHCl, the active site conformation of the enzyme was not appropriate for catalysis. This may have occurred because the tertiary structure was altered or the dimeric protein was dissociated into the monomeric form. To answer this question, the studies mentioned above were performed.

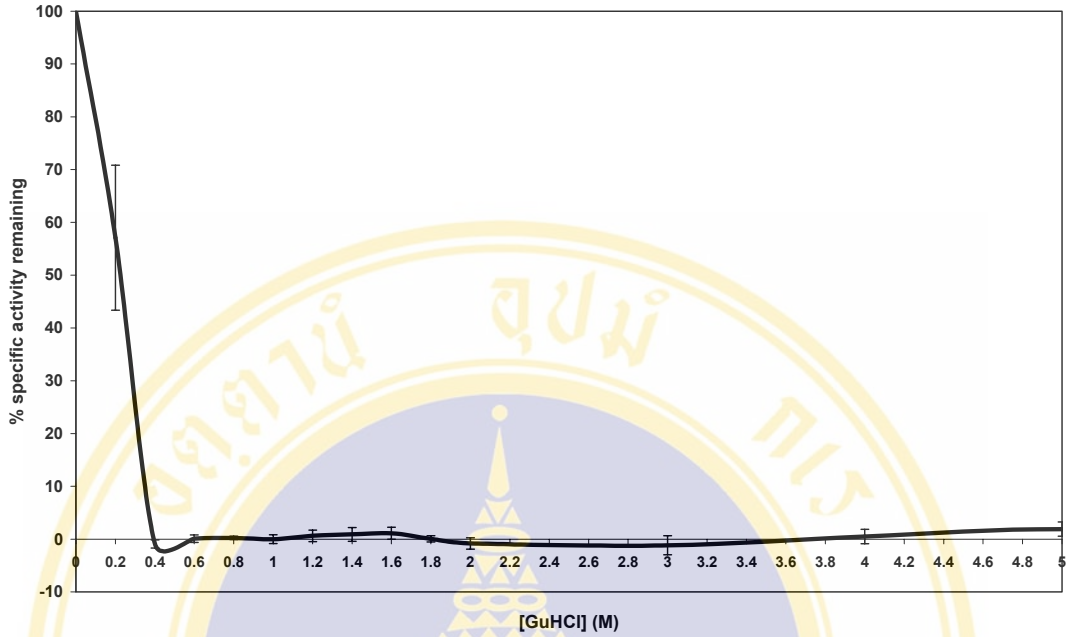

Figure 6.1 % Specific activity remaining of adGSTD3-3 after equilibrated at different guanidinium chloride concentrations. The data are mean ± standard deviation from 3 independent experiments.

6.2 Intrinsic Fluorescence Spectroscopy

Fluorescence spectroscopy was used as a probe to obtain unfolding curves (**Figure 6.2**). An unfolding curve was determined by plotting fluorescence intensity ratio of 350nm (for unfolded protein) and 330 nm (for folded protein) against guanidinium chloride concentration (**Figure 6.3**). From the unfolding curve, there are five phases of fluorescence transitions; 0 – 0.2 M, 0.4-0.8 M, 1-1.6 M, 2.2-2.8 M and 3-5 M GuHCl. However, the number of transition states was confirmed by the following techniques. The emission maximum of tryptophan shifts from 330 nm to 335 nm in the second and the third fluorescence phase (0.4 M -2.4 M GuHCl) as the fluorescing tryptophan becomes partially exposed and then from 335 nm to 348 nm in the fourth fluorescence phase (2.6 M-5 M GuHCl) as the tryptophan becomes fully exposed to solvent upon complete unfolding (confirmed by circular dichroism (see below)).

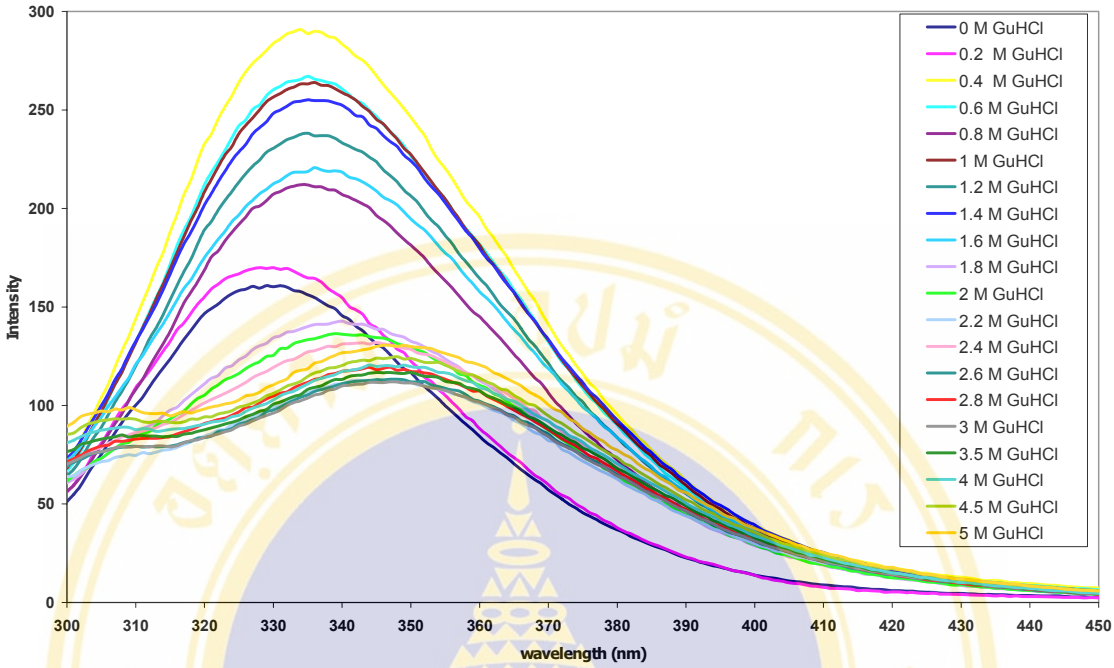

Figure 6.2 Fluorescence Spectra of adGSTD3-3 after equilibration at different guanidinium chloride concentrations. The data are mean ± standard deviation from at least 3 independent experiments.

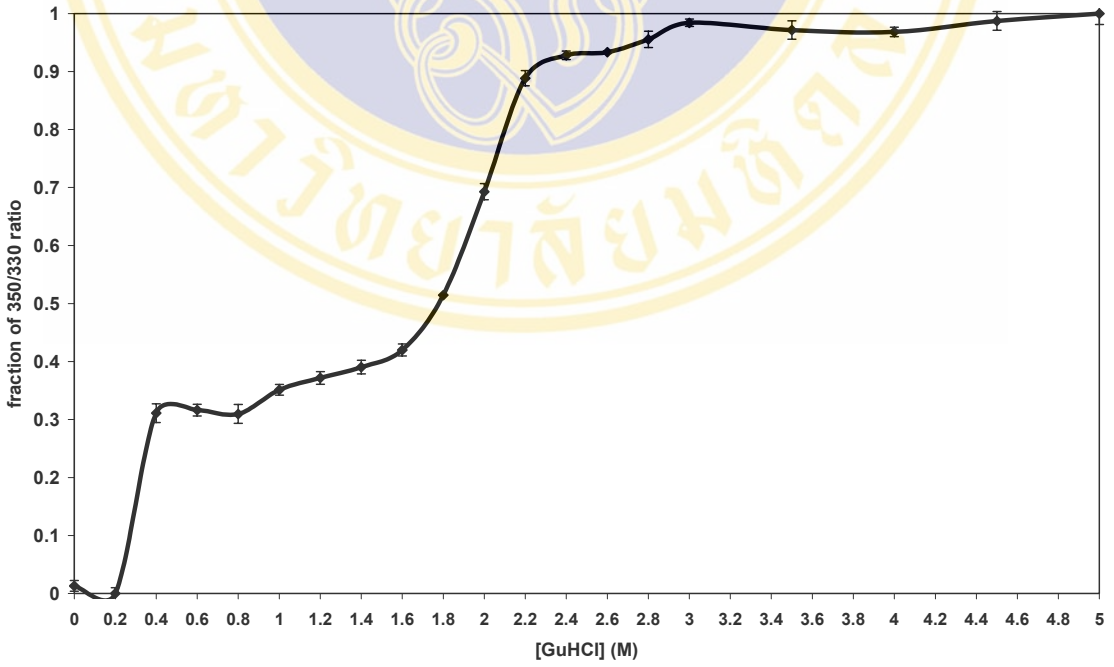

Figure 6.3 The GuHCl fluorescence unfolding curve of adGSTD3-3.
GuHCl-induced unfolding transitions for 0.1 mg/ml of adGSTD3-3 in 20 mM Na_2HPO_4, 5 mM DTT, 1 mM EDTA, pH 6.5. The data are mean ± standard deviation from 3 independent experiments.

6.3 ANS Binding Assay

In general this technique is used to determine the exposure of hydrophobic regions and formation of compact hydrophobic states during unfolding (95;96). For example, the enhanced ANS binding and the blue shift in the emission maximum during the unfolding process demonstrate that the binding environment becomes more hydrophobic (**Figure 6.4**). The unfolding curve which shows ANS binding at 480 nm (maximum intensity of the enzymes in 0 M guanidinium chloride) against guanidinium chloride concentration was determined (**Figure 6.5**).

The change of ANS spectra during the unfolding process was accompanied by shifts in the emission maximum for protein-bound ANS; a blue shift from 480 nm (0 M GuHCl) to 470 nm (0.2 M GuHCl), a red shift to 485 nm (0.4 M GuHCl0, a blue shift to 470 nm (0.6-4 M GuHCl) and a red shift to 520 nm (4.5-5 M GuHCl) (**Figure 6.4**), demonstrating that the binding environment became even more hydrophobic when a blue shift occurred and more hydrophilic when a red shift occurred.

Because ANS fluorescence is quenched by water, the increase or decrease of the fluorescence intensity of the protein bound ANS is highly dependent upon its accessibility to water. Although the location of the ANS binding sites is unknown for delta class GST, it is reasonable to assume that it binds at or near the dimer interface. ANS has been shown to bind at the solvent-exposed cleft in the subunit interface of alpha and pi class enzymes (97;98). In **Figure 6.5**, there are two peaks of ANS binding; the first enhancement from 0 M to 0.4 M GuHCl coincided with the initial tryptophan fluorescence change and the second enhancement from 1 M to 1.2 M GuHCl coincided with the second tryptophan fluorescence change, demonstrating that the hydrophobic interaction motif of the enzyme was altered. To observe the structural change during the unfolding pathway, the interesting points, 0 M, 0.4 M, 1.2 M, 2.6 M and 4 M GuHCl concentrations, were selected to be studied further by circular dichroism (CD) and size-exclusion chromatography.

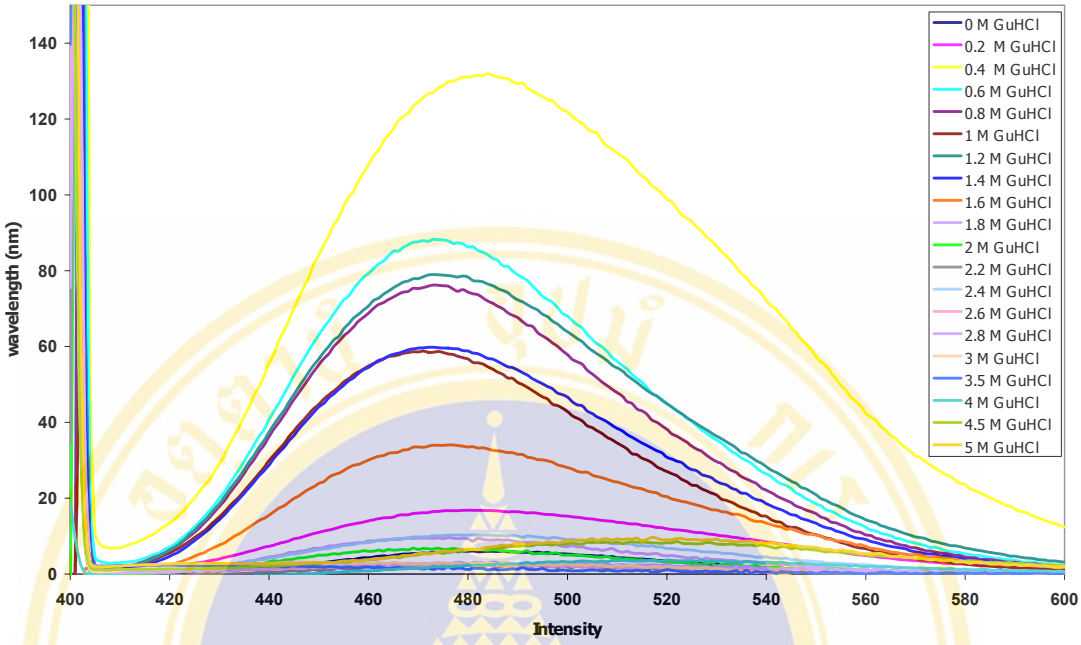

Figure 6.4 Fluorescence emission spectra of ANS bound to adGSTD3-3 after equilibration at different GuHCl concentrations. The data are mean ± standard deviation from at least 3 independent experiments.

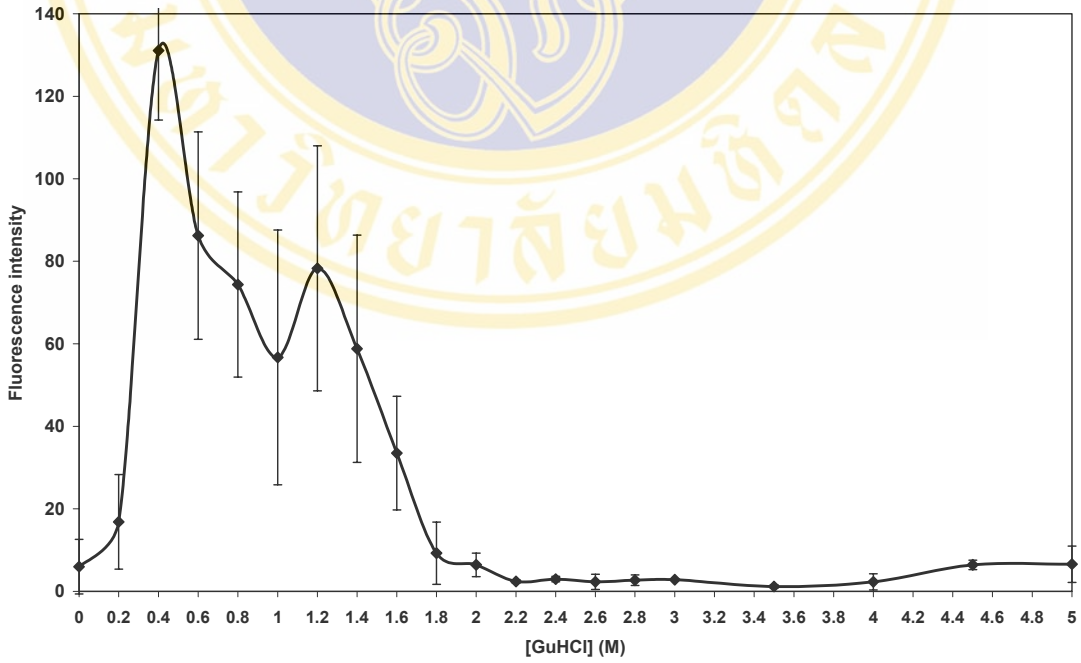

Figure 6.5 Relative ANS binding at 480 nm of adGSTD3-3.

GuHCl-induced unfolding transitions for 0.1 mg/ml of adGSTD3-3 in 20 mM Na_2HPO_4, 5 mM DTT, 1 mM EDTA, pH 6.5. The data are mean ± standard deviation from 3 independent experiments.

6.4 Circular Dichroism Spectroscopy

Circular dichroism (CD) is the ideal technique for studying chiral molecules in solution. It is uniquely sensitive to the asymmetry of the system. These features make it particularly attractive for biological systems. CD is now a routine tool in many laboratories. The most common applications include proving that a chiral molecule has indeed been synthesized or resolved into pure enantiomers and probing the structure of biological macromolecules, in particular determining the α-helical content of proteins (94). UV spectra of proteins are usually divided into the 'near' and 'far' UV regions. The near UV in this context means 250-300 nm and is also described as the aromatic region, though transitions of disulphide bonds (cystines) also contribute to the total absorption intensity here. The far UV (<250 nm) is dominated by transitions of the peptide backbone of the protein, but transitions from some side chains also contribute in this region and, especially if the protein α-helical content is low, may give rise to erroneous protein structure determinations (99).

At present the main use of CD in the study of proteins is as an empirical gauge of protein structure and conformation using the CD measuring the backbone amide transitions from ~190-240 nm (the far UV or peptide region of the spectrum). Distinctive CD spectra (**Figure 6.6**) have been described for pure conformations such as the α-helix, β-sheets and random coil. Employing CD, in unfolding pathway study we used this technique to monitor the disruption of protein secondary structure.

To determine the secondary structure of the different protein conformations, far-UV **c**ircular dichroism spectroscopy (200-260 nm) was used (**Figure 6.7)**. The native protein showed a trough at 222 nm as would be expected for a predominantly α-helix protein. The spectrum for protein in 0.4 M GuHCl showed a small change in the secondary structure in the characteristic region for α-helix by decreases of about 30% ellipticity. The spectrum for the enzyme in 1.2 M GuHCl showed a more substantial loss in secondary structure with less than half of the native ellipticity at 222 nm. The spectra of 2.6 and 4 M GuHCl confirmed that the protein is unfolded under these conditions and approximate a random coil conformation.

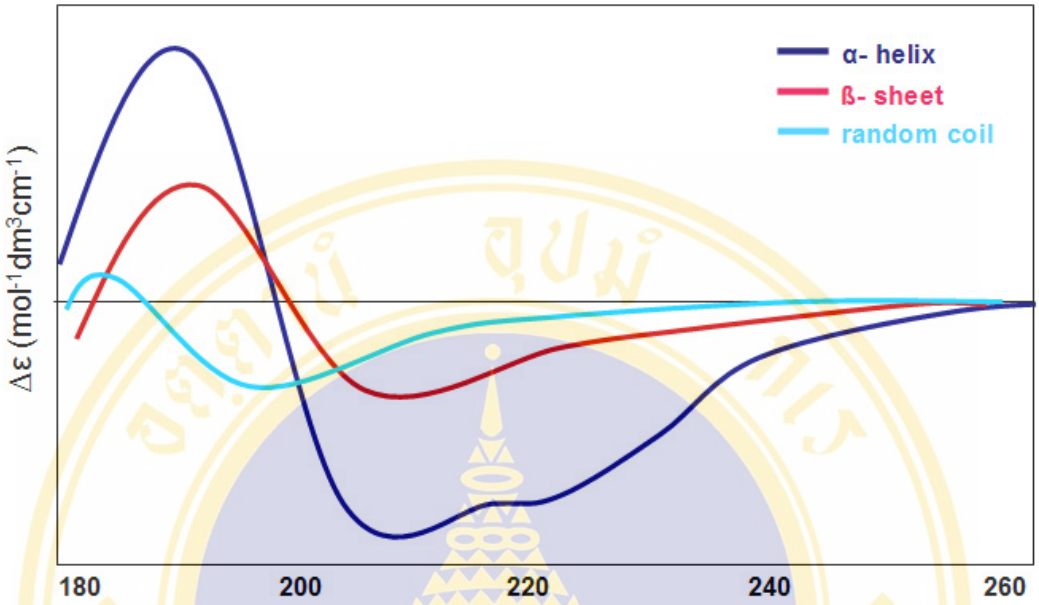

Figure 6.6 Typical protein CD spectra for particular secondary structural motifs of proteins in different conformations.

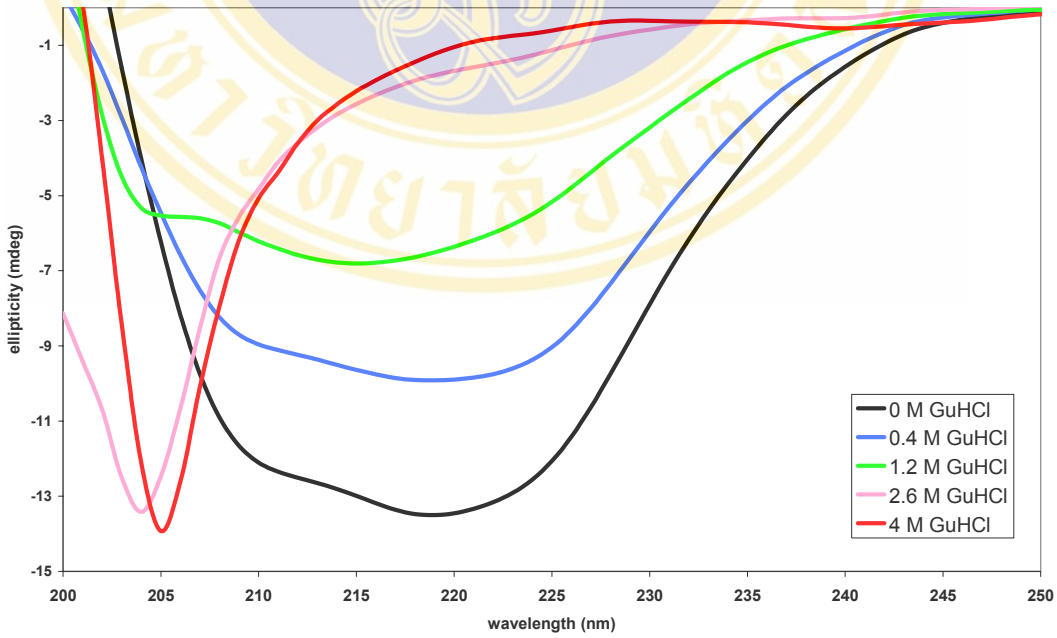

Figure 6.7 Far-UV circular dichroism spectra of adGSTD3-3 in different GuHCl concentrations. The data are mean from 3 independent experiments.

6.5 Size-Exclusion Chromatography

This method was performed to assess the quaternary structure of the enzyme under a range of GuHCl concentrations. Albumin, ovalbumin, chymotrypsinogen A and ribonuclease A which molecular weights of 67, 43, 25 and 14 kDa, respectively, were used as standard proteins (**Figure 6.8**). The elution profiles of the protein in various concentrations of GuHCl are shown in **Figure 6.9**. At 0.4 M GuHCl where the GST lost 100% activity, the enzymes had elution volumes that corresponded to a molecular mass of 50 kDa, as expected for the dimeric protein. This shows that at this concentration, the enzyme was still in dimeric form but the conformation was altered so the enzyme processed no activity. For 1.2 M GuHCl, there was no peak in the elution profile, indicating that at this concentration the protein did not perform like a globular protein that can be solved on column properly. At 2.6 M GuHCl, there was a peak that corresponded to the void volume, indicating that the protein was completely unfolded and most likely had aggregated and eluted as a large complex.

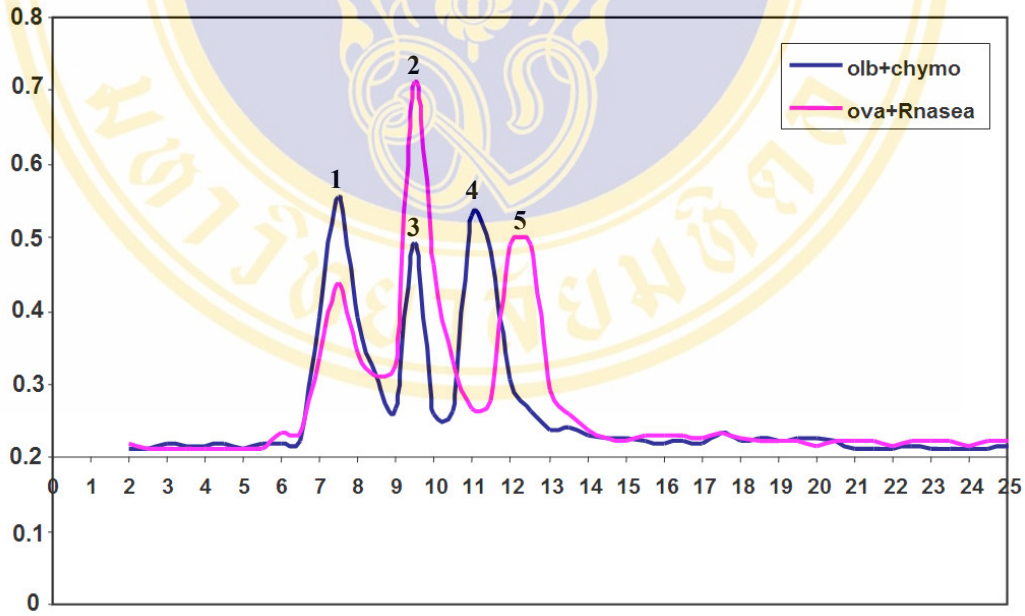

Figure 6.8 FPLC elution profiles of the standard proteins.
(1) blue dextran (void volume), (2) ovalbumin, (3) albumin, (4) chymptripsinogen A and (5) ribonuclease A.

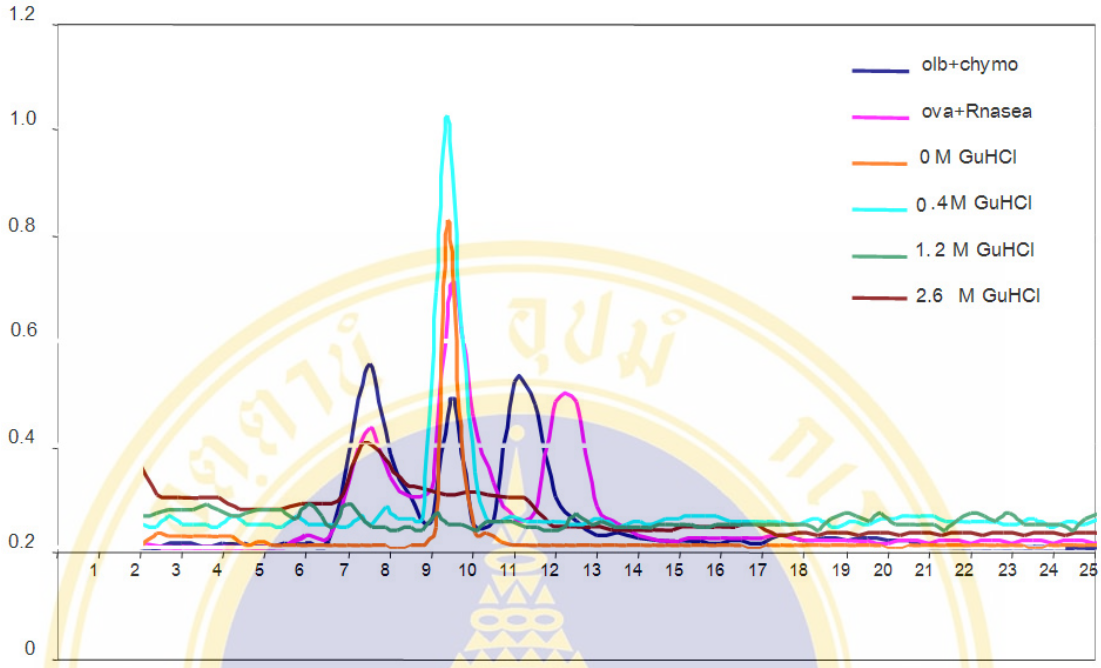

Figure 6.9 FPLC elution profiles of adGSTD3-3 incubated with increasing concentrations of GuHCl compared to the standard proteins. The data are mean from 2 independent experiments.

CHAPTER 7
DISCUSSION

7.1 The inter- and intra-subunit electrostatic interactions at the top of subunit interface are important interactions that help to maintain tertiary and quaternary structures of both isozymes.

The dimerization of the GSTs not only allow for the construction of a fully functional active site, part of which is situated near the subunit interface, but also contributes to the stabilization of the subunit tertiary structure. Although tertiary structures of all classes of GSTs are similar, dimerization is highly specific and occurs only between subunits within the same class. It is assumed that the difference in the structure of the subunit interface among the various GSTs is the basis for this discrimination. The structural features at the dimer interface of the GSTs suggest at least two major types of interactions, a hydrophobic ball-and-socket motif and electrostatic interactions at the subunit interface. The former has been wildly investigated in many classes of GSTs while the latter has been studied only in the alpha class. In insect delta class, the dimer interface features extensive hydrophobic and hydrogen bonding interaction in two major areas; the hydrophobic interactions at both sides of the interface which is the equivalent location of the ball-and-socket motif in the α/μ/π/Sj26 subunit type and the various interactions at the middle of the interface (**Figure 1.13**). In this thesis project, we are interested in the latter area which consists of the conserved electrostatic interactions at the top, the hydrophobic interactions at the center and the ionic interactions at the edge of the subunit interface (**Figures 1.15-1.18**).

The conserved electrostatic interactions at the top of the subunit interface are formed by four amino acid residues from different helices from both subunits (Glu75 in α3 and Arg96 in α4). These interactions are of interest because the directions of the four amino acids side chain interact with each other as a rectangle square planar

within 2.57-3.99 Å (**Figure 1.16**). These interactions are highly conserved among the GST classes; delta, sigma and theta, however there have been no investigations of these interactions in any of the three classes. These interactions are also present in the human GST classes, alpha, pi and mu, but the interactions are located in a different site of the subunit interface (**Figure 1.6**). The conserved salt-bridge in the alpha class showed that these residues are important in the monomer-dimer equilibrium(46).

Breaking these electrostatic interactions by the generation of two mutants of adGSTD4-4, Glu75Ala and Arg96Ala, showed that the interactions make an important contribution to stabilization and folding of the enzymes. The mutants expressed in both inclusion and soluble forms, with the Arg96Ala mutant being mostly expressed as inclusion body (**Figures 3.2 and 3.3**). This evidence and the results from the refolding assay (**Table 3.5** and **Figure 3.6**) indicated that the folding process was altered by the mutations. Moreover, from the enzyme purifications, only approximately 1-5 % of the total GST proteins from the bacterial lysate were obtained from glutathione affinity column (**Table 3.1**). This lower yield results from a reduction in binding affinity to the GSH on the gel matrix of the GSTrap column by disruption of the G-site conformation, the site providing amino acids which bind to GSH, as indicated by the K_m values (**Table 3.3**). Not only effecting the active site architecture as shown in **Table 3.2-3.3**, substitution by alanine at Arg96 also effected the tertiary and quaternary structure of the protein as shown by the intrinsic tryptophan fluorescence spectrophotometry (**Figure 3.5**) and ANS binding assay (**Figure 3.8**). The λ_{max} values of the mutants were similar to the wild type, indicating that a similar polarity characterizes the environment of the tryptophan residues present in all enzyme variants. However, the normalized intensities of fluorescence of the Arg96 mutants were approximately 66% decreased. This finding suggests that there are significant conformational changes characterizing the environment of the tryptophan residues located near the subunit interface and the mutation site. The ANS fluorescence intensity reflected the number of ANS bound to the protein and Arg96Ala appeared to significantly exhibit a lower capacity to bind ANS as suggested by the 5-fold decrease in ANS fluorescence intensity. This implies that the mutation alters the subunit interface conformation. Loss of the electrostatic interactions not only affected the protein folding and catalytic properties, but also affected the protein

stability as shown by the half-life values. The substitutions by alanine at both positions significantly decreased the half-life by approximately 7.4- and 15.4-fold for Glu75Ala and Arg96Ala, respectively (**Table 3.4**).

Although the charged residues are not involved in the active site pocket, the mutations at these positions affected the active site conformation, especially the Arg96Ala mutant (**Tables 3.2 and 3.3**). The available crystal structure of the enzyme showed that Glu75 is far from the substrate binding site; the shortest distance is ~10 Å between it and the GSH binding site of the same subunit. Therefore a mutation at this position should have a small effect on the catalytic properties of the enzyme. However, the Arg96 is a neighbor of Ala97, His100 and Ala68 (**Figures 7.1 and 7.2**) which have side and main chain hydrogen bonds with each other and other residues in the active site pocket an interaction network from arginine96 to the active site residues. Therefore, the mutation at arginine also alters the active site architecture by disruption of this network.

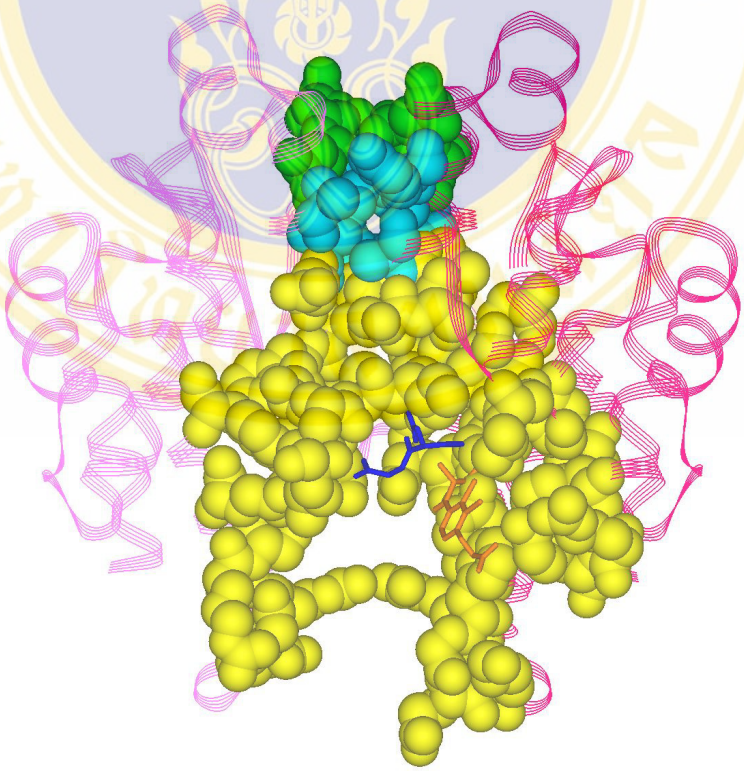

Figure 7.1 The CPK representation of the amino acid residues in the conserved electrostatic interactions (green), the network to the active site (blue) and the active site (yellow). The different colored ribbons represent the different subunits.

The substrates are represented as stick forms, dark blue is GSH and orange is EA.

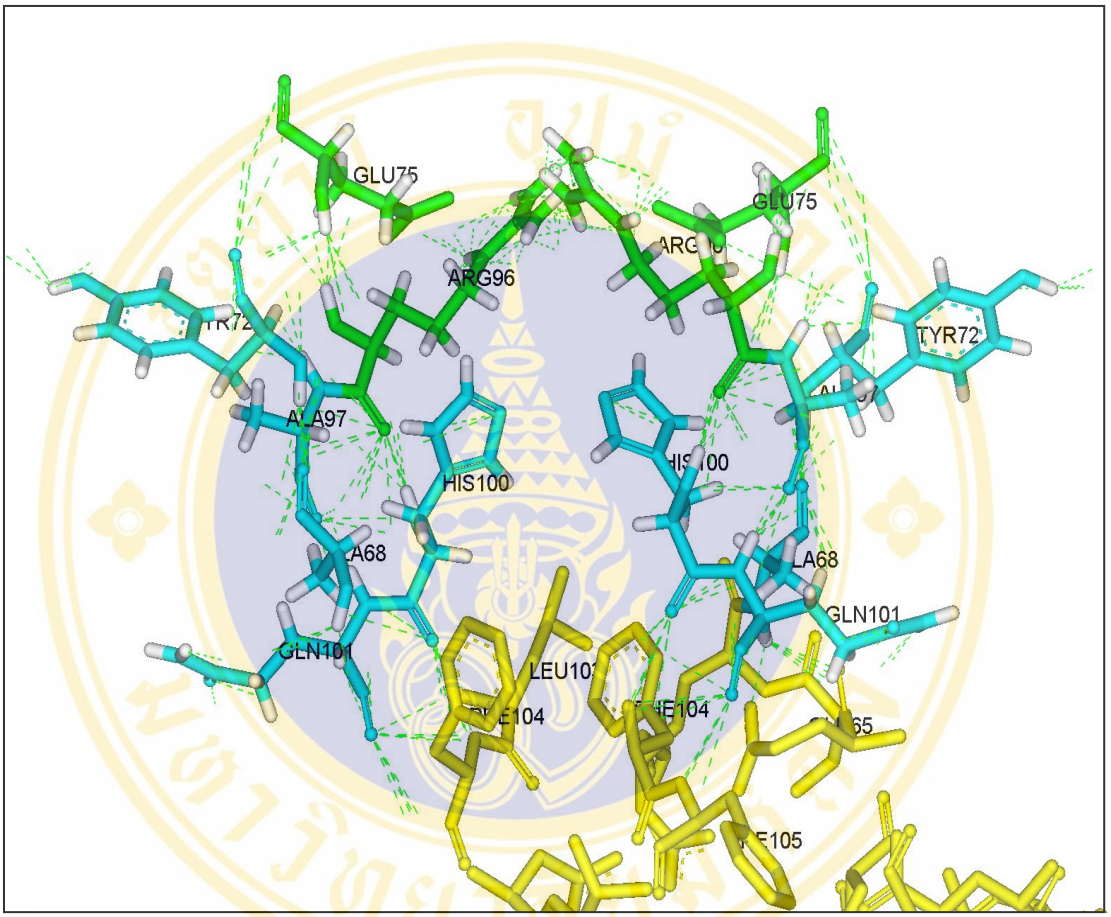

Figure 7.2 The interaction network from the conserved electrostatic interaction residues to the active site residues. The hydrogen bonds are shown as dashed lines. The conserved electrostatic interactions, the network to the active site and the active site residues are shown as green, blue and yellow stick models, respectively.

The alanine replacement of the arginine96 residue showed a dramatic effect on the tertiary structure, the subunit interface integrity and the folding of the protein. The crystal structure suggests that not only the conserved electrostatic interactions, but also the interaction and amino acid packing surround Arg96 are disrupted by the Arg96Ala mutation (**Figure 7.3**).

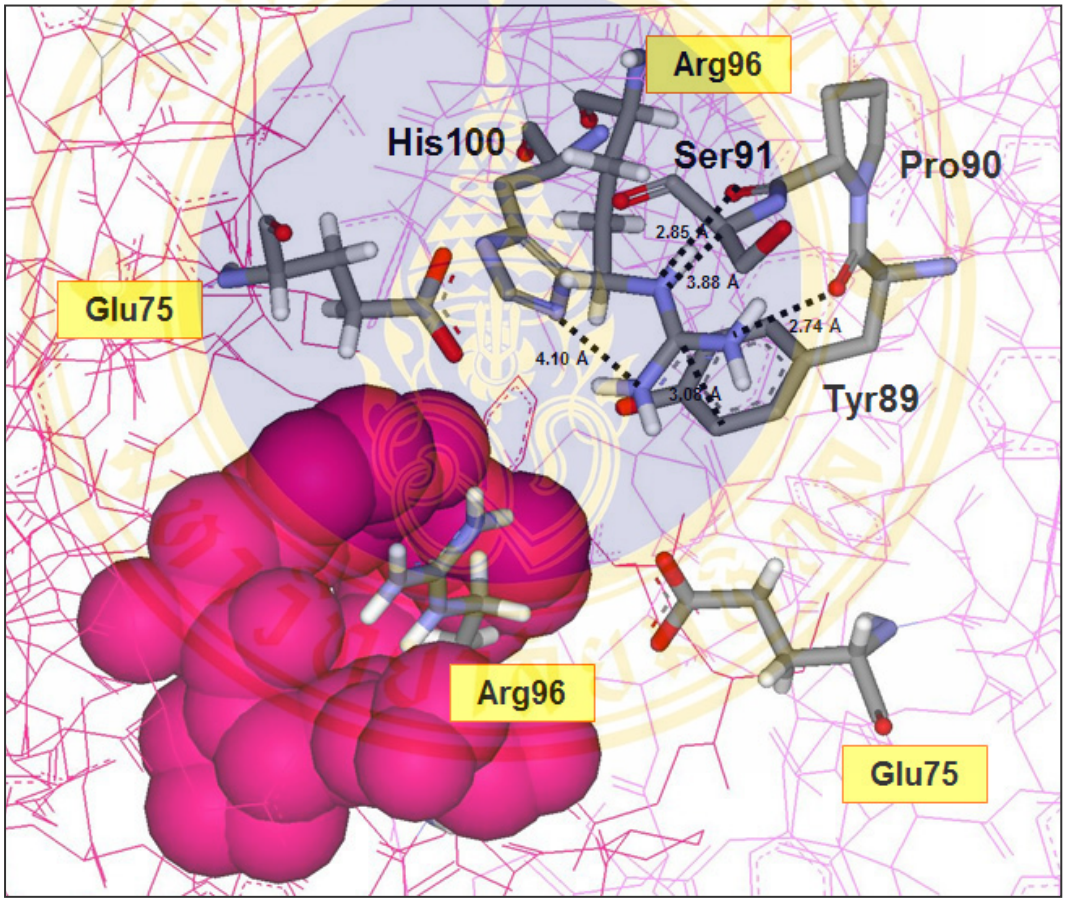

Figure 7.3 The environment residues of Arg96. The stick and CPK models are represented the amino acid around the Arg96 residues in subunit A and subunit B, respectively. The distances between the amino acid side chains are indicated by dash lines.

7.2 The variant hydrophobic amino acids at the center of the subunit interface influence the specific property of the individual spliceform.

Although this subunit interface region shows the most variation in amino acid residues at the equivalent positions between adGSTD3-3 and adGSTD4-4, the amino acid side chain directions are conserved (**Figure 1.13 circle B**). These subunit interface residues are of interest because they are not only the interface residues but also active site residues with several of them involved in both active sites (**Figure 7.4**). Therefore the effects of the different hydrophobic amino acids at the equivalent positions of the two isozymes was studied by disruption of the amino acid side chain packing by switching the equivalent amino acids with these mutations; Tyr98Phe, Met101Val, Gly102Ala and Tyr98Phe/Met101Val/Gly102Ala for adGSTD3-3 and Phe104Tyr, Val107Met, Ala108Gly and Phe104Tyr/Val107Met/ Ala108Gly for adGSTD4-4.

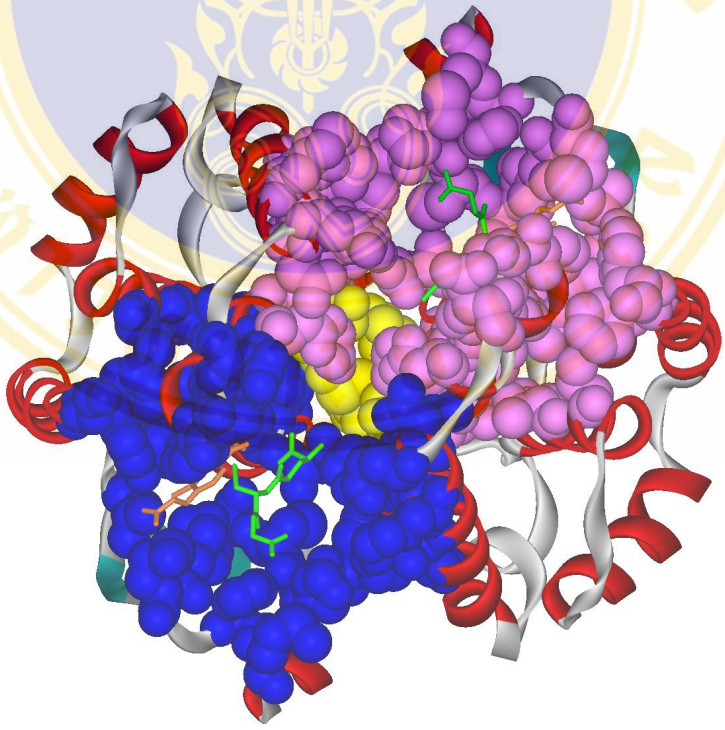

Figure 7.4 The CPK of the active site pocket residues of adGSTD3-3.
Pink and blue color represents the active site pocket of different subunit. The yellow are the three equivalent positions at the center of subunit interface, Tyr98, Met101 and Gly102. The sticks represent the substrates, the green is GSH and the orange is EA.

Each of these mutants expressed as a soluble form at 37ºC and yield approximately 40-80 % of total purified proteins from glutathione affinity column. It implies that the mutations did not have much effect on protein folding in the individual subunits which was confirmed by the intrinsic fluorescence spectroscopy that showed that every mutant had the same λ_{max} as the wild types (**Figures 4.12 and 4.13**). The different intensities of several mutants may be caused from conformational changes of the tryptophan environment which is located near the subunit interface and the mutation site. The electric properties of the tryptophan excited state highly dependent on the nature of its environment (**Figure 7.5**). Intra-molecular interactions; an electrostatic exchange process of disulfide bonds, the neutral amide of glutamine and asparagines as well as a short range electron transfer from the close proximity of the indole ring to the amide backbone of the protein, can enhance or quench the fluorescence. Moreover, the enhancement of fluorescence intensity can occur when the Trp residue is located in a hydrophobic environment.

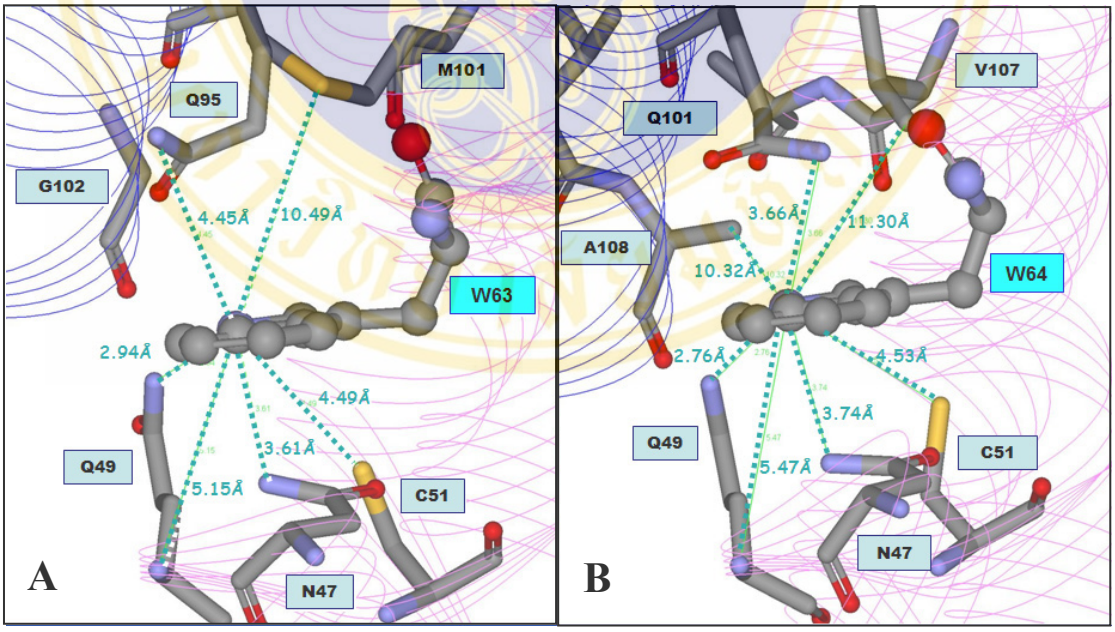

Figure 7.5 The amino acid environment of tryptophan residues.

Tryptophan residues were represented by ball-and-stick models and the residues around the tryptophans were shown by stick models. (A) adGSTD3-3 and (B) adAGSTD4-4

The refolding experiments demonstrated that every enzyme could be refolded back to the same back bone architecture as the native form as showed by similar λ_{max} values (**Figures 4.14 and 4.15**) although the % activity recovery of the mutants varied (**Tables 4.8 and 4.9**). This indicates that the mutations have only slight effect on the tertiary structure folding of each subunit but have more influence on the dimerization process which is necessary for an appropriate active site conformation. For example, the adGSTD4-Val107Met mutant could not recover catalytic activity implying that this residue plays a critical role in the dimerization of the enzymes.

For the protein characterizations to determine whether the mutations alter the catalytic activity, the thermal stability or the subunit interface conformation, the results showed that the mutations at the equivalent positions of both isozymes showed various effects on the enzyme properties.

When comparing between the two isoforms in terms of changes in catalytic activity, the mutations affected the proteins in different ways for the equivalent residues as shown in **Tables 4.2-4.4**. The crystal structures show that all selected equivalent positions are located in the active site pocket indicating that the whole electrostatic field in the active site pocket was disturbed by the mutations which thereby altered the catalytic parameters of the enzymes (**Figure 7.6**). Moreover, these residues are also located at the interface of the two domains which provided different substrate binding sites, for GSH and the hydrophobic substrate. These positions allowed the residues to influence both substrates binding as shown by the K_m values.

Several mutants possessed similar stability as the wild type enzymes (**Tables 4.6 and 4.7**). However, there were three mutants which had thermal stability significantly changed. Two of them were the mutants at the same equivalent position, adGSTD3-Gly102 and adGSTD4-Ala108. Replacement of glycine by alanine of adGSTD3 at this position caused decreases of about 8-fold in half-life, whereas, glycine substitution of adGSTD4 showed an increase of about 4.7-fold. The mutations at this equivalent position showed that this position impacted upon the structure as shown by the increase in stability. This influence was also observed when increasing the side chain from glycine to alanine which made the protein less stable. Other mutant that showed stability change was the adGST4-4 mutant in which valine107

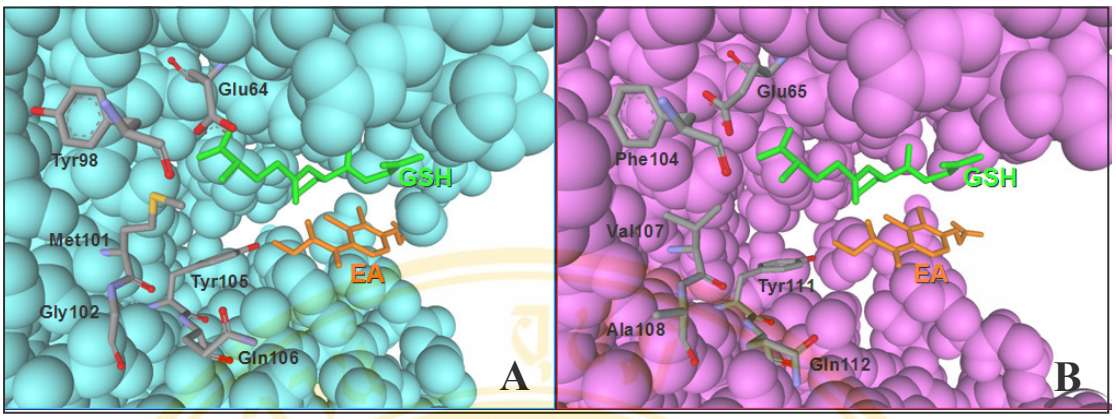

Figure 7.6 The active site pocket of adGSTD3-3 (A) and adGSTD4-4 (B).
The sticks represent the interface residues and substrates, the green stick is GSH and the orange stick is EA.

was replaced by Methionine. This mutant stability was approximately 3-fold less than the wild type while the equivalent position mutant of adGSTD3-3, Met101Val, had no effect. Alanine mutations at this equivalent position in the two splice forms, showed a huge effect to the protein stability by increasing the half-life approximately 17-fold in adGSTD4-4 while the adGSTD3-3 mutant showed only a slight effect (**Table 1.1**). The crystal structure demonstrated that the first sphere milieu of this position, M101 of adGSTD3-3 and Val107 of adGSTD4-4, have seven amino acids of which only two residues are different between the two isoforms, adGSTD3-Tyr98 and adGSTD4-Phe104 and adGSTD3-Gly102 and adGSTD4-Ala108 (**Figure 7.7**). However, the triple mutations, which changed all three amino acids at these equivalent positions to the amino acid of the another isoform, showed that they had only a slight effect on the half-life (**Tables 4.6 and 4.7**). Due to the hydrophobicity of these residues, the steric interactions and Van der Waals force are important interactions for the stability of the proteins (100;101). Therefore, the side chain size of the three amino acids at these equivalent positions had a major impact on the subunit interface between the two splice forms especially Met101 and Gly102 of adGSTD3-3 and Val107 and Ala108 of adGSTD4-4. Although the amino acids display similar properties, the amino acid replacement can alter the protein properties.

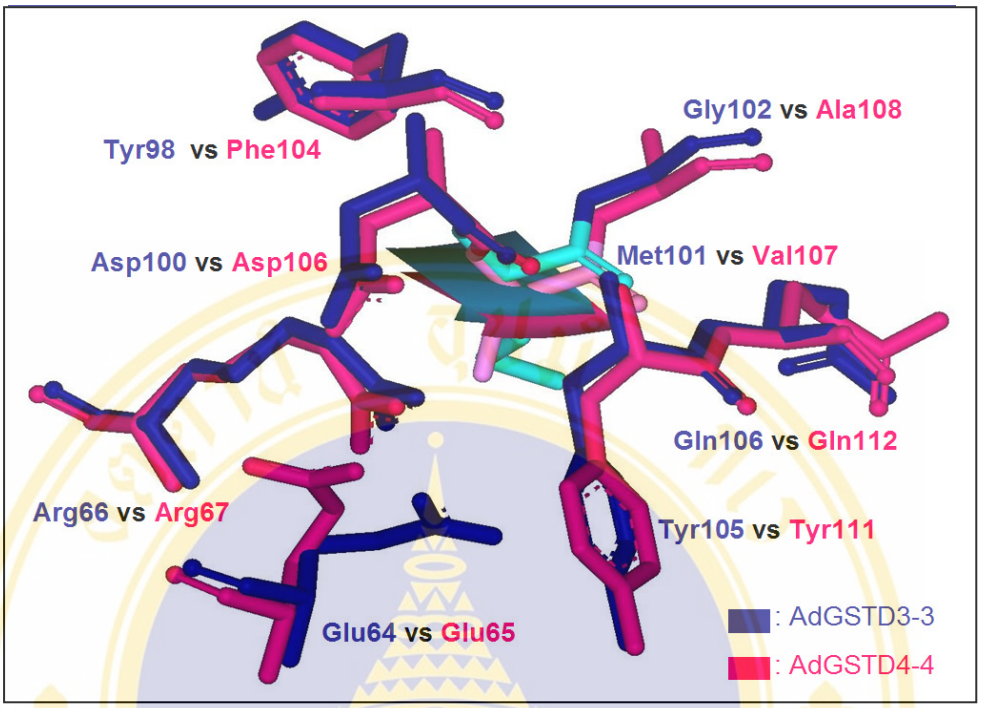

Figure 7.7 The amino acids milieu of adGSTD3-Met101 and asGSTD4-Val107. The different colors represent the different isoform; blue is adGSTD3-3 and pink is adGSTD4-4.

In conclusion, this subunit interface region which has the most variation in amino acid residues at the equivalent positions between adGSTD3-3 and adGSTD4-4 showed that although the mutations did not alter the overall protein folding, the enzyme properties were changed by the mutations especially the catalytic activity, thermal stability and subunit interface. The amino acid replacement can change the protein properties even though the replacement did not much differ in properties that is tyrosine and phenylalanine, methionine and valine, and glycine and alanine. This implies that even the splicing products from the same gene may also have specific features in the subunit interface area.

7.3 The charge-charge network at the edge of adGSTD4-4 subunit interface is an important interaction that helps to maintain tertiary and quaternary structure of the enzymes.

From the conserved electrostatic interactions at the top to the hydrophobic region at the center of the subunit interface, every residue appears to be important to neither maintain structure or for subunit binding. The last area is the hydrophilic region at the bottom edge of the subunit interface, Asp110 and Asn126 of adGSTD3-3 and Glu116 and Arg134 of adGSTD4-4. Not only are these subunit interface residues, but these two equivalent positions also are involved in the active site pockets in part of the H-site (a hydrophobic substrate binding site). Asp110Ala of adGSTD3-3 and Glu116Ala of adGSTD4-4 were generated to study the role of the interactions at this area. Both positions affected the catalytic activity in terms of both specific activity and kinetic parameters. However, only the Glu116Ala mutant showed that it is an important residue for protein stability and the dimerization process as shown by stability assay (**Table 5.4**), refolding assay (**Table 5.5**) and ANS binding assay (**Figures 5.7 and 5.8**).

7.4 adGSTD3-3 shows four-state unfolding pathway.

Equilibrium denaturation studies of proteins provide valuable information on the autonomous folding of domains, the relationship of folding and oligomerization process, and determination of the thermodynamic significance of subunit interface interactions. Most of our knowledge on protein folding derives from studies on small monomeric proteins (47;48;102). However, the majority of native proteins are more complex, composed of several subunits that in turn consist of domains. The extrapolation of results obtained in the study of small proteins to larger ones is not always appropriate, and it is therefore important to investigate proteins composed of more than one subunit (49). GSTs provide a useful model for studying stability and folding within a well-characterized super family of dimeric proteins with conserved overall structures and diverse functional properties. From the equilibrium unfolding study of four classes of GSTs, μ, α, π, and σ class, the σ, GSTS1-1, is the most stable

and unfolds via a four-state pathway ($N_2 \leftrightarrow I_2 \leftrightarrow 2M \leftrightarrow 2U$) (49;59). While μ class, GSTM1-1 and GSTM2-2, unfold via a three-state pathway ($N_2 \leftrightarrow 2M \leftrightarrow 2U$) (42) and other classes unfold via a two-state pathway ($N_2 \leftrightarrow 2U$) (54;55). Polar interactions predominate at the subunit interface for example the electrostatic forces and the charge cluster of GST σ class and μ class, respectively, suggests ionic strength has major affect on stability. The GST solvation by water and/or shielding by salt during unfolding most likely affects subunit association and facilitates the formation of the stable dimeric and monomeric intermediates (59).

In this thesis, the unfolding pathway investigation of adGSTD3-3 and adGSTD4-4 which the subunit interface has extensive hydrophobic and hydrogen bonding interaction in two major areas; the hydrophobic interactions at both sides of the interface which is the equivalent location of the ball-and-socket motif in the α/μ/π/Sj26 subunit type and the variant interactions at the middle of the interface (**Figure 1.13**). Moreover, due to the different amino acid sequence and the enzymatic properties, the unfolding pathway was studied to determine whether these two splicing products show the same or a different unfolding pathway.

The fluorescence unfolding curve of adGSTD3-3 (**Figure 7.8**) demonstrated that the presence of multiple transitions is highly suggestive of the existence of two stable intermediates. The first unfolding transition from native dimer (N_2) to a dimeric intermediate (I_2) was confirmed by the size-exclusion chromatography (FPLC) at 0.4 GuHCl, the concentration that the intermediate is well-populated. The dimeric intermediate is completely inactive as seen by the remaining activity assay and ANS binding assay which showed the combined effect of the partial unfolding producing the dimeric intermediate and the dissociation into the monomeric state. The CD and fluorescence spectra of the dimeric intermediate showed a small change in secondary and tertiary structure, respectively (103).

The second unfolding transition is the presence of the dissociation of the dimeric intermediate (I_2) to two monomeric intermediates (2I). The CD spectrum demonstrated that the secondary structure of the monomeric intermediate is substantially different from the native state with a decrease in ellipticity to less than half while still retaining significant structure content as confirmed by the ability to bind ANS.

The third transition is a unfolding process from monomeric intermediate (2I) to the unfolded state (2U) which was confirmed by the CD spectrum and the loss of ability to bind ANS.

The results from this study, therefore, are strongly supportive of the following four-state pathway for adGSTD3-3:

Native form ↔ Dimeric intermediate ↔ Monomeric intermediate ↔ Unfolded form
(N_2) (I_2) (2I) (2U)

This unfolding pathway is similar to the pathway which has been observed for class sigma GSTS1-1 as mention above (49;59). However, the dimeric intermediate of adGSTD3-3 in the presence of GuHCl appeared to have a more loosely packed quaternary structure displaying enhanced binding of ANS while the dimeric intermediate of the sigma class showed the same quaternary structure as the native form. The sigma and delta classes have a similar subunit interface feature that is lacking the ball-and-socket motif and consisting of hydrophilic interactions along the subunit interface area. The conserved electrostatic interactions at the top and the ionic interactions at the bottom edge of subunit interface which have been studied in this thesis are important factors that affect the subunit association and facilitate the formation of the stable dimeric and monomeric intermediates. The absence of stable intermediate states along the unfolding pathways of α and π classes could be due to the predominantly hydrophobic nature and the lack of hydrophilic interactions of their subunit interfaces that would be unstable when exposed to solvent.

Although adGSTD3-3 and adGSTD4-4 are highly homologous proteins, they display non-identical conformational dynamics, the structural basis of which is yet unknown. AdGSTD3-3 was soluble in the unfolding solution while adGSTD4-4 aggregated in the unfolding solutions from 0 M to 1.8 M GuHCl concentrations. Therefore, the unfolding pathway of adGSTD4-4 is still unknown. The native tertiary structures of adGSTD3-3 and adGSTD4-4 are similar as shown by similar tryptophan environments (**Figure 4.11)**. However, their N_2 subunit interfaces are not identical as reflected by their different ANS binding spectra and the electrostatic field and the solvent-exposed cleft at the subunit interface (**Figures 4.24 and 7.8**). The subunit

interface of adGSTD4-4 showed less polarity and provides a greater amount of ANS binding sites when compared with adGSTD3-3. This feature may be a factor that influences the different folding dynamics of the two splicing products. A further unfolding experiment utilizing urea as the denaturant should be investigated.

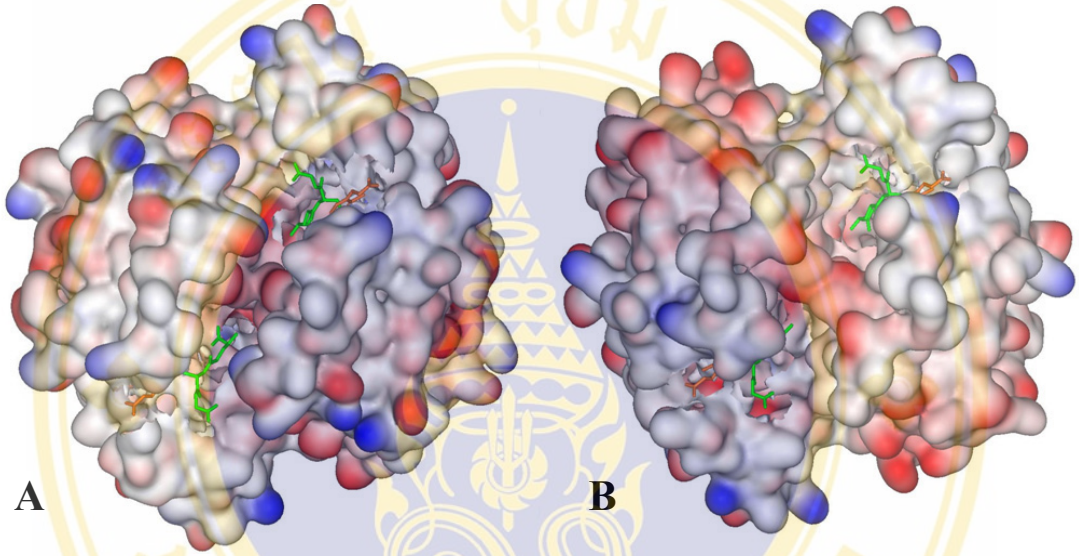

Figure 7.8 The electrostatic field and the solvent-exposed cleft at the subunit interface. (A) adGSTD3-3 and (B) adGSTD4-4. The sticks represent the substrates, the green is GSH and the orange is EA.

CHAPTER 8
CONCLUSION

The results of this thesis project which is the characterizations of the contributions of amino acids at the subunit interface of adGSTD3-3 and adGSTD4-4 in effecting the enzyme properties lead to four conclusions.

1. The conserved electrostatic interactions at the top of subunit interface, which are formed by the two glutamate75 and the two arginine96 of adGSTD4-4, are the critical interactions that help to maintain tertiary and quaternary structures of the enzymes.

2. The variant hydrophobic amino acids at the center of subunit interface influenced the specific property of the individual splice form of the adgst1AS1 gene.

3. The charge-charge network interactions at the edge of adGSTD4-4 subunit interface between Glu116 and Arg134 are the important interactions that help to maintain tertiary and quaternary structures of the enzymes.

4. AdGSTD3-3 unfolding occurs via four-state pathway ($N_2 \leftrightarrow I_2 \leftrightarrow 2I \leftrightarrow 2U$) while the adGSTD4-4 the unfolding pathway is still unknown.

REFERENCES

1. Booth J, Boyland E, Sims P. An enzyme from rat liver catalysing conjugations with glutathione. Biochem J 1961; 79:516-524.

2. Schmidt-Krey I, Mitsuoka K, Hirai T, Murata K, Cheng Y, Fujiyoshi Y et al. The three-dimentional map of microsomal glutathione transferase 1 at 6 Å resolution. EMBO J 2000; 19(23):6311-6316.

3. Hayes JD, Pulford DJ. The glutathione S-transferase supergene family: Regulation of GST and the contribution of the isoenzymes to cancer chemoprotection and drug resistance. CRC Crit Rev Biochem Molec Biol 1995; 30(6):445-600.

4. Armstrong RN. Structure, catalytic mechanism, and evolution of the glutathione transferases. Chem Res Toxicol 1997; 10:2-18.

5. Caccuri AM, Ascenzi P, Antonini G, Parker MW, Oakley AJ, Chiessi E et al. Structural flexibility modulates the activity of human glutathione transferase P1-1. Influence of a poor co-substrate on dynamics and kinetics of human glutathione transferase. J Biol Chem 1996; 271:16193-16198.

6. Armstrong RN, Rife C, Wang Z. Structure, mechanism and evolution of thiol transferases. Chemico-Biological Interactions 2001; 133:167-169.

7. Eaton DL, Bammler TK. Concise review of the glutathione S-transferases and their significance to toxicology. Toxicological Science 1999; 49:156-164.

8. Hemingway J, Hawkes N, Prapanthadara L, Jayawardena KGI, Ranson H. The role of gene splicing, gene amplification and regulation in mosquito insecticide resistance. Phil Trans R Soc Lond B 1998; 353:1695-1699.

9. Brophy PM, Barrett J. Glutathione transferase in helminths. Parasitology 1990; 100:345-349.

10. Marrs KA. The functions and regulation of glutathione *S*-transferases in plants. Ann Rev Plant Physiol Plant Mol Biol 1996; 47:127-158.

11. Lien S, Larsson A-K, Mannervik B. The polymorphic human glutathione transferase T1-1, the most efficient glutathione transferase in the denitrosation and inactivation of the anticancer grug 1,3-bis(2-chloroethyl)-1-nitrosourea. Biochem Pharmacol 2002; 63:191-197.

12. Vuilleumier S. Bacterial Glutathione S-transferases: What are they good for? J Bacteriol 1997; 179(5):1431-1441.

13. Hemingway J. The molecular basis of two contrasting metabolic mechanism of insecticide resistance. Insect Biochem Molec Biol 2000; 30:1009-1015.

14. Bruns CM, Hubatsch I, Ridderstrɔ m M, Mannervik B, Tainer JA. Human glutathione transferase A4-4 crystal structures and mutagenesis reveal the basis of high catalytic efficiency with toxic lipid peroxidation products. J Mol Biol 1999; 288:427-439.

15. Csiszr J, Szab M, Ills E, Kurucz K. Investigations of glutathione S-transferase and peroxidase activities in auxin heterotrophic and autotrophic tobacco calli under salt stress conditions. Acta Biologica Szegediensis 2002; 46 (3-4):79-80.

16. Pettersson PL, Mannervik B. The Role of Glutathione in the Isomerization of Δ^5 -Androstene-3, 17-dione Catalyzed by Human Glutathione Transferase A1-1. J Biol Chem 2001; 276:11698-11704.

17. Pettersson PL, Mannervik B. The isomerization of Δ^5-androstene-3,17-dione catalyzed by human glutathione transferase A1-1. Chemico-Biological Interactions 2001; 133:196-199.

18. Johansson A-S, Mannervik B. Human glutathione transferase A3-3, a highly efficient catalyst of double-bond isomerization in the biosynthetic pathway of steroid hormones. J Biol Chem 2001; 276(35):32061-32065.

19. Lo Bello M, Nuccetelli M, Caccuri AM, Stella L, Parker MW, Rossjohn J et al. Human glutathione transferase P1-1 and nitric oxide carriers : A new role for an old enzyme. J Biol Chem 2001; 276(45):42138-42145.

20. Oakley AJ, Lo Bello M, Nuccetelli M, Mazzetti AP, Parker MW. The ligandin (non-substrate) binding site of human Pi class glutathione transferase is located in the electrophile binding site (H-site). J Mol Biol 1999; 291:913-926.

21. Lyon RP, Atkins WM. Kinetic characterization of native and Cysteine 112-modified glutathione *S*-transferase A1-1: Reassessment of nonsubstrate ligand binding. Biochemistry 2002; 41:10920-10927.

22. Sayed Y, Wallace LA, Dirr HW. The hydrophobic lock-and-key intersubunit motif of glutathione transferase A1-1: implications for catalysis, ligandin function and stability. FEBS Lett 2000; 465:169-172.

23. Adler V, Yin Z, Fuchs SY, Benezra M, Rosario L, Tew KD et al. Regulation of JNK signaling by GSTp. EMBO J 1999; 18(5):1321-1334.

24. Wang T, Arifoglu P, Ronai Z, Tew KD. Glutathione *S*-transferase P1-1 (GSTP1-1) inhibits c-Jun N-terminal kinase (JNK1) signaling through interaction with the C terminus. J Biol Chem 2001; 276(24):20999-21003.

25. Cho S-G, Lee YH, Park H-S, Ryoo K, Kang KW, Park J et al. Glutathione *S*-transferase Mu modulates the stress-activated signals by suppressing apoptosis signal-regulating kinase 1. J Biol Chem 2001; 276(16):12749-12755.

26. Dulhunty A, Gage P, Curtis S, Chelvanayagam G, Board P. The glutathione transferase structural familyincludes a nuclear chloride channel and a

ryanodine receptor calcium release channel modulator. J Biol Chem 2001; 276(5):3319-3323.

27. Harrop SJ, DeMaere MZ, Fairlie WD, Reztsova T, VAlenzuela SM, Mazzanti M et al. Crystal structure of a soluble form of the intracellular chloride ion channel CLIC1 (NCC27) at 1.4-ล Resolution. J Biol Chem 2001; 276 (48):44993-45000.

28. Beckett GJ, Hayes JD. Glutathione S-transferases: Biomedical applications. Adv Clin Chem 1993; 30:281-380.

29. Mannervik B. The isoenzymes of glutathione transferase. Adv Enzymol Relat Areas Mol Biol 1985; 57:357-417.

30. Mannervik B, Danielson UH. Glutathione transferases - structure and catalytic activity. CRC Crit Rev Biochem 1988; 23:283-337.

31. Ketterer B. A bird's eye view of the glutathione transferase field. Chemico-Biological Interactions 2001; 138:27-42.

32. Wilce MCJ, Parker MW. Structure and function of glutathione S-transferases. Biochim Biophys Acta 1994; 1205:1-18.

33. Oakley AJ, Harnnoi T, Udomsinprasert R, Jirajaroenrat K, Ketterman AJ, Wilce MCJ. The crystal structures of glutathione S-transferases isozymes 1–3 and 1–4 from *Anopheles dirus* species B. Protein Science 2001; 10:2176-2185.

34. Reinemer P, Dirr HW, Ladenstein R, Huber R, Lo Bello M, Federici G et al. Three-dimensional structure of class π glutathione S-transferase from human placenta in complex with S-hexylglutathione at 2.8 ล resolution. J Mol Biol 1992; 227:214-226.

35. Sinning I, Kleywegt GJ, Cowan SW, Reinemer P, Dirr HW, Huber R et al. Structure determination and refinement of human Alpha class glutathione

transferase A1-1, and a comparison with the Mu and Pi class enzymes. J Mol Biol 1993; 232:192-212.

36. Patskovska LN, Federov A, Patskovsky YV, Almo SC, Listowsky I. Expression, crystallization and preliminary X-ray analysis of ligand-free human Glutathione S-transferase M2-2. Acta Crystallogr D Biol Crystallogr 1998; 54(1):458-460.

37. Rossjohn J, McKinstry W, Oakley A, Verger D, Flanagan J, Chelvanayagam G et al. Human theta class glutathione transferase: the crystal structure reveals a sulfate-binding pocket within a buried active site. Structure 1998; 6 (3):309-322.

38. Board PG, Coggan M, Chelvanayagam G, Easteal S, Jermiin LS, Schulte GK et al. Identification, characterization, and crystal structure of the omega class glutathione transferases. J Biol Chem 2000; 275:24798-24806.

39. Ji X, Von Rosenvinge EC, Johnson WW, Tomarev SI, Paitigorsky J, Armstrong RN et al. Three-dimensional structure, catalytic properties, and evolution of a sigma class glutathione transferase from squid, a progenitor of the lens S-crystallins of cephalopods. Biochemistry 1995; 34:5317-5328.

40. Rossjohn J, Polekhina G, Feil SC, Allocati N, Masulli M, Di llio C et al. A mixed disulfide bond in bacterial glutathione transferase: functional and evolutionary implications. Structure 1998; 6:721-734.

41. McTigue MA, Williams DR, Tainer JA. Crystal structure of a schistosomal drug and vaccine target: Glutathione S-transferase from *Schistosoma japonica* and its complex with the leading antischistosomal drug praziquantel. J Mol Biol 1995; 246:21-27.

42. Hornby JAT, Luo J-K, Stevens JM, Wallace LA, Kaplan W, Armstrong RN et al. Equilibrium folding of dimeric class μ glutathione transferases involves a stable monomeric intermediate. Biochemistry 2000; 39:12336-12344.

43. Ji X, Zhang P, Armstrong RN, Gilliland GL. The three-dimensional structure of a glutathione S-transferase from the Mu gene class. Structural analysis of the binary complex of isoenzyme 3-3 and glutathione at 2.2-ล resolution. Biochemistry 1992; 31:10169-10184.

44. Sayed Y, Wallace LA, Dirr HW. The hydrophobic lock-and-key intersubunit motif of glutathione transferase A1-1: implications for catalysis, ligandin function and stability. Chemico-Biological Interactions 2001; 133:60-62.

45. Agianian B, Tucker PA, Schouten A, Leonard K, Bullard B, Gros P. Structure of a *Drosophila* Sigma class glutathione S-transferase reveals a novel active site topography suited for lipid peroxidation products. J Mol Biol 2003; 326:151-165.

46. Vargo MA, Nguyen L, Colman RF. Subunit interface residues of glutathione S-transferase A1-1 that are important in the monomer-dimer equilibrium. Biochemistry 2004; 43:3327-3335.

47. Ionescu RM, Eftink MR. Global analysis of the acid-induced and urea-induced unfolding of Staphylococcal nuclease and two of its variants. Biochemistry 1997; 36:1129-1140.

48. Gupta R, Yadav S, Ahmad F. Protein stability: urea-induced versus guanidine-induced unfolding of metmyoglobin. Biochemistry 1996; 35:11925-11930.

49. Stevens JM, Hornby JAT, Armstrong RN, Dirr HW. Class sigma glutathione transferase unfolds via a dimeric and a monomeric intermediate: Impact of subunit interface on conformational stability in the superfamily. Biochemistry 1998; 37:15534-15541.

50. Kong GKW, Polekhina G, McKinstry WJ, Parker MW, Dragani B, Aceto A et al. Contribution of glycine 146 to a conserved folding module affecting stability and refolding of human glutathione transferase P1-1. J Biol Chem 2003; 278(2):1291-1302.

51. Aceto A, Caccuri AM, Sacchetta P, Bucciarelli T, Dragani B, Rosato N et al. Dissociation and unfolding of Pi-class glutathione transferase. Evidence for a monomeric inactive intermediate. Biochem J 1992; 285:241-245.

52. Dragani B, Stenberg G, Melino S, Petruzzelli R, Mannervik B, Aceto A. The conserved N-capping box in the hydrophobic core of glutathione S-transferase P1–1 is essential for refolding. Identification of a buried and conserved hydrogen bond important for protein stability. J Biol Chem 1997; 272:25518-25523.

53. Stenberg G, Dragani B, Cocco R, Mannervik B, Aceto A. A conserved "hydrophobic staple motif" plays a crucial role in the refolding of human glutathione transferase P1-1. J Biol Chem 2000; 275:10421-10428.

54. Dirr HW, Wallace LA. Role of the C-terminal helix 9 in the stability and ligandin function of class a glutathione transferase A1-1. Biochemistry 1999; 38:15631-15640.

55. Wallace LA, Sluis-Cremer N, Dirr HW. Equilibrium and kinetic unfolding properties of dimeric human glutathione transferase A1-1. Biochemistry 1998; 37:5320-5328.

56. Hornby JAT, Codreanu SG, Armstrong RN, Dirr HW. Molecular recognition at the dimer interface of a class Mu glutathione transferase: Role of a hydrophobic interaction motif in dimer stability and protein function. Biochemistry 2002; 41(48):14238-14247.

57. Luo J-K, Hornby JAT, Armstrong RN, Dirr HW. Equilibrium unfolding and enzyme kinetics of chimeric mu class glutathione transferases. Chemico-Biological Interactions 2001; 133:58-59.

58. Luo J-K, Hornby JAT, Wallace LA, Chen J, Armstrong RN, Dirr HW. Impact of domain interchange on conformational stability and equilibrium folding of chimeric class μ glutathione transferases. Protein Science 2002; 11:2208-2217.

59. Stevens JM, Armstrong RN, Dirr HW. Electrostatic interactions affecting the active site of class Sigma glutathione S-transferase. Biochem J 2000; 347:193-197.

60. Bammler TK, Driessen H, Finnstrom N, Wolf CR. Amino acid differences at positions 10, 11, and 104 explain the profound catalytic differences between two murine pi-class glutathione S-transferases. Biochemistry 1995; 34:9000-9008.

61. Xia H, Gu Y, Pan SS, Ji X, Singh SV. Amino acid substitutions at positions 207 and 221 contribute to catalytic differences between murine glutathione S-transferase A1-1 and A2-2 toward (+)-anti-7,8-dihydroxy-9,10-epoxy-7,8,9, 10-tetrahydrobenzo[a]pyrene. Biochemistry 2001; 38(31):19824-19830.

62. Hayes JD, Wolf CR. Role of glutathione transferase in drug resistance. In: Sies H, Ketterer B, editors. Glutathione Conjugation. Mechanisms and biological significance. London: Academic Press, 1988: 315-355.

63. Hemingway J, Malcolm CA, Kissoon KE, Boddington RG, Curtis CF, Hill N. The biochemistry of insecticide resistance in *Anopheles sacharovi*: Comparative studies with a range of insecticide susceptible and resistant *Anopheles* and *Culex* species. Pestic Biochem Physiol 1985; 24:68-76.

64. Motoyama N, Dauterman WC. Interstrain comparison of glutathione-dependent reactions in susceptible and resistant houseflies. Pestic Biochem Physiol 1975; 5:489-495.

65. Grant DF, Matsumura F. Glutathione S-transferase 1 and 2 in susceptible and insecticide resistant *Aedes aegypti*. Pestic Biochem Physiol 1989; 33:132-143.

66. Wang J, McCommas S, Syvanen M. Molecular cloning of a glutathione S-transferase overproduced in an insecticide-resistant strain of the housefly (*Musca domestica)*. Mol Gen Genet 1991; 227:260-266.

67. Clark AG, Shamaan NA, Dauterman WC, Hayaoka T. Characterization of multiple glutathione transferases from the house fly, *Musca domestica* (L). Pestic Biochem Physiol 1984; 22:51-59.

68. Clark AG, Dauterman WC. The characterization by affinity chromatography of glutathione S-transferases from different strains of house fly. Pestic Biochem Physiol 1982; 17:307-314.

69. Clark AG, Dick GL, Martindale SM, Smith JN. Glutathione S-transferases from the New Zealand grass grub, *Costelytra zealandica*. Their isolation and characterization and the effect on their activity of endogenous factors. Insect Biochem 1985; 15:35-44.

70. Toung YPS, Hsieh T-S, Tu CPD. *Drosophila* glutathione S-transferase 1-1 shares a region of sequence homology with the maize glutathione S-transferase III. Proc Natl Acad Sci USA 1990; 87:31-35.

71. Toung YPS, Hsieh T-S, Tu CPD. The glutathione *S*-transferase D genes. A divergently organized, intronless gene family in *Drosophila melanogaster*. J Biol Chem 1993; 268:9737-9746.

72. Grant DF, Dietze EC, Hammock BD. Glutathione S-transferase isozymes in *Aedes aegypti*: purification, characterization, and isozyme-specific regulation. Insect Biochem 1991; 21:421-433.

73. Ketterman AJ. Polymorphisms of human liver carboxylesterases. Biochem Soc Trans 1991; 19:306S.

74. Ketterman AJ, Bowles MR, Pond SM. Purification and characterization of two human liver carboxylesterases. Int J Biochem 1989; 21:1303-1312.

75. Ketterman AJ, Jayawardena KGI, Hemingway J. Purification and characterisation of a carboxylesterase involved in insecticide resistance from the mosquito *Culex quinquefasciatus*. Biochem J 1992; 287:355-360.

76. Ketterman AJ, Karunaratne SHPP, Jayawardena KGI, Hemingway J. Qualitative differences between populations of *Culex quinquefasciatus* in both the esterases A_2 and B_2 which are involved in insecticide resistance. Pestic Biochem Physiol 1993; 47:142-148.

77. Ketterman AJ, Prommeenate P, Boonchauy C, Chanama U, Leetachewa S, Promtet N et al. Single amino acid changes outside the active site significantly affect activity of glutathione S-transferases. Insect Biochem Molec Biol 2001; 31(1):65-74.

78. Ketterman AJ, Pond SM, Becker CE. The effects of differential induction of cytochrome P-450, carboxylesterase and glutathione S-transferase activities on malathion toxicity in mice. Toxicol Appl Pharmacol 1987; 87:389-392.

79. Fournier D, Bride J-M, Poirǐ M, Berǧ J-B, Plapp FW. Insect glutathione S-transferases. Biochemical characteristics of the major forms from houseflies susceptible and resistant to insecticides. J Biol Chem 1992; 267:1840-1845.

80. Toung YPS, Hsieh T-S, Tu CPD. The *Drosophila* glutathione S-transferase 1-1 is encoded by an intronless gene at 87B. Biochem Biophys Res Comm 1991; 178:1205-1211.

81. Chelvanayagam G, Parker MW, Board PG. Fly fishing for GSTs: a unified nomenclature for mammalian and insect glutathione transferases. Chemico-Biological Interactions 2001; 133:256-260.

82. Pongjaroenkit S, Jirajaroenrat K, Boonchauy C, Chanama U, Leetachewa S, Prapanthadara L et al. Genomic organization and putative promotors of highly conserved glutathione S-transferases originating by alternative splicing in *Anopheles dirus*. Insect Biochem Molec Biol 2001; 31(1):75-85.

83. Jirajaroenrat K, Pongjaroenkit S, Krittanai C, Prapanthadara L, Ketterman AJ. Heterologous expression and characterization of alternatively spliced

glutathione *S*-transferases from a single *Anopheles* gene. Insect Biochem Molec Biol 2001; 31:867-875.

84. Wongtrakul J, Udomsinprasert R, Ketterman A. Non-active site residues Cys69 and Asp150 affected the enzymatic 53 properties of glutathione *S*-transferase AdGSTD3-3. Insect Biochem Molec Biol 2003; 33(971):979.

85. Wongsantichon J, Harnnoi T, Ketterman AJ. A sensitive core region in the structure of glutathione S-transferases. Biochem J 2003; 373:759-765.

86. Bradford MM. A rapid and sensitive method for the quantitation of microgram quantities of protein utilizing the principle of protein-dye binding. Anal Biochem 1976; 72:248-254.

87. Habig WH, Pabst MJ, Jakoby WB. Glutathione S-transferases. The first enzymatic step in mercapturic acid formation. J Biol Chem 1974; 249:7130-7139.

88. Vararattanavech A, Ketterman A. Multiple roles of glutathione binding-site residues of glutathione S-transferase. Protein and Peptide Letters 2003; 10 (5):441-448.

89. Ricci G, Lo Bello M, Caccuri AM, Pastore A, Nuccetelli M, Parker MW et al. Site-directed mutagenesis of human glutathione transferase P1-1. Mutation of Cys-47 induces a positive cooperativity in glutathione transferase P1-1. J Biol Chem 1995; 270(3):1243-1248.

90. Hegazy UM, Mannervik M, Stenberg G. Functional role of the lock and key motif at the subunit interface of glutathione transferase P1-1. J Biol Chem 2004; 279(10):9586-9596.

91. Stenberg G, Abdalla A-M, Mannervik B. The dimeric state of glutathione transferases: role of a key residue at the subunit interface in human GSTP1-1. Chemico-Biological Interactions 2001; 133:24-27.

92. Nathaniel C, Wallace LA, Burke J, Dirr HW. The role of an evolutionarily conserved *cis*-proline in the thioredoxin-like domain of human class alpha glutathione transferase A1-1. Biochem J 2003; 372:241-246.

93. Fersht A. Enzyme structure and mechanism. Second ed. W.H.Freeman and company, 1985.

94. Gore MG. Spectrophotometry and spectrofluorimetry. Oxford university press, 2000.

95. Matulis D, Lovrien R. 1-anilino-8-naphthalene sulfonate anion-protein binding depends primarily on ion pair formation. Biophys J 1998; 74:422-429.

96. Matulis D, Baumann CG, Bloomfield VA, Lovrien RE. 1-anilino-8-naphthalene sulfonate as a protein conformational tightening agent. Biopolymers 1999; 49:451-458.

97. Sluis-Cremer N, Naidoo N, Dirr H. Class-pi glutathione S-transferase is unable to regain its native conformation after oxidative inactivation by hydrogen peroxide. Eur J Biochem 1996; 242:301-307.

98. Sayed Y, Hornby JAT, Lopez M, Dirr H. Thermodynamics of the ligandin function of human class Alpha glutathione transferase A1-1: energetics of organic anion ligand binding. Biochem J 2002; 363:341-346.

99. Hennessey JP, Johnson WCJr. Information content in the circular dichroism of proteins. Biochemistry 1981; 20(1085):1094.

100. Otzen DE, Rheinnecker M, Fersht AR. Structural factors contributing to the hydrophobic effect: the partly exposed hydrophobic minicore in chymotrypsin inhibitor 2. Biochemistry 1995; 34:13051-13058.

101. Xu J, Baase WA, Baldwin E, Matthews BW. The response of T4 lysozyme to large-to-small substitutions within the core and its relation to the hydrophobic effect. Protein Science 1998; 7:158-177.

102. Sreerama N, Woody RW. Poly(Pro)II helices in globular proteins: identification and circular dichroic analysis. Biochemistry 1994; 33:10022-10025.

103. Vassilenko KS, Uversky VN. Native-like secondary structure of molten globules. Biochim Biophys Acta 2002; 1594:168-177.

BIOGRAPHY

NAME	Miss Juthamart Piromjitpong
DATE OF BIRTH	9 May 1980
PLACE OF BIRTH	Ubon Ratchatani, Thailand
INSTITUTIONS ATTENDED	Khon Kean University, Thailand: 1998-2002 Bachelor of Science (Chemistry, First Class Honors) Mahidol University, Thailand: 2002-2004 Master of Science (Molecular Genetics and Genetic Engineering)
RESEARCH GRANT	The Development and Promotion of Science and Technology Talent Project (DPST)
HOME ADDRESS	31 Uppareesan Road, A. Moung, Ubon Ratchatani, 34000 Tel. 0-452-425-20